A Study of the Interaction between Botulinum Neurotoxin and Cellular Membranes

Harris, Iain

Award date:
2014

Awarding institution:
University of Bath

A Study of the Interaction between Botulinum Neurotoxin and Cellular Membranes

Iain John Harris

A thesis submitted for the degree of Doctor of Philosophy

University of Bath

Department of Biology and Biochemistry

September 2013

Acknowledgements

Thank you to all of my supervisors both in academia and industry for your constant support and guidance over the past four years. With special thanks to Ravi Acharya, Keith Foster, Matthew Beard, John Chaddock and Elaine Harper.

I would like to extend my thanks to everyone from lab 0.34, past and present, for helping whenever you could.

Thank you to BBSRC for funding my project and to the staff at Diamond Light Source for providing many late nights at the synchrotron.

Thank you to everyone at Syntaxin both past and present for making my stay at the company so enjoyable. There are too many individuals to mention but special thanks to David Burgin, Jolanta Tolkatz, Daniel Kwan and Kevin Moore for your help with molecular biology matters, Mark Elliot and Steve Johnson for your help with Pharmacology assays, Andrew Splevins for your help with developing my vesicle leakage assay and Lewis Burke-Smith for procuring everything I needed.

Thank you to Matthew and Tara for being so supportive both in and out of work over the past four years. I have thoroughly enjoyed your friendship.

Thank you to Tom and Jay for being so supportive and kind and always providing a sofa to sleep on when needed.

And finally my unconditional thanks and love to my mother, father and sister. Your love and support has sustained me through all the highs and lows so far and I know it will be there for all the challenges to come. I could never have got this far without you!

Abstract

Eight genetically distinct serotypes (A-H) of Botulinum neurotoxin (BoNT) cause flaccid muscular paralysis through inhibition of neurotransmission at cholinergic nerve terminals. BoNT binds with specificity to the neuromuscular junction and enters through endocytosis. It translocates its catalytic moiety through the endosomal membrane into the cell cytosol and finally proteolyses soluble N-ethylmaleimide-sensitive-factor attachment protein receptors (SNAREs) inside the neuromuscular junction, thereby preventing synaptic vesicle fusion with the plasma membrane. The action of BoNT is facilitated by its tri-domain structure which includes: the receptor binding domain (H_C), the translocation domain (H_N) and the catalytic domain (LC). Removal of BoNT's H_C domain leaves a stable, catalytically active molecule (LH_N), which lacks specificity for the neuromuscular junction. The least understood step in the mechanism of BoNT action is the translocation of the LC domain through the endosomal membrane into the cell cytosol; this action is thought to be preceded by the formation of an H_N domain pore following acidification of the endosomal compartment. In this study we set out to investigate this step. We investigated the interaction of BoNT and LH_N proteins with cellular and artificial membranes. Firstly, the interaction of LH_N serotype D (LH_D) with Chinese Hamster Ovary cells (CHO-K1 cells) was investigated by measuring an apparent LH_D induced increase in CHO-K1 cell intracellular Ca^{2+} levels. The increase was affected by extracellular Ca^{2+} concentration suggesting that LH_D may permeabilise the membrane of CHO-K1 cells at near neutral pH. Secondly, we developed novel expression and purification methods for BoNT H_N domains (serotypes A, C and D). This allowed us to compare the lipophilicity of the H_N domains from multiple serotypes, further supporting a role for this domain as a pore forming moiety. Thirdly, vesicle leakage assays were explored as a method for determining protein or peptide pore formation in an attempt to further define the pore forming potential of BoNT and LH_N proteins of various serotypes. However, in these experiments, control proteins with no known pore forming ability also caused vesicle leakage at acidic pH; the ability of a vesicle leakage assay to sufficiently demonstrate protein or peptide pore formation has not therefore been confirmed in this study. Investigation into LH_N and BoNT induced pore formation in lipid vesicles via electron microscopy was similarly inconclusive. Together the results presented in this thesis show that the H_N region of BoNT serotypes A, C and D can be purified as isolated lipophilic domains, furthermore, the interaction of BoNT constructs containing the H_N domain with membranes is consistent with a function in transmembrane protein translocation.

List of Abbreviations

A_{280} - Absorbance at 280 nm

ADP – Adenosine diphosphate

AMP - Adenosine monophosphate

ANTXR – Anthrax Toxin Receptor

ATP – Adenosine triphosphate

B1 – Bradykinin B1 receptor

BIS-TRIS - Bis(2-hydroxyethyl)-amino-tris(hydroxymethyl)-methane

BoNT – Botulinum Neurotoxin

BSA - Bovine serum albumin

C. argentinense - *Clostridium argentinense*

C. baratii - *Clostridium baratii*

C. botulinum - *Clostridium botulinum*

C. butyricum - *Clostridium butyricum*

C. difficile - *Clostridium difficile*

C. perfringens - *Clostridium perfringens*

C. tetani - *Clostridium tetani*

CHO – Chinese Hamster Ovary

Des-Arg^9-BK – Des-Arginine^9-Bradykinin

DLS - Diamond Light Source

DNA - Deoxyribonucleic acid

DOPC – 1,2-dioleoyl-sn-glycero-3-phosphocholine

DOPG – 1,2-dioleoyl-sn-glycero-3-phospho-(-1-race-glycerol)

DTT - Dithiothreitol

E. coli - *Escherichia coli*

EC50 - Half maximal effective concentration

ECL - *Erythrina cristagalli* lectin

EDTA – Ethylene-diaminetetraacetic acid

EF – Edema Factor

EGF - Epidermal growth factor

EGFR (ECD) - Epidermal growth factor receptor (extracellular domain)

eSCN - Embryonic spinal cord neuron

$F_{(0)}$ – Florescent level before protein addition

$F_{(t)}$ – Florescent level at time t

F_{max} – Maximum Fluorescence

GALA – 30 amino acid pore forming peptide

GD1b – Disialo gangliosides

GH – Growth Hormone

GHRH – Growth Hormone Receptor Hormone

GPCR – G-protein Coupled Receptor

GT1b – Trisialo gangliosides

HA - Hemagglutinin

HC – Heavy Chain

H_C – Receptor Binding Domain

H_{CC} – Receptor Binding Domain (C-terminal)

H_{CN} – Receptor Binding Domain (N-terminal)

HEPES - 4-(2-hydroxyethyl)-1-piperazineethanesulfonic acid

HIC – Hydrophobic Interaction Chromatography

H_N – Translocation Domain

IgG - Immunoglobulin G

IPTG - Isopryl-1-thio-□-galactopyranoside

LC – Light Chain

LH_N - Fragment LC+H_N of BoNT

LOS – Lipoligosaccharide

LPS – Lipopolysaccharide

LT – Lethal Toxin

LUV – Large Unilamellar Vesicle

MAPKK – Mitogen-Activated Protein Kinase

MBP - Maltose binding protein

MoA – Mechanism of Action

MOPS - 3-(N-morpholino)propanesulfonic acid

NGF – Nerve Growth Factor

NTA – Nickel Tagged Agarose beads

NTNH - Non-toxic non-hemagglutinin

PAGE - Polyacrylamide gel electrophoresis

PEG - Polyethylene glycol

PM – Plasma Membrane

rDNA - Ribosomal DNA

RFU – Relative Fluorescent Unit

RNA – Ribonucleic Acid

SDS - Sodium dodecyl sulphate

SNAP – Synaptosomal Associated Protein

SNARE – Soluble N-ethyl-Maleimide Sensitive Fusion Protein Attachment Receptor

SRB – Sulforhodamine B

SV – Synaptic Vesicles

SV2- Synaptic Vesicle Receptor 2

Syt - Synaptotagmin

T50% - Time to 50% vesicle leakage

TB - Terrific Broth

TeNT – Tetanus Neurotoxin

TRIS - Tris(hydroxymethyl)aminomethane

TSI – Targeted Secretion Inhibitor

t-SNARE - Target SNARE

VAMP – Vesicle Associated Membrane Protein

v-SNARE - Vesicle SNARE

WGA - Wheat germ agglutinin

β-o-G – n-Octyl-β-D-Glucopyranoside

Table of contents

Table of contents

Table of contents

Table of contents

Table of contents

Table of contents

List of figures

List of figures

List of tables

1 Introduction

1.1 Bacterial toxigenesis

In 1676 Antonie Van Leeuwenhoek peered down a single lens microscope and observed small organisms which he termed “Animalcules”. Following initial scepticism, his observations were confirmed by Robert Hooke of the Royal Society of London after repetition of the experiment. Unwittingly, Leeuwenhoek had just made undoubtedly one of the most important discoveries in science; he had discovered “Bacteria” (Dobell, 1923; Fred, 1933).

Engaged by the idea of microbiology, Louis Pasteur established fermentation to be as a result of micro-biological growth (1859). This led Pasteur and his contemporary Robert Koch to both subscribe to “the germ theory of disease”, here they hypothesised that bacterial organisms were responsible for certain diseases. Robert Koch developed the idea of germ theory through pioneering work on cholera, anthrax and tuberculosis culminating in his proof of germ theory for which he was awarded the Nobel prize in 1905. “Koch’s postulates”, the criteria with which he determined an organisms potential to cause disease are still used today (Inglis, 2007).

Pioneering work by Koch and Loeffler alluded to the anticipated release of toxic molecules by bacteria as a mechanism for the proliferation of some diseases including cholera (*Vibrio cholerae*) and diphtheria (*Corynebacterium diphtheriae*). Today we define this process as bacterial toxigenesis.

There are two main types of bacterial toxigenesis; cell associated toxins known as endotoxins and extracellular diffusible toxins known as exotoxins. Endotoxins are structural components of the bacteria, specifically lipopolysaccharides (LPS) or lipoligosaccharides (LOS) located on the outer membrane of Gram-negative bacteria. Exotoxins are predominantly secreted by bacteria but may also be released following cell lysis (Rietschel et al., 1994). Exotoxins are predominantly proteins or peptides, when these molecules

interact with a host's cellular environment they elicit specific host responses (Turton et al., 2002).

1.2 Diversity of bacterial exotoxins

Most bacteria capable of producing disease causing exotoxins produce a species specific toxin (e.g. *Clostridium tetani* produces tetanus toxin which causes tetanus and *Corynebacterium diphtheria* produces the diphtheria toxin which causes diphtheria) (Hoch et al., 1985). This is not true for all species of exotoxin, some can be produced by multiple species of bacteria (e.g *Clostridium botulinum, Clostridium butyricum*, *Clostridium baratii* and *Clostridium argentinense* produce botulinum toxin which in turn causes Botulism). The associated exotoxins are normally produced in the exponential phase of bacterial growth (Montal, 2010).

Diversity in bacterial toxins can be seen clearly by distinct differences in their site of action, mechanism of action, potency, size and structure (Table 1-1). Descriptive pre-cursors such as enterotoxin, neurotoxin, leukocidin and haemolysin indicate in generality the sites targeted by the proteins. Enterotoxins, such as cholera enterotoxin (produced by *Vibro cholera*), target the gastrointestinal tract, a common symptom of which is severe diarrhoea and vomiting (de Haan and Hirst, 2000); neurotoxins such as botulinum neurotoxin and tetanus neurotoxin target the nervous system, the details of which are discussed in detail below; leukocidin's, such as Panton-Valentine leukocidin (produced by *Staphylococcus aureus*), are pore forming toxins originally discovered due to their ability to cause leukocyte cytosis (Kaneko and Kamio, 2004); haemolysin toxins, such as alpha-haemolysin (also produced by *Staphylococcus aureus*), are pore forming toxins capable of causing cell lysis through uncontrolled permeation of water ions and small organic molecules, they were originally discovered through monitoring their ability to cause red blood cell cytosis (Gouaux et al., 1997). Toxins without known mechanisms which cause animal death are simply known as lethal toxins. Some toxins, known as invasins, have a less specific site of action and the ability to enable bacterial invasion through breaking down cellular structure (e.g. collagenase, hyaluronidase and streptokinase) (Niemann et al., 2004).

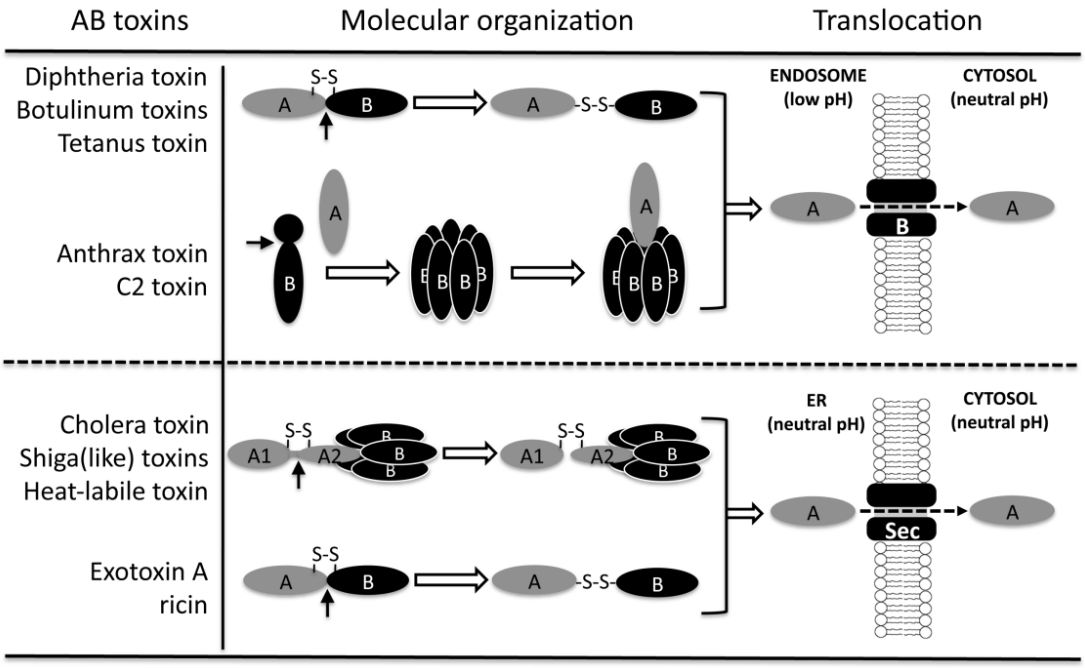

Figure 1-1 The molecular organization of AB toxins during subunit A translocation
The molecular organization of AB toxins prior to and during subunit A translocation (Sun, 2012).

1.3 A plus B subunit arrangement

Many toxins which act at specific intracellular sites adhere to a two domain structure consisting of subunits A and B: subunit A is the catalytically active element, and subunit B is responsible for cell specificity, binding and subunit A translocation (Odumosu et al., 2010).

The A and B subunits are synthesised and arranged in a way which is species dependent. A + B toxins subunits are synthesised separately and eventually interact at the target cell to create a viable toxin (e.g. Bacillus anthracis EF, Anthrax toxin LF); A-B or A-5B refer to A and B subunits synthesised separately and associated by non-covalent bonds during secretion (e.g. Cholera toxin, Pertussis toxin and E.coli heat-labile toxin LT); 5B refers to a pentameric arrangement of the binding and translocation region. A/B toxins are synthesised as a single unit which is separated by proteolytic cleavage (e.g. Botulinum toxin, Pseudomonas Exotoxin A and Tetanus toxin) (Odumosu et al., 2010).

	A Subunit(s)	B Subunit(s)	Enzymatic Activity	Target	Receptors(s)
Cholera toxin	A1: 22 kDa A2:5 kDa	(×5) 10.6 kDa	ADP-ribosyl transferase	Adenylate cyclase *G*-protein (Gsα)	GM1 ganglioside
***E. coli* (LT)**	A1:22 kDa A2: 5 kDa	(×5), 11.6 kDa	ADP-ribosyl transferase	*G*-protein (Gsα)	GM1 ganglioside Asialoganglioside
Shiga toxin	A1: 28 kDa A2: 4 kDa	(×5) 7.7 kDa	*N-glycosylase* (Cleaves adenine 4324)	rRNA (28S)	Gb3 glycolipid
Pertussis toxin	S1: 28 kDa	S2: 23 kDa S3: 22 kDa S4: (×2) 11.7 kDa S5: 9.3 kDa	ADP-ribosyl transferase	*G*-protein (Gsα)	GD1a ganglioside
Anthrax	(LF): 90 kDa (EF): 89 kDa	(PA): (×7) 83 kDa	Zn metalloprotease Adenylate cyclase	MAPKK Protein Kinases	ANTXR 1 ANTXR 2
Ricin	30 kDa	29 kDa	*N*-glycosylase (Cleaves adenine 4324)	rRNA (28S)	Glycoprotein Glycolipid
Botulinum Toxin	Approx 50 KDa	Approx 100 KDa	Zn metalloprotease	Soluble Nsf Attachment protein REceptor (SNARE)	Ganglioside SV2 Synaptotagmin

Table 1-1 A small selection of genetically diverse AB exotoxins
This table demonstrates the diversity of known AB toxins by highlighting difference between their respective catalytic action, subunit organization and receptor binding. (Montecucco and Schiavo, 1995; Odumosu et al., 2010)

Once synthesised there are two prominent ways in which toxins are thought to enter host/target cells, namely direct entry and receptor mediated endocytosis. Direct entry is a mechanism by which the toxins B domain forms a pore in the target cell membrane allowing the A subunit to enter the cytosol of the target cell directly from the cell exterior (Balfanz et al., 1996). Receptor-mediated endocytosis requires the binding of subunit B to the target cell exterior followed by the internalisation of subunits A and B within an endosome. Finally the B subunit permeates the endosomal membrane permitting translocation of subunit A to the cell cytoplasm (Wileman et al., 1985).

1.3.1 Clostridia

The genus *Clostridium* consists of large, Gram-positive, rod-shaped bacteria within the phylum *Firmicutes.* There are over 100 species of *clostridia* characterised by 16s RNA sequencing, all species form endospores and only grow under anaerobic conditions; however, the spores generated by clostridia can survive long periods in aerobic conditions. *Clostridia* will grow in virtually all anaerobic habitats where organic compounds are present, including soils, aquatic sediments and the intestinal tracts of mammalian organisms (Coffield et al., 1994; Shukla and Sharma, 2005).

Through fermenting a large range of organic compounds, clostridia produce waste compounds such as butyric acid, acetic acid, butanol, acetone, carbon dioxide and hydrogen. The bacteria secrete a variety of extracellular enzymes which degrade biological molecules including proteins, lipids, collagen and cellulose. Consequently *Clostridia* is known to play an important role in the carbon cycle (Wang et al., 2013). In *Clostridia* infection, the ability to degrade large biological molecules can play a role in invasion and pathology. Some species of the clostridia are pathogenic for humans, primarily *Clostridium perfringens*, *C. difficile, C. botulinum and C. tetani* produce the most toxic biological molecules known to man (Maclennan, 1962; Shukla and Sharma, 2005).

Tetanus is caused by *C. tetani* exotoxins known as tetanus neurotoxin (TeNT) or tetanospasmin. TeNT targets the central nervous system through inhibiting

neurotransmission leading to potentially fatal spastic paralysis. The toxin binds to cholinergic motor neurones where it is subjected to retrograde axonal transport to spinal cord neurones. Neurotransmission is inhibited through TeNT's cleavage of synaptobrevin preventing cellular secretion. The structure and mechanism of action of TeNT is very similar to that of Botulinum toxins (see below) (Shukla and Sharma, 2005).

1.4 Botulinum neurotoxins and Botulism

Botulism is a rare but severe paralytic disease caused by an exotoxin produced by the bacterial species *Clostridium botulinum, Clostridium butyricum, Clostridium baratii* and *Clostridium argentinense,* namely, Botulinum neurotoxin (BoNT). Justinus Kerner first described Botulism in the 19th century following a severe food poisoning outbreak that was traced back to the ingestion of blood sausage; consequently, the name Botulinum was derived from the Latin term for sausage (*botulus*) (Hatheway, 1990).

Through a mechanism which will be discussed in detail, BoNTs cause muscular paralysis by inhibiting synaptic action and consequently nerve signal transmission at the neuromuscular junction. Portals for BoNT entry into the circulatory system include the pulmonary tract (inhalation botulism), the gastrointestinal tract (food-borne and infant botulism) and through the broken skin of wounds (wound botulism). Regardless of the route of infection, if BoNT enters the circulatory system and is transported to the neuromuscular junction of motor neurones, it has the potential of inhibiting muscle contraction (Montal, 2010).

The clinical hallmark of botulism is an acute flaccid paralysis which begins with bilateral cranial nerve impairment, involving muscles of the eyes, face, head and pharynx and then descends symmetrically to involve muscles of the thorax and extremities. Symptoms which characterise the disease include blurred vision, amblyopia, ptosis and photophobia which can be followed by signs of bulbar nerve dysfunction such as dysarthria, dysphonia and dysphagia. However, early symptoms are mostly non-specific and difficult to distinguish from the over indulgence of alcohol. If Botulism has been contracted from food borne bacteria, initial symptoms may include nausea, abdominal pain and diarrhoea, most

likely caused by other bacterial exotoxins, before any sign of neurologic complication develops (Caya et al., 2004).

If the disease is allowed to progress without treatment, death may result from respiratory failure caused by paralysis of the tongue or muscles in the pharynx causing upper airway occlusion or via paralysis of the diaphragm and intercostals muscles. The severity, rate and duration of Botulism is dependent on the serotype specific action of BoNT and the dose of toxin (Peck, 2009).

Due to its potency and its potential to cause death through muscular paralysis, BoNT has be classified as the most deadly toxin known to mankind and consequently as a "select agent" meaning criminal prosecution for those who do not follow strict government guidelines regarding obtaining, handling and documenting its use. Due to its relative ease of production and virulent potential through aerosol, BoNT's have concurrently been determined a category A biological weapon by the Centres for Disease Control and prevention (CDC), USA. Assuming a 70kg human, death from BoNT toxicity takes just 0.09-0.15 μg when injected, 0.7-0.9 μg when inhaled and 70 μg if ingested. Consequentially 1g of the toxin has the potential to kill approximately 14,000 people if ingested, 1.25 million if inhaled and 8.3 million if injected (Scott and Suzuki, 1988).

1.4.1 The eight serotypes of botulinum neurotoxin

It became apparent that more than one type of Botulinum toxin existed when antitoxin serums, developed to treat Botulism, only proved successful in select outbreaks of the disease (Hatheway, 1990). As the new strains of BoNT were discovered they were labelled chronologically from serotype A (the first serotype to be discovered) to serotype H (the last serotype to be discovered) (Aoki and Guyer, 2001). Variants or subtypes within BoNT serotypes A, B, E and F have been designated by adding an Arabic number to the toxin type, e.g., A_1, A_2.

Botulinum neurotoxins (BoNTs) are produced by at least four diverse groups of Gram positive spore-forming anaerobic bacteria under the taxonomic label of *Clostridium*

botulinum (Hedeland et al., 2011). The only criterion for belonging to the *C. botulinum* species is the ability to produce the exotoxin BoNT. Therefore *C. botulinum* arguably encompasses four separate species of bacteria that can be clearly separated into four distinct groups (Groups I-IV) via phylogenetic analysis of 16S rrn genes (Hill et al., 2009). Group I contains proteolytic serotype A, B and F strains as well as strains that produce two botulinum toxin types (bivalent) including Ab, Ba, Af and Bf strains; Group II consists of nonproteolytic (np) and saccharolytic serotype B, E, and F strains; Group III consists of serotype C and D strains; group IV consists solely of serotype G strains; Group IV has been recognised as a distinct species and has been given the name *C.* argentinense*.* It has been suggested that Groups V and VI should extend to BoNT producing clostridial species such as *C. baratii* (produces BoNT serotype F) and *C*. *butyricum* (produces BoNT serotype E) respectively (Hill et al., 2009).

Each serotype of BoNT is encoded by a ~3.8kb gene which is associated with accessory genes or predicted open reading frames (*orfs*) that are collectively referred to as the BoNT gene cluster. The BoNT gene cluster includes nontoxic and nonhemagglutinin genes and several other genes that encode toxin-associated proteins (hemagglutinins HA-17, HA-33, HA-70 and p21, and/or p47) (Kubota et al., 1998). There are two types of BoNT gene clusters known: the hemagglutinin (*ha*) toxin gene cluster is found within strains that produce toxin types A_1, A_5, B, C, D and G and the *orfX* gene cluster is found in strains that produce toxin types A_1, A_2, A_3, A_4, E and F and in *Clostridium butyricum* type E and *Clostridium baratii* type F strains. The location of gene clusters encoding BoNT proteins varies between serotypes; the genes encoding for BoNT serotypes A, B, E and F are located on bacterial chromosomes, BoNT serotypes C and D are encoded for on a phage genome and BoNT serotype G is located on a plasmid (Hill et al., 2007). Very recently a new serotype of BoNT was discovered and named serotype H, it was found to be located in the *orfX* toxin gene cluster at a unique chromosomal site different from those used by other botulinum toxin gene clusters (Barash and Arnon, 2014).

Comparison of the protein sequences of BoNT serotypes A-G shows that serotype identity ranges from 34%-64% (Hill et al., 2009). This variation in serotype diversity is thought to be as a result of BoNT genes being horizontally transferred between various

clostridial lineages, resulting in the isolated evolution of each BoNT serotype (Hill et al., 2009). In addition, recombination events within BoNT genes have resulted in mosaic serotypes (e.g. BoNT serotypes C/D and A_1/A_3) which contribute even further to BoNT diversity (Hill et al., 2009).

All BoNT serotypes (A, B, C_1, D, E, F, G and H) cause the potentially fatal neuroparalytic disease known as Botulism. Only four of the seven serotypes (A, B, E and F) have been confirmed to cause naturally occurring human botulism, but seven cause inhalational botulism in primates (A-G). There is evidence for the ingestion of serotype C_1 causing human botulism but recent results show serotype D to be largely ineffective in humans (Collins and East, 1998; Eleopra et al., 2013). As the clinical uses of BoNT expand, it has become more important to understand the differences between BoNT serotypes. Although all BoNT molecules are known to inhibit acetylcholine release, they bind to different extracellular receptors, act through different intracellular protein targets, exhibit different durations of effect and have different potencies (Montal, 2010).

1.4.2 The tri-modular architecture of botulinum neurotoxin

All seven serotypes of BoNT are known to be synthesised as single chain polypeptide precursor molecules with approximate masses of 150KDa. The inactive precursor protein is post-translationally cleaved (or activated) into two sections, either by Clostridial or tissue proteases. The two sections, called the heavy chain (HC) and the light chain (LC), create a A-B toxin motif (Figure 1-2). The heavy chain is the larger of the two sections with a molecular weight of ~100KDa. It is attached to the ~50KDa light chain section via a disulphide bond, hydrogen bonding and Van der Waals interactions. Structural elucidation of the toxin has identified that the HC structure is further divided into at least two covalently linked domains, namely, the receptor binding domain (H_C) and the translocation domain (H_N). (Montecucco et al., 1994).

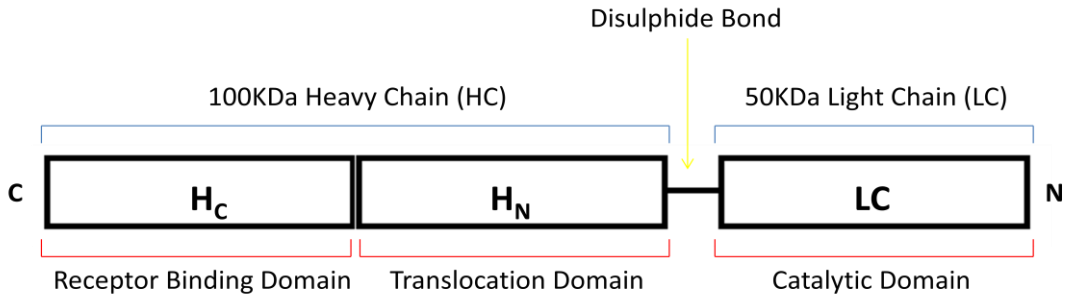

Figure 1-2 Domain organization of Botulinum neurotoxins
There are three domains present in all BoNT molecules, namely, the receptor binding domain (H_C), the translocation domain (H_N) and the catalytic domain (LC). Following post synthetic cleavage these three domains are organized into a 100KDa heavy chain (containing the H_C and H_N domains) and a 50KDa light chain (containing the LC domain). The light chain is joined to the heavy chain via a disulphide bond and many intermolecular interactions.

The three domains of BoNT have been determined functionally and structurally to be common in seven BoNT serotypes (A-G) and are presumed to be present in the recently discovered H serotype (Barash and Arnon, 2014). This tri-modular architecture allows BoNT to inhibit the release of acetylcholine from neuromuscular synapses, ultimately causing flaccid muscular paralysis. Each domain has a specific role in BoNT's mechanism of action: In general, the H_C domain binds specifically to the pre-synaptic membrane of a neuromuscular synapse (see section 1.5.1); BoNT is endocytosed into recycling vesicles where the acidic environment provokes a conformational change (see 1.5.2.5) and ultimately translocation of the LC domain into the cell cytosol through a pore formed by the H_N domain (see section 1.5.2.4); once inside the cell cytosol the LC domain cleaves soluble N-ethyl-maleimide sensitive fusion protein attachment receptor (SNARE) proteins (see section 1.5.3). The general and serotype specific function of each domain will be discussed in greater detail below.

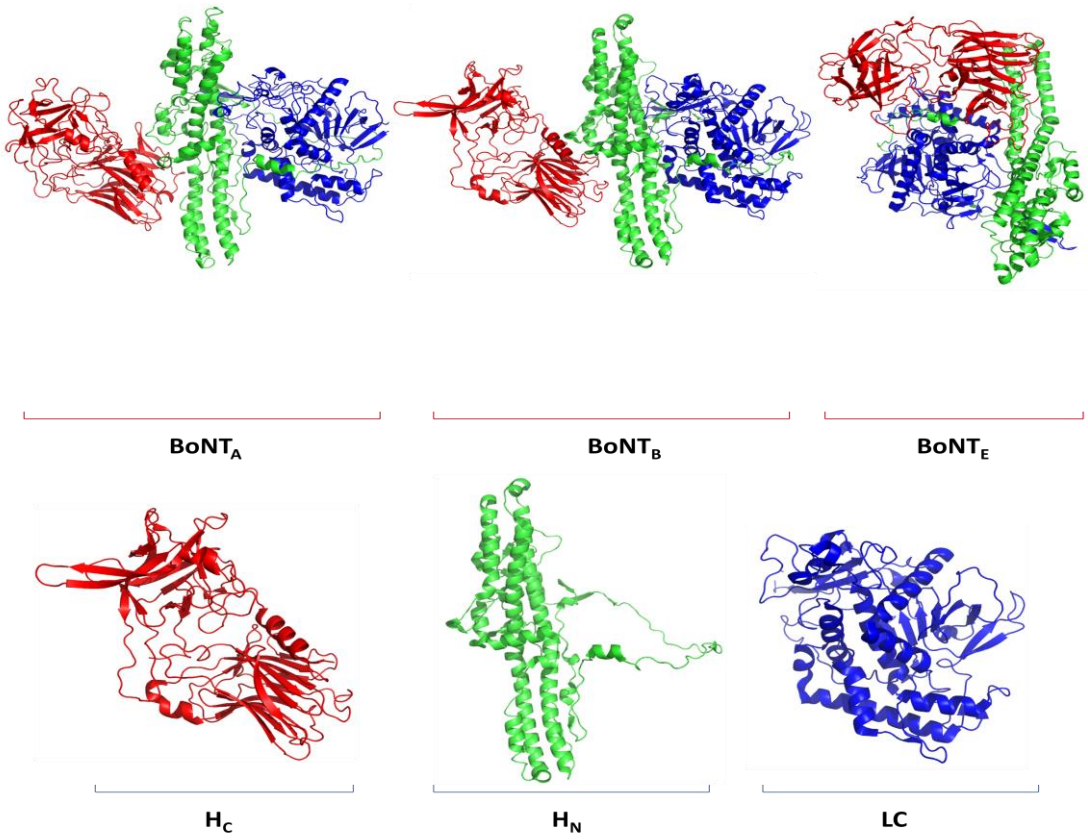

Figure 1-3 The tri-modular domain of BoNT is represented in all seven serotypes
The crystal structures of BoNT$_A$ (3BTA), BoNT$_B$ (1EPW) and BoNT$_E$ (3FFZ) all conform to a tri-modular architecture; the three domains highlighted are the receptor binding domain (H$_C$) (red), the translocation domain (H$_N$) (green) and the catalytic domain (LC) (blue). The three domains of BoNT$_B$ (1EPW) have been separated and defined (Kumaran et al., 2009; Lacy et al., 1998; Swaminathan and Eswaramoorthy, 2000).

1.5 Botulinum neurotoxin mechanism of action

In order to inhibit neuromuscular communication, botulinum neurotoxin must target, infiltrate and disrupt the action of neuromuscular synapses. To understand how one molecule can complete all of these tasks, the physiological representation of BoNT's tri-modular organisation is assessed with relation to the molecules physical properties and three-dimensional structure for characterised serotypes A-G.

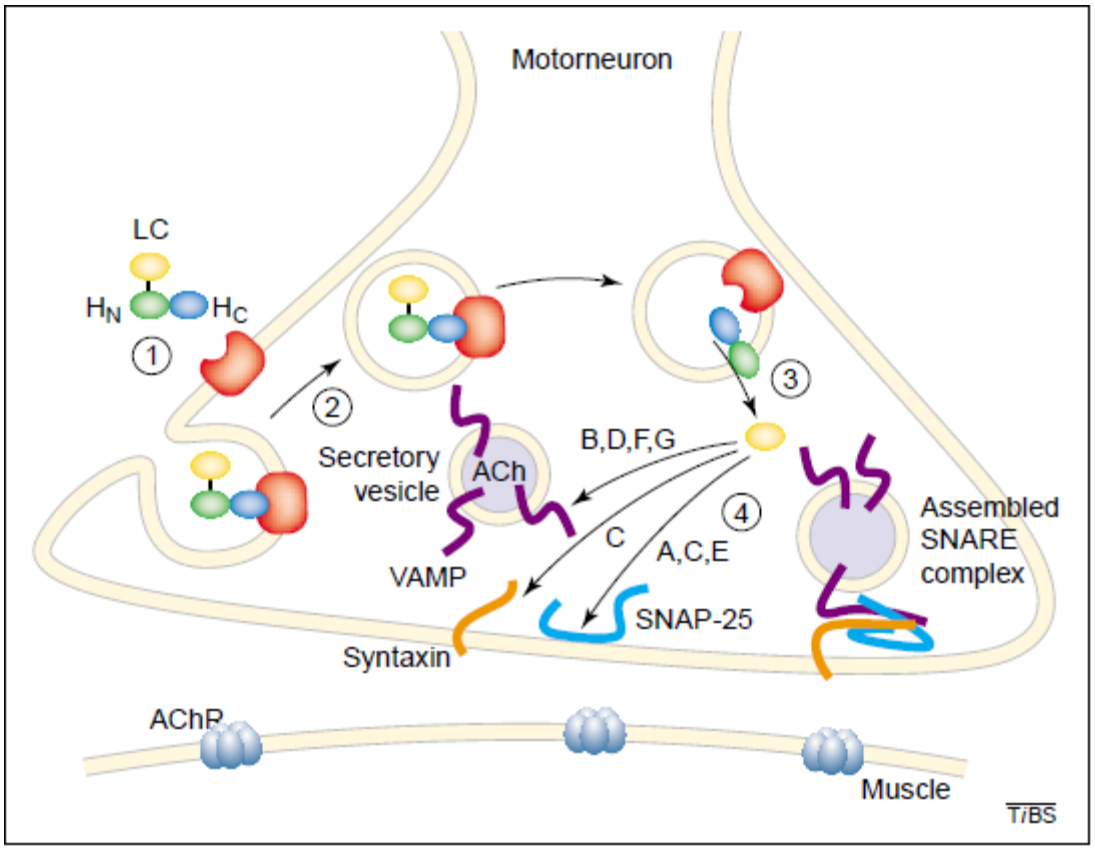

Figure 1-4 Mode of action of botulinum neurotoxins.
Reproduced from (Turton et al., 2002). A four-step mechanism, (1) cell binding, (2) endocytosis, (3) translocation of LC in the cytosol, (4) LC cleavage of one of the SNARE proteins. (Ach, acetylcholine; AChR, acetylcholine receptor).

1.5.1 Receptor binding

As discussed, the binding of BoNT's H_C domain to the neuromuscular junction is the first step required for intoxication. BoNTs are known to enter neurones by a dual host receptor mechanism which either requires binding to two ganglioside receptors or binding to a ganglioside receptor and a synaptic vesicle (SV) associated protein receptor (Benson et al., 2011; Montecucco, 1986).

Ganglioside binding:

Gangliosides are glycosphingolipids which have a ceramide component, imbedded in the outer layer of the plasma membrane, and a carbohydrate moiety extending into the extracellular space (Figure 1-5). The composition of the carbohydrate moiety of complex

gangliosides includes a sugar backbone consisting of glucose, galactose and N-acetylgalactosamine with attached sialic acids to varying degrees and positions (Lopez and Schnaar 2009).

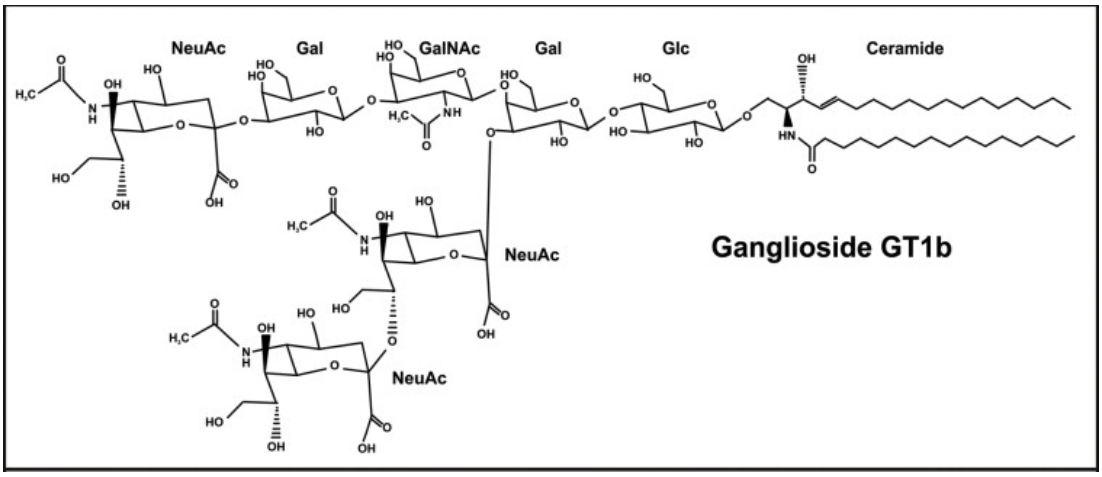

Figure 1-5 Structure of the GT1b ganglioside
BoNT serotypes A, B, C, E and G have affinity for the GT1b ganglioside which is found on the pre-synaptic terminal of neuromuscular synapses. (Lopez and Schnaar, 2009)

The abundance of gangliosides on the surface of presynaptic membranes lead to an investigation which aimed to determine whether or not they interacted with BoNT molecules. Through this investigation it was demonstrated that members of the G1b class of ganglioside (specifically GT1b (trisialo gangliosides) and GD1b (disialo gangliosides)) have a high affinity for BoNT (Montecucco, 1986). In an effort to further determine the importance of gangliosides in BoNTs mechanism of action, monoclonal antibodies specific to the GT1b ganglioside were introduced to rat brain synaptosomes, eliminating the toxicity of $BoNT_A$ and $BoNT_B$ respectively (Kozaki et al., 1998). Furthermore, it was demonstrated that gangliosides were essential to the binding of $BoNT_A$ to ganglioside-deficient murine or human neuronal cells (Yowler et al., 2002).

As its name suggests, BoNTs receptor binding domain (H_C) is responsible for the binding of ganglioside receptors (Swaminathan, 2011). The binding of gangliosides has been demonstrated to be serotype specific. BoNT serotypes A, B, C and F bind to gangliosides GT1b, GD1b and GD1a; serotype E binds to GT1b and GD1a; and serotype G recognises all gangliosides with similar affinity (Montal, 2010). Recently it has been demonstrated that

BoNT serotypes C and D have the potential to simultaneously bind to two ganglioside receptors. $BoNT_C$ endocytosis requires dual ganglioside binding facilitated by two separate binding sites known to have affinity for GD1b and either GD1a or GT1b receptors respectively (Karalewitz et al., 2012). Mutagenesis studies of the H_C domain of $BoNT_C$ and $BoNT_D$ have shown the toxins potential to bind two ganglioside receptors at separate sites including GM3, GM2 GM1 and GDa1 (Strotmeier et al., 2010). Neither of these observations precludes BoNT serotypes C and D from concurrently binding proteinous receptors although it is likely that their affinity for more than one ganglioside will increase their probability of binding to the neuronal cell surface.

Protein receptor binding:

Ganglioside binding alone does not account for the specificity of most, if not all, BoNT serotypes binding to the presynaptic terminal of motor neurones (serotypes C and D are possible exceptions as discussed above). After BoNT has bound to gangliosides on the neuronal cell surface, a depolarisation event triggers an influx of extracellular Ca^{2+} which in turn promotes the fusion of synaptic vesicles with the neurones plasma membrane, exposing luminal domains of synaptic vesicle proteins to the extracellular environment (Verderio et al., 2006). Specific luminal domains of synaptic vesicle proteins function as the co-receptors for BoNT. When BoNT binds to these co-receptors, it is endocytosed into recycling synaptic vesicles (Montecucco, 1986; Zimmermann et al., 1993). Protein receptors were found to be key to the BoNT mechanism of action following the discovery that treatment of cells with a protease to deplete protein surface receptors protected cells from BoNT action (Nishiki et al., 1994). The first synaptic vesicle associated protein receptor determined to be essential to the neuronal uptake of BoNT molecules (specifically $BoNT_B$) was synaptotagmin (Syt) (Nishiki et al., 1996). BoNT serotypes which share close sequence homology within the H_C domain recognise the same protein receptors, in summary: $BoNT_B$ was found to adopt a dual receptor binding complex with synaptotagmin II and GT1b; $BoNT_G$ was found to require binding to synaptotagmin I or II; and it was found that serotypes A, E and F utilise synaptic vesicle protein 2 (SV2) proteins as receptors (Benson et al., 2011; Montal, 2010; Peng et al., 2012; Schmitt et al., 2010). The H_C domain of $BoNT_D$ has been shown to have affinity for the SV2 receptor, however the role of this interaction in the

mode of action of $BoNT_D$ is not clear (Kroken et al., 2011). There is no known protein receptor for $BoNT_C$. A crystal structure demonstrating that the H_C domain of $BoNT_B$ is capable of binding Synaptotagmin and GD1a at the same time, has recently been released supporting a dual receptor binding model (Berntsson et al., 2013).

The architecture of the H_C domain of BoNT is a well conserved structure throughout all seven serotypes (see Figure 1-6). It is composed of two subdomains, N-terminal (H_{CN}) and C-terminal (H_{CC}), which are connected by a short helix (Swaminathan, 2011). The crystal structure of BoNT serotypes A and B bound to GT1b and synaptotagmin respectively have provided evidence that the H_{CC} subdomain is responsible for binding both ganglioside and proteinous receptors (Chai et al., 2006; Jin et al., 2006; Stenmark et al., 2008). The two sites on the H_{CC} domain include a hydrophobic cavity containing a conserved lactose binding motif (H...SXWY...G) separated by a single loop from the protein binding region, which contains a hydrophobic pocket within two β-strands (part of a β-trefoil fold). Following the elucidation of a crystal structure showing both Syt and GD1a bound to $BoNT_B$ it has been confirmed that the two respective binding sites do not overlap (Berntsson et al., 2013).

Although the crystal structures of seven serotypes (A-G) of BoNTs H_C domain have been solved, the function of the H_{CN} subdomain has still not yet been elucidated. The H_{CN} domain adopts a conserved jelly-roll fold typical of lectins and other proteins involved in sugar binding and protein interactions. Recent studies have shown its interaction with sphingomyelin-enriched membrane micro-domains (Muraro et al., 2009), molecules involved in vesicular trafficking (e.g. phosphatidyinositol phosphates (PIPs)) and potential binding with PIP binding protein, known to promote diphtheria toxin pore formation (Donovan et al., 1982). However, if PIP does play a role in BoNT internalisation and translocation it is not yet known.

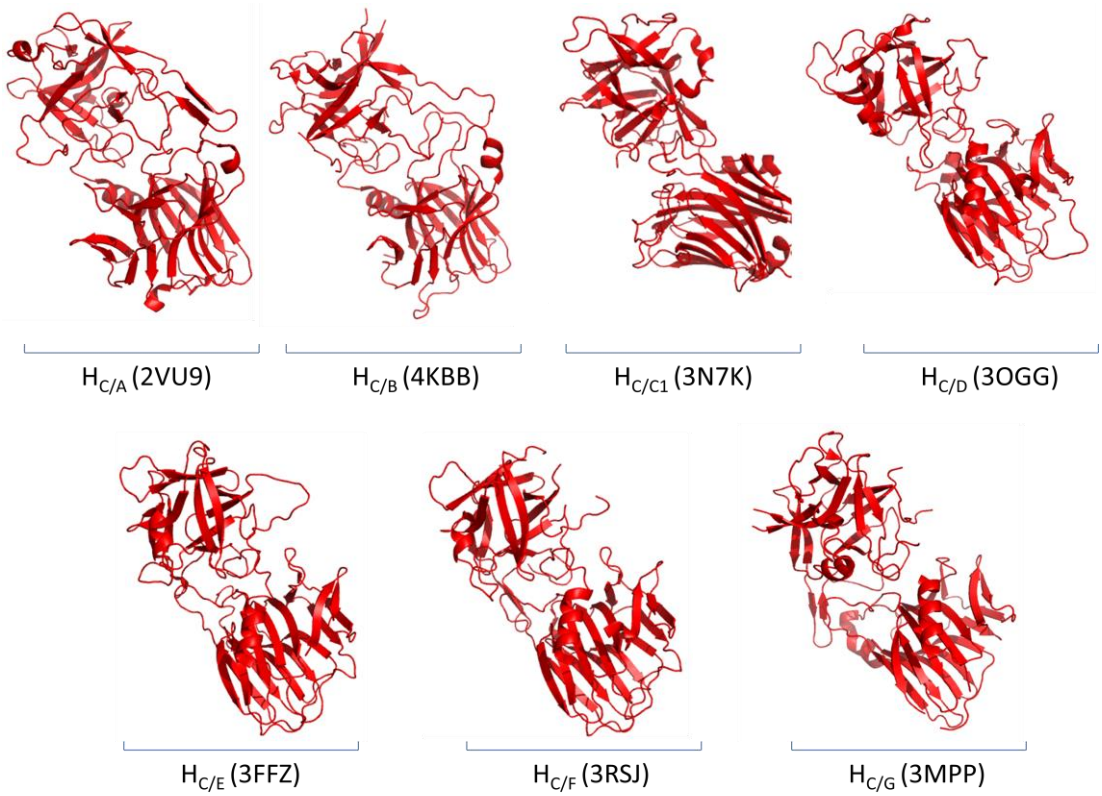

Figure 1-6 The BoNT H_C domain
The crystal structures of all seven serotypes of the BoNT H_C domain are displayed with PDB codes. (Benson et al., 2011; Berntsson et al., 2013; Karalewitz et al., 2010; Kumaran et al., 2009; Schmitt et al., 2010; Stenmark et al., 2008; Zhang et al., 2010)

1.5.2 Pore formation and light chain translocation

1.5.2.1 *BoNT is endocytosed inside synaptic vesicles*

Once BoNT molecules are bound to the pre-synaptic membrane of motor neurones, they are endocytosed into synaptic vesicles (see Receptor binding). The evidence for this process is substantial including confirmation by immuno-electron microscopy of BoNT in synaptic vesicles (Colasante et al., 2013) and the inhibition of BoNT action following the proteolysis of BoNT protein receptors known to be recycled within the lumen of synaptic vesicles (Nishiki et al., 1994). Following endocytosis, the BoNT molecule is still contained within a synaptic vesicle, in order to reach the cell cytosol, BoNT must transfer its catalytic LC domain from the synaptic vesicle, through the vesicle membrane and into the cell

cytosol (Montal, 2010). This process is undoubtedly the least understood mechanism of BoNT action.

1.5.2.2 *Synaptic vesicles are acidified*

Once inside synaptic vesicles, BoNT molecules are exposed to the conditions imposed by synaptic vesicle recycling, including the acidic environment induced by endosomal proton pumps (H^+-ATPase's) (Zimmermann et al., 1993). Inhibition of these protein pumps (by bafilomycin) blocks BoNT activity in mouse phrenic nerve-hemidiaphragm preparations, confirming that the translocation of BoNT's LC domain into the cell cytosol is dependent on exposure of BoNT to an acidic environment (Simpson et al., 1994).

1.5.2.3 *The LC domain of BoNT unfolds under acidic conditions*

Published crystal structures identify the BoNT light chain to be a large globular protein approximately 5.5 x 5.5 x 6.2nm in size (Lacy et al., 1998). Due to its large size some degree of unfolding is considered to be necessary to facilitate the LC domains translocation into the cell cytosol. Indeed, increasing the size of the LC domain and making it more resistant to unfolding conditions using anti-LC monoclonal antibody fab fragments was found to arrest translocation through excised Neuro 2A membrane fragments (Fischer and Montal, 2007b). Furthermore, spectroscopic analysis showed structural changes in the LC domain of $BoNT_A$ at pH values similar to those found in synaptic vesicles (Koriazova and Montal, 2003) and analysis of lipophilic dye binding to solvent exposed hydrophobic patches supported the unfolding of the LC domain at acidic pH (Cai et al., 2006). Conflicting results have been obtained when using circular dichroism to measure the degree to which the fold of the LC domain changes under acidic conditions (Koriazova and Montal, 2003; Li and Singh, 2000), this difference of opinion has not been settled, however the crystal structure of the LC domain of $BoNT_B$ does not appear to be altered for that resolved at near neutral pH compared to acidic pH (Eswaramoorthy et al., 2004).

1.5.2.4 *The H_N domain of BoNT forms a pore in the synaptic vesicle membrane*

There is relatively little structural information known regarding the H_N domain of BoNT proteins. However, the crystal structures of holotoxin BoNT serotypes A, B and E have been solved providing evidence of a long thin domain consisting of antiparallel and amphipathic α-helices (approximately 100Å in length) that form a coiled coil. A shorter α-helix structure packs in parallel on both sides of the larger helices and a large relatively unstructured "belt region" forms a loop which wraps around the LC domain either covering or near to the catalytic pocket ($BoNT_A$ and $BoNT_B$ respectively) (Kumaran et al., 2009; Lacy et al., 1998; Swaminathan and Eswaramoorthy, 2000). The H_N domains of BoNT serotypes C, D, F, G and the newly discovered serotype H are the only BoNT domains not to have been solved by X-ray crystallography (excluding subserotypes).

Acidification of the synaptic vesicle not only causes a structural change in the LC domain but simultaneously triggers the insertion of the translocation domain (H_N) into the synaptic vesicle membrane (Brunger et al., 2007; Galloux et al., 2008; Lai et al., 2010; Shone et al., 1987). The protonation of charged groups on the surface of the H_N domain (and on the H_N domain belt region) reduces the molecules electrostatic repulsion from lipophilic environments and consequently facilitated H_N domain interaction with the phospholipid membrane. This observation is supported by an increase in H_N domain interaction with synthetic lipid vesicles following a decrease in NaCl concentration under acidic conditions (Lai et al., 2010).

The mechanism by which a pore is formed by the H_N domain is still elusive. Whether or not BoNT forms a multimeric channel is debated by researchers in the field. The argument for oligomeric pore formation is compelling; evidence for oligomeric pore formation includes (1) a low resolution electron micrograph of the interaction of $BoNT_B$ with synthetic vesicle membranes showed evidence for a tetrameric "doughnut shaped" channel (Schmid et al., 1993) and (2) the GT1b mediated interaction of $BoNT_B$ with lipid bilayers suggesting an oligomeric pore, seen using atomic force microscopy (Sun et al.,

2011). The argument against oligomeric pore formation centres around immune-electron microscopic observations that only one molecule of BoNT (maximum two) is endocytosed per synaptic vesicle; this conclusion is based on counting the number of immune-labelled BoNT molecules detected within synaptic vesicles (Pirazzini et al., 2011).

Further evidence that the H_N domain of BoNT forms a pore was provided by the electrophysiological analysis of the interaction between holotoxin BoNT molecules and BoNT derivatives with cellular membranes. These studies monitor pores formed in excised segments of either Neuro 2A or PC12 cellular membranes through measuring the electrical current between the side of the membrane exposed to BoNT (called the cis side) and the side of the membrane not exposed to BoNT (called the trans side). Through these experiments it was determined that conditions at the cis side of the excised membrane must be acidic and oxidising, whereas conditions at the trans side must be neutral and reducing for BoNT pore formation to occur (Fischer and Montal, 2006; Koriazova and Montal, 2003). Concurrently, the need for acidic pH to trigger BoNT pore formation has also been determined in artificial membranes by measuring the leakage of fluorescent or charged molecules from within large unilamellar vesicles (LUV's) (Hoch et al., 1985; Shone et al., 1987). Evidence that the H_N domain of BoNT may form pores in both cellular and synthetic membranes without either the H_C or LC domains respectively, has been collected using both electrophysiological and vesicle leakage techniques (Fischer and Montal, 2007b; Galloux et al., 2008; Lai et al., 2010).

The diameter of the H_N pore has been estimated by electrophysiological methods and by measuring the escape of various differently sized fluorescent labelled molecules from inside lipid vesicles (Fu et al., 2002; Koriazova and Montal, 2003; Shone et al., 1987). The results of these investigations have determined the diameter of the pore to be between 1.5nm and 2.4nm. This variation in size may be evidence that the H_N pore is a highly dynamic structure and alternates between open and closed conformational states.

1.5.2.5 *The LC domain of BoNT translocates into the synaptic cell cytosol*

The purpose of the pore formed by the H_N domain is to facilitate the translocation of the LC domain from the interior of a recycling synaptic vesicle into the cell cytosol (Montal, 2010). If the LC domain is replaced by an alternative (non-light chain) cargo protein, translocation does not occur suggesting that an ordered and specific set of interactions between the heavy chain and LC domain are required in order to facilitate LC movement (Goodnough et al., 2002).

The electrophysiological investigation of BoNT pore formation (see section 1.5.2.4) reported a series of blocked and unblocked pore states which have been interpreted as showing progression of the LC domain through the individual stages of translocation (Figure 1-7). Firstly the pore appears blocked demonstrating a low conductance (approximately 13 pS) followed by a series of intermediate stages thought to be the partial occlusion of the pore by the LC domain (24, 47 and 55pS), before finally the conductance stabilizes at a higher conductance (approximately 67pS) determined to be a unblocked pore state (Fischer and Montal, 2007b). Direct evidence that this electrophysiological method reports the translocation of the light chain domain, comes from observations that SNARE protein substrates added to the trans compartment are only proteolysed in experiments where all the electrophysiological stages are observed (Fischer et al., 2008b; Koriazova and Montal, 2003).

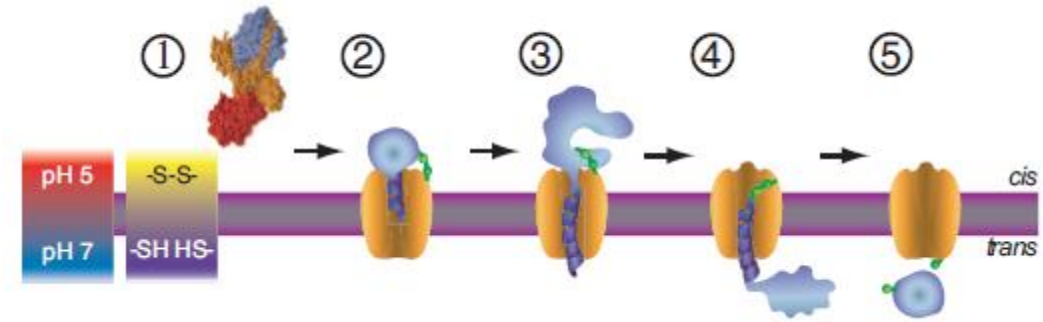

Figure 1-7 Sequence of events underlying BoNT LC translocation through the HC channel. Step 1, Crystal structure of BoNT/A holotoxin before insertion in the membrane. Then is shown a schematic representation of the membrane inserted BoNT/A during an entry event (step 2), a series of transfer steps (steps 3 and 4), and an exit event (step 5). (reproduced from (Fischer and Montal, 2007b)).

An elegant series of studies identified that channel formation and LC domain translocation rely on three gradients between the cis and trans side of excised Neuro 2A cells: a pH gradient, a redox gradient and the transmembrane potential. If any of these gradients becomes disrupted LC translocation will not occur.

As has already been discussed, an acidic pH is required for LC domain unfolding and H_N domain insertion into membranes; however, if a pH is not near neutral at the trans side of the membrane LC translocation will not occur. For example removal of the pH gradient prevented the heavy chain of $BoNT_B$ from forming conducting channels at acidic but symmetrical pH, upon neutralization of the trans compartment an acidic gradient was created restoring channel activity within 30 seconds (Hoch et al., 1985).

Similarly, a redox gradient is required (oxidizing cis and reducing trans) to facilitate LC domain translocation. The cis side of the membrane must be kept under reducing conditions otherwise the disulphide bond connecting the H_N and LC domains will be reduced and only open pore formations will be observed. Concurrently, a reducing environment is needed at the trans side of the membrane to reduce the disulphide bond post translocation so that the LC domain may leave the pore formation assembly. (Koriazova and Montal, 2003). There is experimental evidence that the NADPH-thioredoxin reductase-thioredoxin system is responsible for reducing the BoNT disulphide bond in a cellular system (Pirazzini et al., 2013).

Once inside the cytoplasm the LC domain must refold in order to restore its enzymatic protease activity. This process is thought to prevent any reverse translocation which is shown in patch clamp assays as a permanent blocked pore (Koriazova and Montal, 2003). It is not fully understood whether the refolding of the LC domain is spontaneous and unregulated but it has been hypothesized that the H_N domain belt region may assist in this process (Fischer et al., 2008b).

1.5.3 LC domain SNARE cleavage prevents neurotransmission

Once the LC domain of BoNT has refolded in the physiological conditions of the cell cytoplasm it is free to locate SNARE protein substrates. SNARE proteins are core components of the vesicle membrane fusion apparatus and as such facilitate the interaction between vesicles containing molecules to be exocytosed and the cellular membrane. There disruption therefore is instrumental in preventing the release of acetylcholine into the synaptic cleft of motor neurones, resulting in flaccid muscular paralysis (Montal, 2010).

SNARE substrates are found at multiple locations; SNAP-25 and Syntaxin are attached to the plasma membrane and synaptobrevin (also called VAMP) is attached to vesicular membranes (Südhof and Rothman, 2009). Each BoNT serotype has developed ways of accessing their respective substrate targets; for example, the localisation of the LC domain of serotypes A and E have been studied using fluorescent fusion proteins which show their localisation to the plasma membrane (LC_A) and the cell cytoplasm (LC_E) respectively (Fernandez-Salas et al., 2004).

The crystal structures of all seven serotypes of the BoNT LC domain have been solved providing evidence of a zinc protease domain which has similarities to thermolysin (Agarwal et al., 2005; Agarwal et al., 2009; Arndt et al., 2006; Arndt et al., 2005; Jin et al., 2007; Segelke et al., 2004). The LC structure is constituted of a mixture of α-helicies and β-strands and much like the H_C domain displays a similar structure throughout all seven serotypes with an approximate sequence identity of 35%. Conserved residues which make up a tetrahedral co-ordination, characteristic of a HEXXH zinc binding motif, have been determined through mutation studies to be essential to the domains function (Binz et al., 2002). Inactivation of BoNT's SNARE catalysis through the select mutation of LC domain residues produces a non-toxic form of BoNT (also known as endonegative BoNT).

Each serotype of LC domain acts as a remarkably specific protease which shows specificity for a single peptide bond at a single SNARE proteins (with the exception of serotype C_1 which is known to cleave both SNAP-25 and Syntaxin) (Binz, 2013). BoNT serotypes B, D, G and F proteolyse VAMP/Synaptobrevin-2 at separate peptide bonds identified in Figure 1-8; BoNT serotypes A, C and E proteolyses SNAP-25 at peptide bonds

identified in Figure 1-8; and BoNT serotype C has the capability to cleave two types of SNARE protein, namely, SNAP-25 and Syntaxin 1A (Binz, 2013).

It is known that exocytosis is a common process that occurs in most eukaryotic cell types. It is used for processes as diverse as membrane expansion during cell growth and the release of neurotransmitters from neurones (Darios and Davletov, 2006). This process, similar to cholinergic nerve terminal exocytosis, is regulated by SNARE proteins which form a complex essential for the docking and fusion of synaptic vesicles with the plasma membrane.

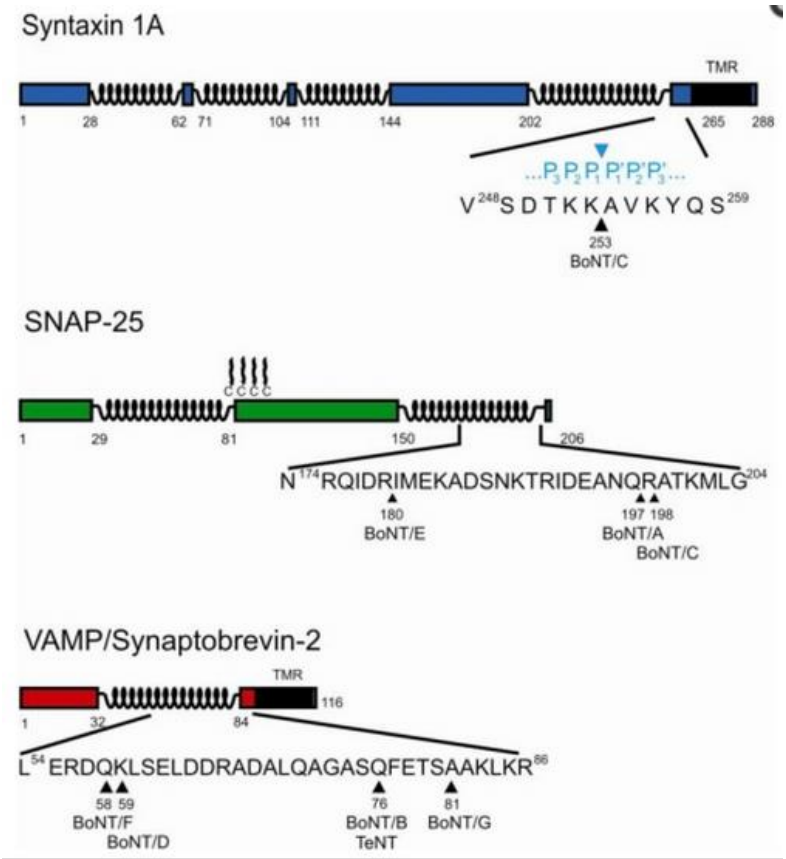

Figure 1-8 Schematic drawing of the substrate recognition sites for BoNT LC serotypes A-G
The SNARE proteins known to be proteolysed by the Zn^{2+} dependent catalytic ability of BoNT are identified above. The position at which BoNT serotypes A-G cleave SNARE proteins has been labeled (reproduced from (Foster et al., 2006)).

1.5.4 Composition of the synaptic vesicle

As discussed, the endocytosis and translocation of BoNT relies on the toxins interaction with eukaryotic membranes. Consequently, to understand this interaction requires analysis of the composition of these membranes and specifically the endocytotic compartment (or synaptic vesicle, SV).

In 2006, the purification and analysis of rat brain synaptic vesicles provided the first detailed picture of SV composition and physical characteristics by identifying and quantifying their proteinaceous and phospholipid components. Proteomic analysis identified 410 different proteins, of which, more than 80 were identified as integral membrane proteins. Quantitative western blot and dot blot analysis of a select few of these proteins identified a high proportion of previously known SV associated proteins, including, synaptophysin, synaptobrevin 2, syntaxin1, SNAP 25 and synaptotagmin 1 (~10%,~8.6%,~2%,~0.4% and ~7% of total SV proteins respectively). The lipid composition of SVs was measured via electrospray ionization (ESI) coupled with collision-induced dissociation (CID) and mass spectrometry to contain a high cholesterol content, a low concentration of phosphatidylinositol and a high proportion of phosphatidylethanolamine (see Table 1-2) (Takamori et al., 2006).

Quantitative analysis of the physical parameters of rat brain SVs determined the average proportions of protein, phospholipids and cholesterol per vesicle to be (17.1 ± 0.19) x 10^{-18}, 8.8 x 10^{-18} and 3.7 x 10^{-18} g/vesicle respectively, resulting in a total predicted dry mass of 29.6 x 10^{-18} g/vesicle. Further inspection of rat brain SVs using cryo-electron microscopy determined the average diameter of a vesicle to be ~40-45nm. Using this quantitative analysis of SV components and physical parameters, a molecular model was constructed using structurally defined membrane proteins. This model suggests a high density of membrane proteins on the surface of SVs (Figure 1-9) (Takamori et al., 2006).

Membrane Lipids	ng lipid/µg protein
Phosphatidylcholine	186 ± 37
Phosphatidylethanolamine	
1- Ester	120 ± 18
1- ester (plasmalogen)	96 ± 14
Phosphatidylserine	68 ± 7.2
Phosphatidylinositol	9.73 ± 10
Sphingomyelin	37 ± 5.1
Cholesterol	215 ± 25
Hexylceramide	8.6 ± 4
Ceramide	1.2 ± 0.1
Protein : Phospholipid (w/w)	1.94 ± 0.23

Table 1-2 Quantitative measurement of rat synaptic vesicle lipids via electrospray ionization coupled with collision-induced dissociation (CID) and mass spectrometry. (Takamori et al., 2006)

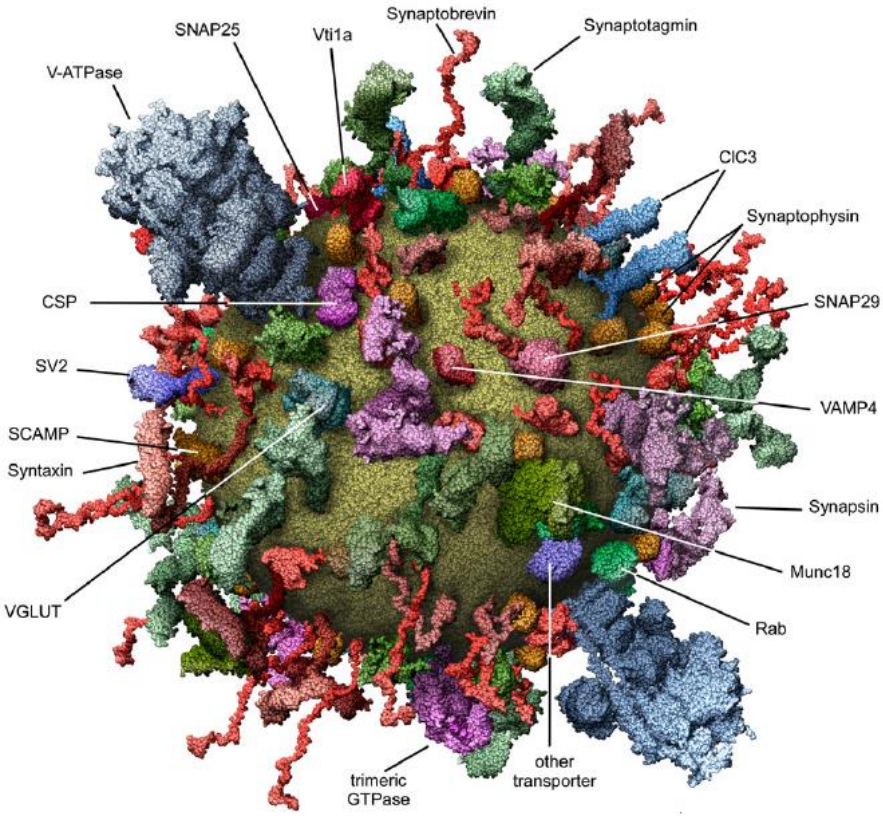

Figure 1-9 Molecular model of an average rat Brain SV based
Reproduced from (Takamori et al., 2006)

1.5.5 Retargeting botulinum neurotoxin (targeted secretion inhibitors)

In 1985, trypsin was used to separate the receptor binding domain (H_C) of $BoNT_A$ from the holotoxin molecule, thus leaving a seemingly stable protein composed of the light chain domain (LC) and translocation domain (H_N) (Shone et al., 1985). This combination of the LC and H_N domains was termed LH_N. The LH_N molecule was "activated" by cleaving a protease bond between the H_N and LC domains using exoprotease to mimic host protease activation (Shone et al., 1985). LH_N serotype A (LH_A) was further determined to retain its catalytic activity and its ability to form pores under acidic conditions demonstrated though a vesicle leakage assay (Shone et al., 1987). However, removing the H_C domain removed the inherent toxicity of the BoNT molecule by taking away its protein specific binding mechanism with cholinergic nerve terminals (Chaddock et al., 2002).

The recombinant production of LH_N has since been further optimised leading to the expression and isolation of LH_N serotypes A, B, C and D respectively. These constructs were codon optimised for recombinant expression in *E.coli* and included an affinity tag to aid in their purification (e.g. Maltose Binding Protein (MBP) or Histidine Tag). A specific activation site was added between the LC and H_N domains to allow activation by specific proteases and thereby minimise non-specific enzyme digestion during production. LH_N molecules were found to be suitable for vaccine preparation and for tools to investigate SNARE-mediated exocytosis (Fdez et al., 2008).

The three dimensional structures of LH_A and LH_B molecules have been defined through X-ray crystallography. Through comparison of LH_A and LH_B molecules with the three-dimensional structures of $BoNT_A$ and $BoNT_B$ respectively, it has been determined that the removal of the H_C domain does not significantly affect the structure of either the H_N or LC domains (Masuyer et al., 2011; Masuyer et al., 2009).

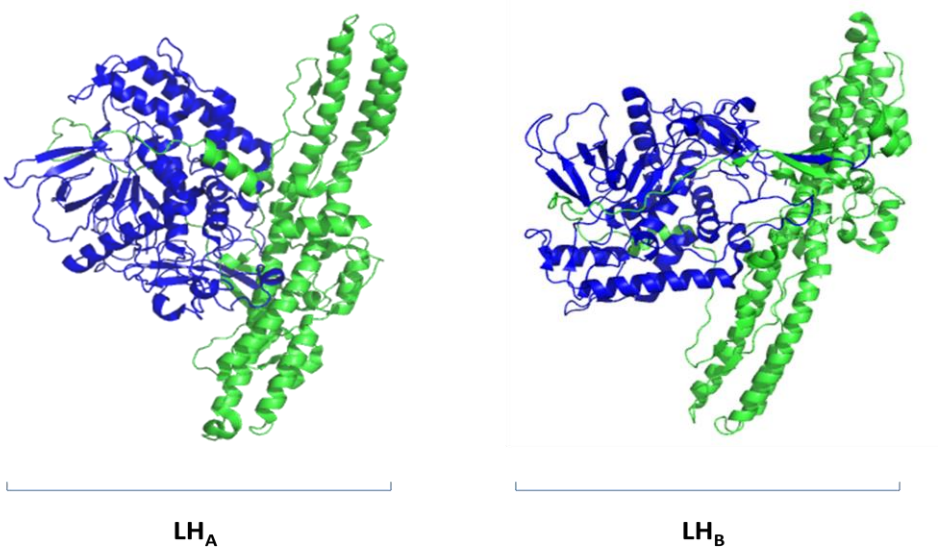

Figure 1-10 The crystallographic structures of LH_A and LH_B proteins
The crystallographic structures of LH_A and LH_B demonstrate that the H_N and LC domains of $BoNT_A$ and $BoNT_B$ are stable in the absence of the H_C domain. (Masuyer et al., 2011; Masuyer et al., 2009)

Following removal of BoNTs specificity for the cholinergic nerve terminal, the concept of targeting the catalytic action of BoNT molecules to various cell types was investigated. The principle of retargeting BoNT derivatives has been demonstrated in four studies in which LH_N serotypes A, C and D have been successfully targeted towards both neuronal and non-neuronal cell types.

When LH_A was chemically conjugated to nerve growth factor (NGF) or wheat germ agglutinin (WGA), it was shown to inhibit the release of noradrenaline in neuronal cells and insulin secretion in a pancreatic cell lines respectively, through the cleavage of intracellular SNAP-25 protein. This demonstrates the ability of LH_N molecules to bind with, translocate into and have catalytic effect in both neuronal and non-neuronal cell lines (Chaddock et al., 2000b).

The first in-vivo demonstration of targeted LH_N action was seen following its chemical conjugation with a lectin from *Erythrina cristagalli* (ECL) which was shown to specifically bind to nociceptive afferent neurones (Duggan et al., 2002). This molecule was shown to have the ability to successfully inhibit the release of substance P in several models of pain. This was the first example of the specific targeting of LH_N to a particular cell type.

To target the action of LH_N toward non-neuronal cell lines, LH_C was expressed in conjugation with epidermal growth factor (EGF). This molecule was proven to inhibit the in-vitro release of mucin in human pulmonary epithelial cells, thus showing a therapeutic potential in the treatment of chronic obstructive pulmonary disease (Foster et al., 2006).

Most recently, the recombinant expression of LH_D with a growth hormone receptor hormone (GHRH) binding domain specifically inhibited the release of pituitary somatotroph growth hormone (GH) release though the intercellular cleavage of vesicle associated membrane proteins (VAMP) in-vitro and in-vivo. This presents further evidence of the potential of targeted secretion inhibitors (TSI) for targeting diseases caused by the hyper-secretion of hormones (Leggett et al., 2013)

1.5.6 Aims of the project

Botulinum neurotoxins inhibit neurotransmission at cholinergic nerve terminals through entering a neuromuscular junction and cleaving SNARE proteins (which are critical for exocytosis). Much is known regarding the specificity with which BoNT targets motor neurones and the mechanism by which they cleave SNARE proteins, however, only limited and sometimes conflicting information is available regarding how BoNT interact with cellular membranes. Here we investigate the interactions between recombinant, endopeptidase inactive BoNT proteins and catalytically active LH_N proteins, with cellular and artificial membranes to provide insight into the way in which BoNTs and their derivatives interact with membranes.

Firstly, an interaction between LH_N serotype D and CHO-K1 cells was investigated to detect whether LH_D proteins interact with membrane bound G-protein coupled receptors (GPCRs). This was completed both to assure that LH_D did not serendipitously interact with G-protein coupled receptors (GPCR's) and to further assess whether LH_D interacts with cellular membranes at physiological pH (section 3.1).

Secondly, to further investigate the serotype specific differences inherent in BoNT structure, LH_D was recombinantly expressed, purified and crystallised in an attempt to elucidate its novel three-dimensional structure via X-ray crystallography. Furthermore, novel purification procedures were developed to isolate the H_N domain of BoNT serotypes A, C and D so to further understand their physical properties (section 3.2).

Finally, to further investigate the method by which BoNT and LH_N proteins interact with phospholipid membranes, a 96 well vesicle leakage assay was designed and developed to quickly and efficiently provide evidence of the pore forming potential of BoNT and LH_N molecules. This was performed to uncover for the first time, differences in the pore forming potential of various BoNT and LH_N serotypes (section 3.3, 3.4 and 3.5).

2 Methods

2.1 Chemicals and reagents

All chemicals and reagents were purchased from Sigma-Aldrich unless otherwise stated.

2.2 DNA processing

2.2.1 Agarose gel electrophoresis

1% agarose gels were prepared by dissolving 1g agarose powder (Quiagen) in 100ml's of TAE buffer (40mM Tris Acetate, 1mM EDTA, pH8) whilst heating. The agarose solution was poured onto a gel mould and left to cool and set. 50µl DNA samples were prepared with SYBR safe stain (Invitrogen) prior to loading into the agarose gel (15µl's per well). NEB DNA ladders were used as molecular weight markers (1kbp or 100bp). Electrophoresis was carried out in TAE buffer using a Bio-Rad gel tank at 150 Volts. The DNA bands were analysed under UV light (InGenious, Syngene).

2.2.2 DNA plasmid isolation

Microbank beads coated with Top 10 cells pre-transformed with recombinant DNA by Syntaxin Ltd, were placed in 10ml modified Terrific Broth (mTB, #T0918) with an appropriate antibiotic and grown overnight at 37°C in a shaking incubator (200rpm). The cells were harvested via centrifugation and the DNA isolated using a Wizard® plus SV miniprep system (Promega) as per the manufacturer's instructions.

2.2.3 Restriction endonuclease digestion

Specific recognition sites were identified in the DNA sequence using SeqBuilder® (DNASTAR), the restriction sites were then cleaved using restriction enzymes from NEB with NEB digestion buffers according to the manufacturers protocols.

Digestions were either completed as sequential digestions or double digestions; sequential digestions were completed using two individual (single) digestions separated by a DNA purification step (Wizard® plus SV DNA purification system (Promega) using the manufacturers protocol); double digestions were completed using one digestion step (two restriction sites cleaved) again following the manufacturers protocols. All digestions were completed over 3hrs at 37°C. The subsequent DNA fragments were purified using 1% agarose gel electrophoresis (section 2.2.1).

2.2.4 DNA ligation

DNA ligation was completed in a microcentrifuge tube placed on ice. A mixture of 2µl 10x T4 DNA Ligase Buffer, 50ng Vector DNA, 50ng Insert DNA and 1µl DNA ligase was pippetted into the microcentrifuge tube before making up the solution volume to 20µl using Nuclease-free water. The reaction was briefly mixed by gently pipetting up and down within the microcentrifuge tube. The reaction was then incubated at room temperature for 3 hours to allow ligation to occur before subsequent transformation into a 50µl's volume of competent cells.

2.2.5 Transformation

A 50µl vial of TOP 10 cells (NEB) was thawed from -80°C on ice before the addition of 5µl's ligations mixture (section 2.2.4), it was then gently mixed by flicking the vials base. Following mixing, the vial and its contents were incubated on ice for 20 minutes prior to placing in a water bath heated to 42°C for 45 seconds (heat shock) before it was transferred back to ice for 10 minutes (care was taken not to agitate the mixture so to not shear DNA being taken up by cells). 150µl of modified Terrific Broth (mTB, #T0918) was then added to the mixture before incubating at 37°C for 60 minutes in a shaking incubator (225rpm). The mixture was then plated out onto pre-prepared agar plates inoculated with 1ng/ml Kanamycin and left to dry for 30 minutes. Finally, the agar plates were placed in a 37°C incubator overnight and inspected for the growth of bacterial colonies the following day.

2.2.6 Sequencing

After transformation of ligations in TOP10 competent cells, three individual colonies were selected from the agar plate and transferred into three 50ml falcon tubes containing 10ml modified Terrific Broth (mTB) growth media. DNA plasmid isolation (section 2.2.2) was then used to produce sufficient quantities of plasmid DNA for sequencing.

Samples were sent for sequencing to Source BioScience (Oxford, UK). The results generated were examined using the SeqMan software (StarLabs).

2.3 Protein methods

2.3.1 SDS-PAGE and western blot analysis

Protein samples were mixed with LDS sample buffer (x4) (Life Technologies) and heated to 90°C for five minutes before centrifuging for 1 minute on a bench top centrifuge. NuPAGE 4-12 % bis-tris gels were loaded with samples and ran at 200 Volts for 55 minutes. Gels to be stained were washed with dH_2O and stained with warm Coomassive SafeStain for 30 minutes before de-staining by washing several times with dH_2O and finally leaving in dH_2O for up to an hour. Gels to be blotted were assembled in the transfer assembly and blotted at 0.4mA for 1 hour onto nitrocellulose membrane in methanol free blotting buffer (Pierce cat no.350400).

Nitrocellulose blots were blocked for 1 hour with 0.5% BSA in PBS-0.1% Tween 20 (PBS-T) before they were probed with in-house rabbit polyclonal antibody (5 µg/ml, 1:1000 dilution) in 0.5 % BSA/ PBS-T for 1 hour. The blots were washed with 3 changes of PBS-T over 15 minutes before incubating with secondary antibody at 1:1000 dilution in PBS-T for 1 hour. The blots were washed again and developed with SuperSignal DuraWest substrate as per the manufacturer's instructions. All incubations and washes were carried out at room temperature with gentle rocking. The developed blots were imaged using a Syngene Imaging Instrument as were the stained gels.

Gels used for SDS-PAGE analysis were loaded with 5µl of Benchmark ladder (NEB) in the left-hand lane and 10µl of protein sample/LDS sample buffer in subsequent wells. Gels used for western blott analysis were loaded with 3µl of Magicmark (NEB) in the left-hand lane and 15µl of protein sample/LDS sample buffer in subsequent wells.

2.3.2 Protein expression

100 ml of modified Terrific Broth (mTB) in a 250 ml plastic flask was supplemented with 0.2% glucosamine and 30µg/ml kanamycin before inoculating with one microbank bead coated with BL21 DE3 cells (from Syntaxin Ltd expression microbanks) and incubated at 37 °C, 225 rpm.

The next day, 10 ml of the overnight culture was used to inoculate 1L of modified TB containing 0.2% glucosamine, 30µg/ml Kanamycin and 20mL of 50mM Hepes, 500mM NaCl, pH7.2. An OD_{600} value of the overnight culture was determined by making 1:10 or 1:20 dilution in the appropriate media. After inoculation, the flasks were returned to the incubator and incubated at 37°C, until an OD_{600} of 0.5-0.6 was reached, at which point the incubator temperature was dropped to 16°C for 1 hour before inducing the cultures with 1mM IPTG. Again, the OD600nm value was determined by making 1:2 or 1:10 dilution in the appropriate media. The expression cultures were then incubated overnight for approximately 20 hours.

Prior to harvest OD_{600} values for each culture were determined by making a 1:20 dilution with the appropriate media. Cultures were then transferred to 1L pots and harvested by centrifugation at 5000rpm for 20 minutes (4°C). The supernatant was decanted and the cell pellets were resuspended in 20ml's of lysis buffer (see section 3.2.2). The cell pastes were then weighed and the wet cell weight was calculated before storing the cell pastes in 50mL centrifuge tubes at -80°C.

2.3.3 Cell homogenisation

The expression cell paste was removed from the -80°C freezer and thawed by incubating the tubes in a beaker of cold water before being re-suspended in 60-70ml of lysis buffer. After re-suspension the sample was incubated for 1 hour under stirring in a cold room (2-8°C). When the cell paste was completely re-suspended, cells were homogenized at 20kPsi with a single pass through a Constant Systems homogenizer, previously washed using 0.1M NaOH then dH_2O before equilibriating with the determined lysis buffer. After homogenization the cell debris was removed by centrifugation. The samples were spun at 13,500 rpm for 60 minutes at 4°. Supernatant finally filtered using a 0.45µm syringe filter.

3 Results

3.1 LH_D causes an increase in CHO-K1 cell intracellular Ca^{2+}

3.1.1 Introduction

3.1.1.1 *LH_N proteins inhibit cellular secretion*

The intoxication of Botulinum neurotoxin (BoNT) (serotypes A-H) is thought to occur in three distinct phases: a receptor binding phase, an internalization phase and a catalytic phase, ultimately causing the inhibition of presynaptic neurotransmitter release. The structure of all BoNT serotypes is thought to conform to a tri-modular architecture which facilitates these three stages using three domains: the receptor binding domain (H_C), translocation domain (H_N) and catalytic domain (LC) (Turton et al., 2002). Removing the H_C domain of BoNTs, either by proteolytic cleavage or cloning and expression, produces LH_N molecules (Chaddock et al., 2004). LH_N molecules possess the translocation and catalytic ability of BoNT molecules without possessing their potential to specifically bind to the pre-synaptic terminal of motor neurons (Chaddock et al., 2004). By adding a new specifically designed targeting domain to the LH_N protein it is possible to target their effect to non-neuronal and neuronal cells of potential therapeutic interest (Chaddock et al., 2004; Chaddock et al., 2000a; Chaddock et al., 2000b; Leggett et al., 2013).

The targeting and effect of LH_N molecules has been demonstrated in four studies. In the first study, Nerve Growth Factor targeted LH_A (NGF-LH_A) was targeted to nerve growth factor receptors causing SNAP-25 cleavage and consequently inhibiting the release of noradrenalin from neuronal cells (Chaddock et al., 2000a). In the second study, Wheat Germ Agglutinin lectin receptor targeted LH_A (WGA-LH_A) was targeted to wheat germ agglutinin lectin receptors inhibiting neurotransmission from several neuronal cell types and insulin secretion from a pancreatic cell line (Chaddock et al., 2000b). In the third study, LH_A was chemically conjugated with a lectin from *Erythrina cristagalli* to target primary nociceptive afferents and inhibit the release of neurotransmitters, glutamate and substance P with a duration of action similar to that of its holotoxin equivalent. This study confirmed

the efficacy of targeted LH_N proteins in-vivo. (Chaddock et al., 2004). Finally, LH_D recombinantly expressed with a Growth Hormone Receptor Hormone (GHRH) binding domain successfully inhibited the release of pituitary somatotroph growth hormone (GH) in-vitro and in-vivo (Leggett et al., 2013).

3.1.1.2 *Bradykinin B1 receptor targeting*

Kinins are a group of biologically active peptides that exert a number of physiological effects, including vasodilatation, smooth muscle contraction, inflammation and pain induction. The physiological effects of Kinin molecules are mediated through the stimulation of bradykinin B1 and B2 G-protein coupled receptors. B1 receptors have been shown to have a low level of expression which is up-regulated in the presence of cytokines and endotoxins or during tissue injury. The B1 receptor participates in chronic inflammation and pain and has been identified as a potential drug target for the treatment of those conditions (Wu et al., 2012). In vivo studies indicate that B1 receptor antagonists can reverse streptozotocin-induced chronic pain in rate models of diabetes (Dias et al., 2007).

Agonist stimulation of the bradykinin B1 receptor results in the receptor mediated stimulation of phospholipase C and hydrolysis of phosphatidylinositol bisphosphate, leading to the formation of the two second messengers, namely, $Ins(1,4,5)P_3$ and diacylglycerol. $Ins(1,4,5)P_3$ interacts with a receptor on the endoplasmic/sarcoplasmic reticulum that functions as a Ca^{2+} release channel which serves to increase cytosolic free Ca^{2+} ultimately stimulating inflammatory responses (Mathis et al., 1996).

Des-Arg^9-BK is a kinin metabolite which selectively activates Bradykinin B1 receptors. By assessing Des-Arg^9-BK potency it is possible to determine stability in the recombinant expression of the Bradykinin B1 receptor and lack of Bradykinin B2 receptor expression on select cell types (Leeb-Lundberg et al., 2005).

3.1.1.3 *Investigation of LH_D effects on Bradykinin B1 receptors*

Experiments were conducted by Syntaxin Ltd aimed at targeting LH_N towards the Bradykinin B1 receptor so to prospectively inhibit cellular secretion at sites of inflammation and pain. To confirm that a targeting domain is necessary for LH_N proteins to bind to the Bradykinin B1 receptor, LH_N molecules (serotypes A-D) with no targeting domain were assessed for their ability to stimulate intracellular Ca^{2+} release in cells engineered to stably express the Bradykinin B1 receptor. Experiments completed by Syntaxin Ltd demonstrated that LH_D stimulated an unexpected increase in intracellular Ca^{2+} ion concentration in CHO-K1 cells which expressed the recombinant Bradykinin B1 receptor.

Here we investigate the interaction of LH_N serotype D (LH_D) with recombinant Bradykinin B1 receptors expressed on CHO-K1 cells. Through comparison of the interaction of LH_D with CHO-K1 cells which do and do not express the Bradykinin B1 receptor respectively, we were able to determine that LH_D induced increases in intracellular Ca^{2+} were not related to activation of the Bradykinin B1 receptor.

3.1.2 Methods

3.1.2.1 *Culture of CHO-K1-B1 cells*

CHO-K1 cells with stable recombinant expression of the human Bradykinin B1 receptor (CHO-K1-B1 cells) were cultured in media (Ham's F12, 2mM glutamine, 10% FBS and 400µg/ml G418) at 37°C, 5% CO_2. Cells were passaged when they reached 80% confluency (every 3 to 5 days). The media was removed and the cells washed twice with PBS. Cells were harvested in PBS-based non-enzymatic cell dissociation buffer (37°C) for 2 minutes, pelleted by centrifugation (1,500rpm; 3 minutes), re-suspended in cell culture media and seeded into fresh T500 flasks.

3.1.2.2 *Ca^{2+} mobilisation assay*

The intracellular increase of cytosolic free Ca^{2+} was measured in-vitro using Ca^{2+} sensitive dye (FLIPR® Calcium Assay Kit) (Simpson et al., 2000). CHO-K1-B1 cells (20,000 cells.well^{-1}) were seeded into 96 well black walled/clear bottomed half area plates (costar) 16 hours prior to performing the assay. On the day of the assay, plates were incubated (37^{o}C; 5% CO_2) in HBSS modified assay buffer containing 0.5X Ca^{2+} sensitive dye and probenecid (2.5 mM). After 1 h, increasing concentrations of des-Arg^{9}-BK (3pM-3µM) or LH_D (10pM- 1µM, provided by Syntaxin Ltd) were added to the cells in triplicate rows by the FlexStation3® (height 70µl; speed 16µl.s^{-1}; 37^{o}C). Fluorescence was measured at 525nm measured over 60 seconds and recorded as RFU signal. Ca^{2+} mobilisation was quantified as % increase in baseline RFU (Equation 1).

3.1.2.3 *Data handling and statistical analysis*

All data have been analysed using Graph pad Prism 6.01 (San Diego, USA).

Raw Ca^{2+} fluorescence traces were converted into single numerical values of maximum minus minimum (RFU units) using Softmax Pro software. The minimum RFU point was subtracted from the peak RFU point during the 60 second total read time.

Data points were plotted on the y-axis as percentage increase in baseline RFU measurements using Equation 1. Baseline RFU was estimated from the first 20 seconds of reading (before addition of agonist or LH_D), this normalised the response measured in each well of the plate using the baseline value, thus correcting for any slight variation in cell density between wells.

$$\% \text{ Increase Baseline} = \frac{(\text{peak RFU} - \text{baseline RFU})}{\text{Baseline RFU}} \times 100 \qquad \textbf{(Equation 1)}$$

Potency of agonist was estimated by fitting RFU data (% increase in baseline) and logarithmic agonist concentration into a four parameter logistic equation (a modified Hill equation; Equation 2). The four parameters of this equation include minimum response (basal), maximum response (max or Emax), the concentration required to produce a response half way between the minimum and maximum response (EC^{50}) and the slope factor (Hill slope (nH)).

$$y = \text{basal} + \frac{(\text{max-basal})}{1+10(pEC^{50} - x)^{nH}} \qquad \textbf{(Equation 2)}$$

3.1.3 Results

3.1.3.1 *LH_D induces an increase in CHO-K1 intracellular calcium*

Des-Arg^9-Bradykinin (des-Arg^9-BK) binds to and activates the Bradykinin B1 receptor, this activation can be monitored through measuring an increase in intracellular Ca^{2+} using Ca^{2+} sensitive dye (Simpson et al., 2000). Consequently, by measuring the intracellular Ca^{2+} levels of cells, following their incubation with des-Arg^9-BK, it is possible to determine the presence or absence of the Bradykinin B1 receptor.

The increase in intracellular Ca^{2+} levels caused by the incubation of CHO-K1-B1 cells with des-Arg^9-BK (0.3pM to 0.3µM) demonstrated the presence and stable recombinant expression of the Bradykinin B1 receptor on CHO-K1-B1 cells (Figure 3-1, A). Specifically, des-Arg^9-BK induces a concentration dependent increase of intracellular Ca^{2+} in CHO-K1-B1 cells, demonstrating a pEC_{50} of 10.21 ± 0.10 standard error mean (s.e mean). A similar incubation of des-Arg^9-BK (0.3pM to 0.3µM) with wild type CHO-K1 cells (not transfected with the receptor) did not trigger an increase in intracellular Ca^{2+} demonstrating that the Bradykinin B1 receptor is not expressed on CHO-K1 cells.

It was found that incubating concentrations of 1, 0.33 and 0.1µM LH_D with CHO-K1-B1 cells caused a small but measurable increase in intracellular Ca^{2+} levels (Figure 3-1, B). In an effort to determine whether the increase in intracellular Ca^{2+} was due to LH_D activation of the Bradykinin B1 receptor, the same experiment was repeated using CHO-K1 cells; the incubation of CHO-K1 cells with 1, 0.33 and 0.1µM LH_D caused a similar increase in intracellular Ca^{2+} levels (Figure 3-1, D). Specifically, 1, 0.33 and 0.1µM LH_D caused increases of 46%, 28%, and 13.5% (CHO-K1-B1) and 66%, 30% and 13% (CHO-K1).

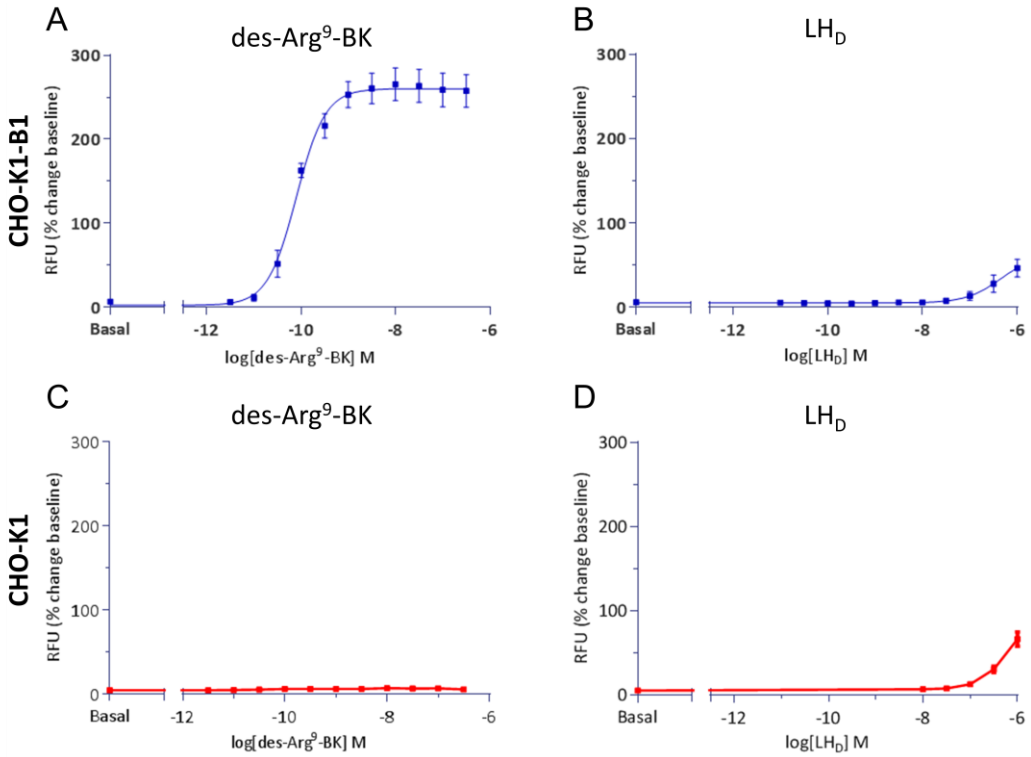

Figure 3-1 LH_D causes an increase in intracellular calcium levels in CHO-K1-B1 and CHO-K1 cells.
Through measuring intracellular Ca^{2+} levels the effect of des-Arg^9-BK and LH_D on CHO-K1-B1 and CHO-K1 cells is shown (A) Effect of des-Arg^9-Bradykinin (0.3µM- 0.3pM) on CHO-K1-B1 cells (pEC_{50} = 10.10 ± 0.06 s.e mean, nH = 1.41 ± 0.24 s.e mean) (B) Effect of LH_D (1µM-10pM) on CHO-K1-B1 cells (n=3). (C) Effect of des-Arg^9-Bradykinin (0.3µM- 0.3pM) on CHO-K1 cells (D) Effect of LH_D (1µM- 0.01µM) on CHO-K1 cells (n=3).

3.1.3.2 *Reducing extra-cellular Ca^{2+} levels inhibits LH_D induced intra-cellular Ca^{2+} increase*

Repeating experiments to determine the LH_D induced increase of intracellular Ca^{2+} at CHO-K1 and CHO-K1-B1 cells respectively (Figure 3-2, A) identified a similarity between the two responses. Specially, an LH_D concentration of 1µM induced a mean increase in intracellular Ca^{2+} of 64.4% and 63.7% in CHO-K1-B1 and CHO-K1 cells respectively.

In order to investigate whether extracellular Ca^{2+} concentration affects the increase in intracellular Ca^{2+} concentration caused by 1, 0.33 and 0.1µM LH_D, the experiment was repeated using two different formulations of extracellular buffer (with and without Ca^{2+}).

Removing extracellular Ca^{2+} decreased the potential of LH_D to increase intracellular Ca^{2+} levels in CHO-K1 cells, suggesting that LH_D facilitates an influx of extracellular Ca^{2+} to the intracellular compartment (Figure 3-2, B). When the concentration of extracellular $CaCl_2$ was decreased by 1.26mM, the intracellular Ca^{2+} fluorescence decreased from 37.5% to 12.2% (1µM LH_D).

Variability of LH_D induced increase in intracellular Ca^{2+} concentration for both CHO-K1 and CHO-K1-B1 cells respectively was evident throughout this study. Further investigation into LH_D induced increase in intracellular Ca^{2+} resulted in an inability to reproduce the response. For this reason the previous results identifying LH_D induced increase in intracellular Ca^{2+} could not be qualified as significant and the investigation was terminated.

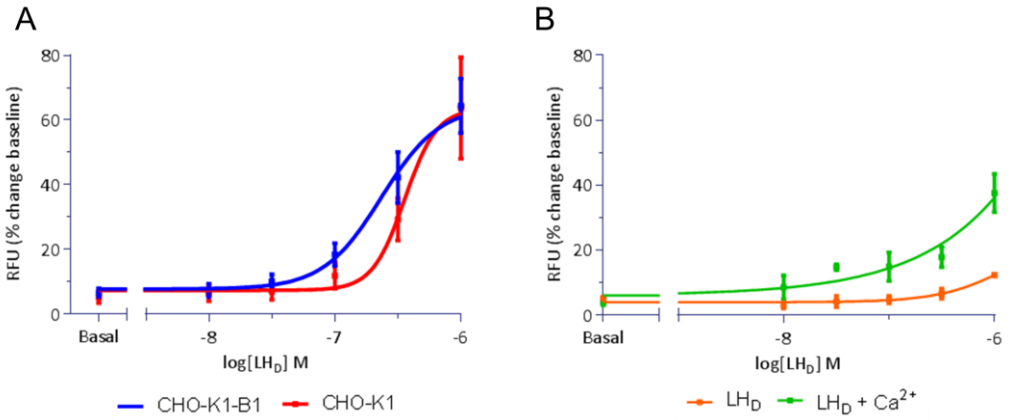

Figure 3-2 Reducing the concentration of extracellular Ca^{2+} inhibits LH_D induced increases in intracellular calcium.
Through measuring intracellular Ca^{2+} levels, the effect of LH_D on CHO-K1-B1 and CHO-K1 cells is determined with and without extracellular Ca^{2+} (A) A comparison of the effect of LH_D (1µM- 10pM) on CHO-K1-B1 and CHO-K1 cells (n=3). (B) The effect of removing extracellular Ca^{2+} on LH_D (1µM- 10pM) induced intracellular Ca^{2+} fluorescence.

3.1.4 Discussion

Removing the H_C domain of BoNT proteins, removes their specificity for the pre-synaptic terminal of neuromuscular synapses and consequently their natural toxicity. BoNT proteins without H_C domains are termed LH_N proteins; by fusing a ligand with affinity for specific cell surface protein receptors of a target cell, the SNARE cleavage potential of LH_N proteins has been targeted to specific cell types. (Chaddock et al., 2004; Chaddock et al., 2000a; Chaddock et al., 2000b). The activity of targeted LH_N molecules has lead to the development of a range of targeted secretion inhibitors (TSI's) by Syntaxin Ltd with an objective to develop therapeutic molecules. To qualify that LH_N proteins are targeted towards specific cell types, they should not bind serendipitously to cellular receptors. Any random binding of LH_N molecules to cellular receptors may suggest inherent toxicity in the molecule and cast doubts on to the molecules potential as a therapeutic.

Here we investigate LH_D induced increase in intracellular Ca^{2+} in CHO-K1 cells in an attempt to further understand how LH_D interacts with eukaryotic cells.

3.1.4.1 *Bradykinin B1 receptors are stably transfected onto CHO-K1 cells*

The Bradykinin B1 receptor was confirmed to be stably expressed on CHO-K1-B1 cells through detecting Bradykinin B1 receptor activation via a des-Arg^9-BK induced increase in intracellular Ca^{2+} (Mathis et al., 1996; Simpson et al., 2000). Similarly, the absence of the Bradykinin B1 receptor on CHO-K1 cells was determined through a lack of response to the des-Arg^9-BK agonist (Figure 3-1, C). By determining the presence and absence of the Bradykinin B1 receptor on CHO-K1-B1 and CHO-K1 cells respectively, whether or not a cellular response is directly attributable to Bradykinin B1 receptor activation can be assessed.

3.1.4.2 *LH_D facilitates an increase in CHO-K1 and CHO-K1-B1 cell intracellular Ca^{2+} levels*

CHO-K1 and CHO-K1-B1 cells demonstrate an increase in intracellular Ca^{2+} concentration in the presence of LH_D (Figure 3-1, B and D). This implies that LH_D either stimulates an increase in intracellular Ca^{2+} from an intracellular source, activates an endogenous receptor or Ca^{2+} channel on the cell surface, or uses its ability as a pore forming protein (Fischer and Montal, 2007b) to form ion channels in the cellular membrane through which extracellular Ca^{2+} may permeate.

Through determining that LH_D has a similar effect at both CHO-K1 and CHO-K1-B1 cells (Figure 3-1, A and Table 3-1), we can conclude that LH_D proteins are not causing an increase in intracellular Ca^{2+} by activating the Bradykinin B1 receptor.

Cell Type	Molecules	pEC^{50}	nH	Emax
CHO-K1-B1	Des-Arg^9-BK	10.01 ± 0.06	1.41 ± 0.24	257.5 ± 11.33
CHO-K1	Des-Arg^9-BK	n/a	n/a	n/a
CHO-K1-B1	LH_D	n/a	n/a	46.58
CHO-K1	LH_D	n/a	n/a	66.34

Table 3-1 Measured increase in CHO-K1 and CHO-K1-B1 cell intracellular Ca^{2+} following addition of Des-Arg^9-BK or LH_D
Through measuring intracellular Ca^{2+} levels, the effects of des-Arg^9-BK and LH_D on CHO-K1-B1 and CHO-K1 cells are shown. pEC^{50}, nH and Emax data presented for the agonist response of des-Arg^9-BK at CHO-K1-B1 cells is from curve fitting within GraphPad Prism; n = 3 experiments in all cases (pEC^{50}, nH and Emax values are shown within 95% confidence limits). Emax values presented for the effect of LH_D upon CHO-K1 and CHO-K1-B1 cells represent the mean maximum response measured for the respective interaction (n = 3).

Decreasing the concentration of extracellular Ca^{2+} effectively reduced the increase in intracellular Ca^{2+} levels induced by the interaction of LH_D with CHO-K1 cells (Figure 3-2, B). There are many possible explanations for this, which include: (1) the binding of LH_D to an unknown endogenous receptor is Ca^{2+} dependent, when bound this elicits a G-protein response and release of intracellular calcium stores; (2) LH_D induces an influx of extracellular Ca^{2+} through a mechanism ultimately causing the flow of Ca^{2+} ions through

Ca^{2+} channels; (3) LH_D interacts with CHO-K1 cells forming a pore through which extracellular Ca^{2+} enters the cell, causing an increase in intracellular Ca^{2+} levels (LH_Ns are pore forming proteins capable of forming pores through which conductance has been measured (Fischer et al., 2008b)).

If LH_D is capable of forming a pore in the membrane of CHO-K1 cells under near physiological conditions this would suggest that LH_D does not conform to the low pH induced pore forming model currently accepted for BoNT proteins. Concurrently, the endogenous expression of GPCR's in CHO-K1 cells is well established (Holdsworth et al., 2005); if LH_D is effecting the release of intracellular Ca^{2+} through activating an endogenous GPCR, it should be possible to determine a dose response effect through increasing the concentration of LH_D beyond 1µM.

Ultimately, the effect elicited by LH_D in CHO-K1 cells could not be isolated due to a lack of reproducibility. To determine whether LH_D does permeate cellular membranes further analysis would be required; analysis of LH_D membrane interaction through either vesicle leakage or patch clamp analysis may provide evidence of the proteins potential to permeate membranes at a physiological pH (Fischer et al., 2009; Lai et al., 2010).

3.1.5 Conclusion

LH_D has been assessed for its potential to cause an increase in CHO-K1 cell intracellular calcium in the absence and presence of the Bradykinin B1 receptor. These results suggest that the Bradykinin B1 receptor has no bearing on any effect of LH_D on Ca^{2+} influx into CHO-K1 cells.

The apparent LH_D induced increase in intracellular Ca^{2+} was small and poorly reproducible. Initially we were concerned that it might represent an off-target effect of LHD that could be problematic for development of therapeutic proteins incorporating that backbone. However the evidence presented in this chapter does not support that. If LH_D does have the potential to stimulate Ca^{2+} signalling or form pores in cellular membranes directly, then further analysis, through an assay known to have the capability to measure

pore formation (e.g. vesicle leakage or patch clamp assays) would be required to investigate it. Based on these results there is no strong evidence to suggest LHD is unsuitable as a backbone for new therapeutic proteins.

3.2 Purifying the derivatives of botulinum neurotoxins

3.2.1 Introduction

Following the discovery that Botulinum toxins (BoNTs) are the causative agents of Botulism, efforts have been made to isolate BoNTs from bacteria using recombinant technology to express the desired protein and purification techniques to extract it. Subsequent development of these techniques has not only facilitated the elucidation of the crystallographic structure of BoNT serotypes A, B and E, but has also allowed the investigation of BoNTs mechanism of action (MoA) and the industrial production of BoNT serotypes A and B as pharmaceutical products (Kumaran et al., 2009; Lacy et al., 1998; Swaminathan and Eswaramoorthy, 2000).

3.2.1.1 *Purification of singular botulinum toxin domains*

Following the elucidation of $BoNT_A$'s crystallographic structure, it was clear that it contained three separate domains, namely, the receptor binding domain (H_C), the translocation domain (H_N) and the catalytic domain or light chain (LC) (Figure 3-3) (Lacy et al., 1998); the tri-modular architecture of BoNT has subsequently also been seen in the crystallographic structures of BoNT serotypes B and E respectively (Kumaran et al., 2009; Swaminathan and Eswaramoorthy, 2000). Given that separate functions have been proposed for each BoNT domain, there is great intrinsic value in the expression and purification of isolated BoNT domains so that their physical properties and function may be studied in isolation.

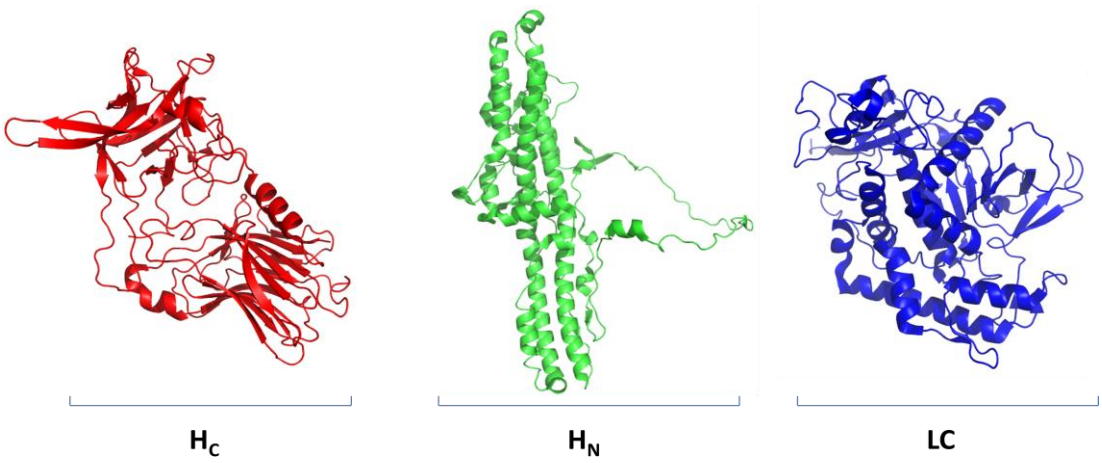

Figure 3-3 The three domains of Botulinum toxins
The receptor binding domain (H_C), translocation domain (H_N) and catalytic domain or light chain (LC) of Botulinum neurotoxin serotype B (Swaminathan and Eswaramoorthy, 2000).

Seven serotypes (A-G) of the H_C and LC domains of BoNT have been expressed, purified and crystallised in isolation. In contrast, the H_N domain for only one serotype has been expressed and purified in isolation (serotype A). Previous expression and purification of H_N domain (serotype A) has identified a hydrophobic protein which requires detergent to remain soluble before and during purification (Lai et al., 2010). When purified, the H_N domain has provided information as to how $BoNT_A$ may form pores in vesicle and cellular membranes (Fischer et al., 2012; Lai et al., 2010).

The crystallographic structures of BoNT serotypes A, B and E have revealed the three dimensional structure of the H_N domain; however, the crystallographic structures of H_N domain serotypes C, D, F, G and H are without structural solution. Through the expression, purification and crystallisation of the remaining H_N domain proteins, it may be possible to gain further insight into the least understood mechanism of BoNT action, namely, the way in which it forms a pore in synaptic vesicles at acidic pH (see Introduction 1.5.2.4).

3.2.1.2 *Purification and crystallization of LH_N proteins*

The expression and purification of recombinant LH_N proteins (serotypes A and B) has been completed to discover their functional properties and crystallographic structure

(Masuyer et al., 2011; Masuyer et al., 2009). This has demonstrated that LH_N proteins can be purified, are stable when crystallized and their domains show little structural variation in comparison to full length BoNT molecules. (Chaddock et al., 2004). Given the successful expression and purification of recombinant LH_N molecules and their inherent lack of toxicity, LH_N proteins may be a promising and convenient way of solving unknown H_N domain structures via X-ray crystallography.

3.2.1.3 *Aims*

Analysis of protein purification has for years provided a much needed insight into the physical properties of isolated proteins in solution. In this chapter we explore the purification of protein domains derived from various BoNT serotypes to assess their physical properties and to use these proteins in further studies (e.g. crystallisation trials and vesicle leakage assays).

The following molecules have been expressed and purified. (1) **LH_N serotype D (LH_D)**; LH_D has been expressed, purified and crystallised in an attempt to elucidate its three-dimensional structure via X-ray crystallography. (2) **H_N domain serotype D**; The LC and H_N domains of LH_D have been separated in order to further understand the interaction between these two domains and to isolate the H_N domain for further studies. (3) **H_N domain serotype A**; the H_N domain of BoNT serotype A has been cloned, expressed and purified to further understand its physical properties and for use in further experiments. (4) **H_N domain serotype C**; this is the first recorded cloning, expression and purification of the H_N domain of BoNT serotype C, this was completed to understand its physical properties and for its potential use in further experiments.

3.2.2 Materials and methods

3.2.2.1 *C and N-terminal His-tagged LH_D cloning and expression*

Synthetic genes were designed encoding LH_D with a C or N terminal 10x Histidine tag (His-tag); and with either Enterokinase (DDDK) or Factor Xa (IEGR) cleavage sites (separating the LC and H_N domains). These were cloned into a modified pMAL-c2x vector (NEB, UK) and transformed into E. coli BL21 cells by Syntaxin Ltd. Expression of these LH_D constructs was carried out by inoculating a 100ml volume of terrific broth complex medium containing 100µg/ml Kanamycin (mTB) with expression cells. Following a 12 hour incubation at 37°C (shaken at 200rpm), 10ml of cell culture was transferred to a 1L volume of mTB in a 2L conical flask subsequently shaken at 200 rpm (37°C) until the OD_{600} reached a value of 0.6. The temperature was then lowered to 16°C for induction with 1mM IPTG and left to grow overnight. The cells were then harvested, re-suspended in a minimal volume of 25mM Tris, 500mM NaCl pH8 (suspension buffer) and stored at -80°C until further use.

3.2.2.2 *C and N-terminal His-tagged LH_D purification*

Cell paste was thawed at a ratio of 1g cell paste: 100ml suspension buffer before lysis using a homogeniser (Constant Systems Ltd). The lysate was centrifuged at 20,000 g for one hour. The supernatant was filtered and loaded onto a 20ml Ni^{2+} charged chelating sepharose column (GE Healthcare). Fractions were eluted at imidazole concentrations of 30, 100, and 250mM imidazole respectively (25mM Tris, pH8, 200mM NaCl) (Figure 3-4, (A)). The fractions of interest (determined by SDS page) were pooled together and dialysed overnight at 4°C against 25mM Tris, pH8, 200mM NaCl. Enterokinase and Factor Xa (New England Biolabs) treatment was carried out to mimic the native protein endoprotease activation by *C. botulinum* for N terminal and C-terminal his-tagged LH_D, allowing formation of a two-chain (LC and H_N) protein. Enterokinase digestion was completed by adding 1 unit of Enterokinase per 0.1mg LH_D followed by incubation at room temperature for four hours. Factor Xa digestion was completed by adding 1 unit of Factor Xa per 0.1mg LH_D at 25^{o}C for 12 hours. Ammonium sulphate solution was added to the cleaved fusion protein to reach a loading concentration of 1M before loading onto a 20ml phenyl sepharose hydrophobic

interaction chromatography column (HIC) equilibrated with 25mM Tris, pH8, 200M NaCl, 1M $(NH_4)_2SO_4$. Elution was performed in steps at over a gradient of 1-0 M $(NH_4)_2SO_4$, 25mM Tris, pH8, 200mM NaCl (3ml samples). LH_D elution was confirmed by SDS page analysis and corresponding fractions were pooled together. Pooled sample was dialysed overnight against 10L's dialysis buffer (25mM Tris, pH8, 200mM NaCl) at 4°C. The sample was finally concentrated using Vivaspin 50000 MWCO concentrator (Millipore), spinning at 3000 g until concentration reached approximately 4 mg/ml. All concentrations were determined by absorbance measurement at 280nm. Protein was stored in 1ml aliquots at -20°C until further use.

3.2.2.3 *Crystallisation of LH_D*

Initial screening for crystallisation conditions was completed using a crystallisation robot (Phenix, Art Robbins instruments) with PGA Screen (Molecular Dimensions). The condition was repeated using the hanging-drop vapour diffusion method, with 3µl drops (2µl protein and 1µl mother liquor) against a reservoir (500µl) at 16°C. LH_D crystals were obtained using 15% PEG 2K MME, 0.3M (NH4)2SO4, 0.1M NaC2H4O2, pH4.6 (Figure 3.2).

3.2.2.4 *Data collection*

X-ray diffraction data for LH_D was collected at Diamond Light Source (DLS, UK), beamline I03. Prior to data collection, LH_D crystals were transferred to a cryoprotectant solution with 25% (v/v) glycerol for 1 min, and then flash-frozen under a nitrogen stream. Data processing and space group determination was performed using MOSFLM version 7.0.3.

3.2.2.5 *Purification of H_N serotype D from N-terminal his-tagged LH_D*

A 3ml Ni-NTA agarose (Quiagen) drip column was equilibrated with 25mM Tris, 200mM NaCl, 0.5% n-Octyl-β-D-Glucopyranoside, pH8. 1mg/ml N-terminal his-tagged LH_D

was loaded “dripwise” onto the column before subsequently washing with 25mM Tris, 200mM NaCl, 0.5% n-Octyl-β-D-Glucopyranoside, 10mM DTT, pH8.

3.2.2.6 *H_N domain cloning and expression (serotype A and C)*

Plasmids encoding for LH_N serotypes A and C respectively were supplied by Syntaxin Ltd. Plasmids were digested sequentially using SalI and HindIII (New England Biolabs) to isolate H_N domain DNA, H_N domain DNA was then purified using agarose gel electrophoresis before ligation into the pMAL-c2x vector (NEB, UK). Following conformation of the DNA composition through sequencing the vector was transformed into E. coli BL21 expression cells for expression.

H_N domain expression was completed as per section 3.2.2.1. The cells were then harvested, re-suspended in a minimal volume of 25mM Tris, 500mM NaCl, pH8, 1% Triton X-100, 1% Tween 20 and stored at -80$_o$C until further use.

3.2.2.7 *H_N domain serotype A purification*

Cells were resuspended in 25mM Tris, pH 8, 0.5M NaCl, 1% Triton X-100, 1% Tween 20 (1g cell paste: 100ml re-suspension buffer) and lysed using a homogeniser (Constant Systems Ltd). The lysate was centrifuged 20,000 g for one hour. The supernatant was filtered and loaded onto a 20ml Ni^{2+}-charged chelating sepharose column (GE Healthcare). Fractions were eluted over an imidazole gradient (0-400mM Imidazole) (25mM Tris, pH8, 200mM NaCl, 0.5% Triton X-100, 0.5% Tween 20) (Figure 3-8 (A)). The fractions of interest were pooled together before adding a solution of 2M $(NH_4)_2SO_4$ slowly to achieve a final $(NH_4)_2SO_4$ concentration of 0.5M. The sample was filtered before overnight dialysis against 25mM Tris, pH8, 200mM NaCl, 0.5% Triton X-100, 0.5% Tween 20 at 4°C. The sample was loaded onto a Superdex size exclusion column (GE Healthcare) equilibrated with 25mM Tris, pH8, 200mM NaCl, 0.5% n-Octyl-β-D-Glucopyranoside to remove previous detergent. Protein was stored at 4°C until further use.

3.2.2.8 *H_N domain serotype C purification*

Cells were resuspended in 25mM Tris, pH 8, 0.5M NaCl, 1% Triton X-100, 1% Tween 20 (1g cell paste: 100ml resuspention buffer) and lysed using a homogeniser (Constant Systems Ltd). The lysate was centrifuged at 20,000 g for one hour. The supernatant was filtered and loaded onto a 20ml Ni^{2+} chelating sepharose column (GE Healthcare). Fractions were eluted over an imidazole gradient (0-400mM Imidazole) and checked via SDS-page electrophoresis for content (25mM Tris, pH 8, 200mM NaCl, 0.5% Triton X-100, 0.5% Tween 20). The fractions of interest were pooled together and dialysed overnight at 4 °C against 25mM Tris, pH 8, 200mM NaCl, 0.5% Triton X-100, 0.5% Tween 20. Ammonium sulphate solution was added to the cleaved fusion protein to reach a loading concentration of 0.5M before loading onto a phenyl sepharose hydrophobic interaction chromatography column (HIC) equilibrated with 25mM Tris, pH8, 200M NaCl, 0.5M $(NH_4)_2SO_4$ 0.5% Triton X-100, 0.5% Tween 20. Elution was performed at over a gradient of 0.5M- 0M $(NH_4)_2SO_4$. The sample was loaded onto a Superdex size exclusion column (GE Healthcare) equilibrated with 25mM Tris, pH8, 200mM NaCl, 0.5% n-Octyl-β-D-Glucopyranoside to remove previous detergent. Protein was stored at 4°C until further use.

3.2.3 Results

3.2.3.1 *The purification, crystallization and diffraction of C-terminal His-tagged LH_D*

LH_D has been successfully expressed, purified and crystallized in an attempt to elucidate its three-dimensional structure via X-ray diffraction.

Expression and purification

Using a pre-optimized expression cell bank provided by Syntaxin Ltd, C-terminal His-tagged LH_D was expressed in *E*.Coli BL21 cells. The protein was then successfully solubalised via cell lysis (Figure 3-4, C, lane 2). Affinity of LH_D's C-terminal His-tag for a Ni^{2+}-charged chelating column allowed immobilization of the protein and removal of a large proportion of cellular contaminants (Figure 3-4, C, Lane 3). LH_D was then activated via proteolytic cleavage using Enterokinase, this evidently broke covalent bonds between the LC and H_N domains of LH_D, seen following reduction of the disulphide linkage known to exist between the LC and H_N domains, displaying a 50KDa domain (Figure 3-4, C, Lanes 5 and 6). Hydrophobic interaction chromatography (HIC) was used to remove contaminants and produce approximately 80% pure LH_D (Figure 3-4, C, Lane 4).

The purified protein was subject to automated crystallization screening using over 500 different crystallization conditions. Finally, crystals of LH_D were formed using the sitting drop method of crystallization. LH_D was crystallised in the presence of 15% PEG 2K MME, 0.3M $(NH_4)_2SO_4$, 0.1M $NaC_2H_4O_2$, pH4.6 (Figure 3-5, C).

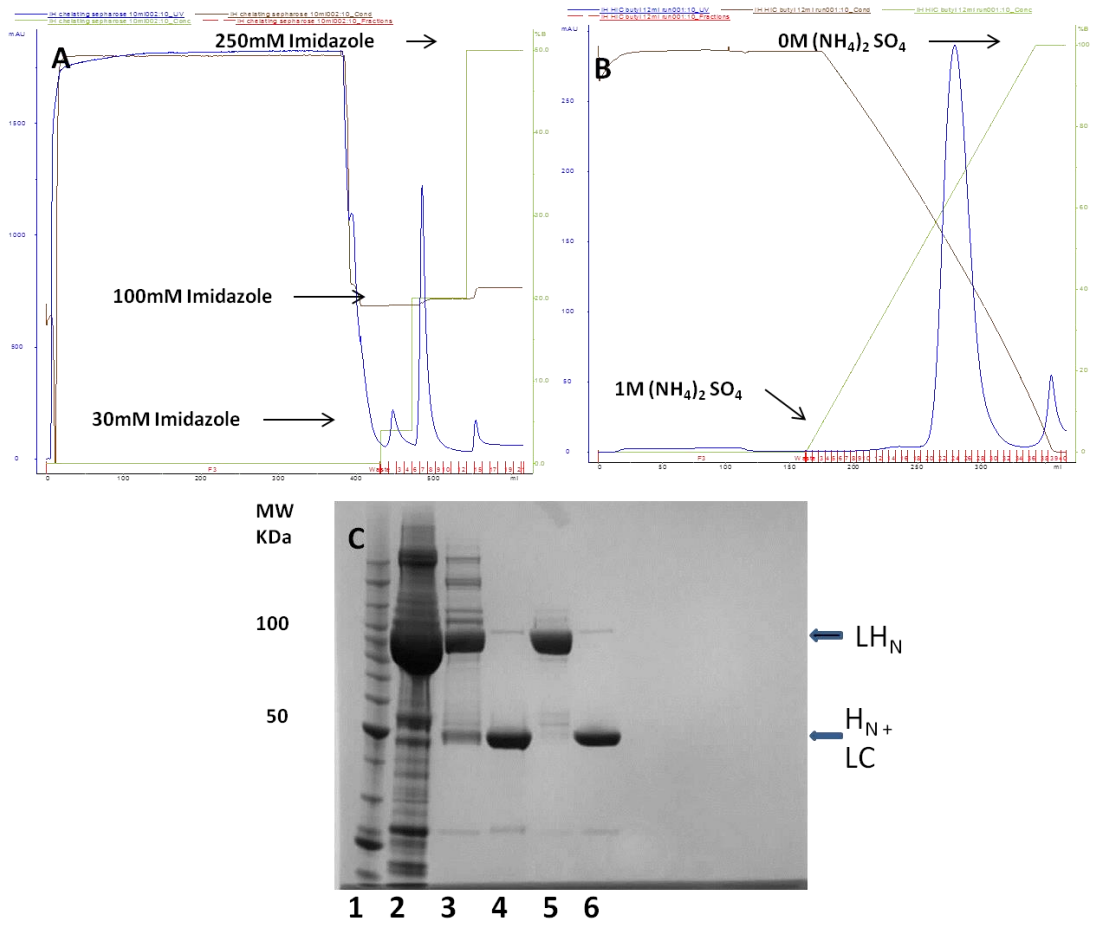

Figure 3-4 Purification of C-terminal His-tagged LH_D for crystallization
(A) Purification step 1 (PS1); Chromatograph of elution from a Ni^{2+} chelating column at imidazole concentrations of 30, 100 and 250mM respectively. (B) Purification step 2 (PS2); Elution from a hydrophobic interaction column (HIC, Phenyl Sepharose) over a gradient of 1 to 0M $(NH_4)_2SO_4$. (C) SDS-page summary of purification; Lane 1 Benchmark, 2 Cell lysate, 3 PS1 100mM elution, 4 Sample post activation + 10mM DTT, 5 PS2 elution, 6 PS2 elution + 10mM DTT.

The protein crystals diffracted to 3.5Å (Figure 3-5, A) before succumbing to radiation damage when exposed on the high power synchrotron beam at Diamond Light Source, Oxfordshire (DLS, Figure 3-5, B). The radiation damage suffered was too severe to record a dataset from which the three-dimensional structure of LH_D could be solved. Subsequent attempts to reproduce and to further optimise crystallisation conditions were unsuccessful.

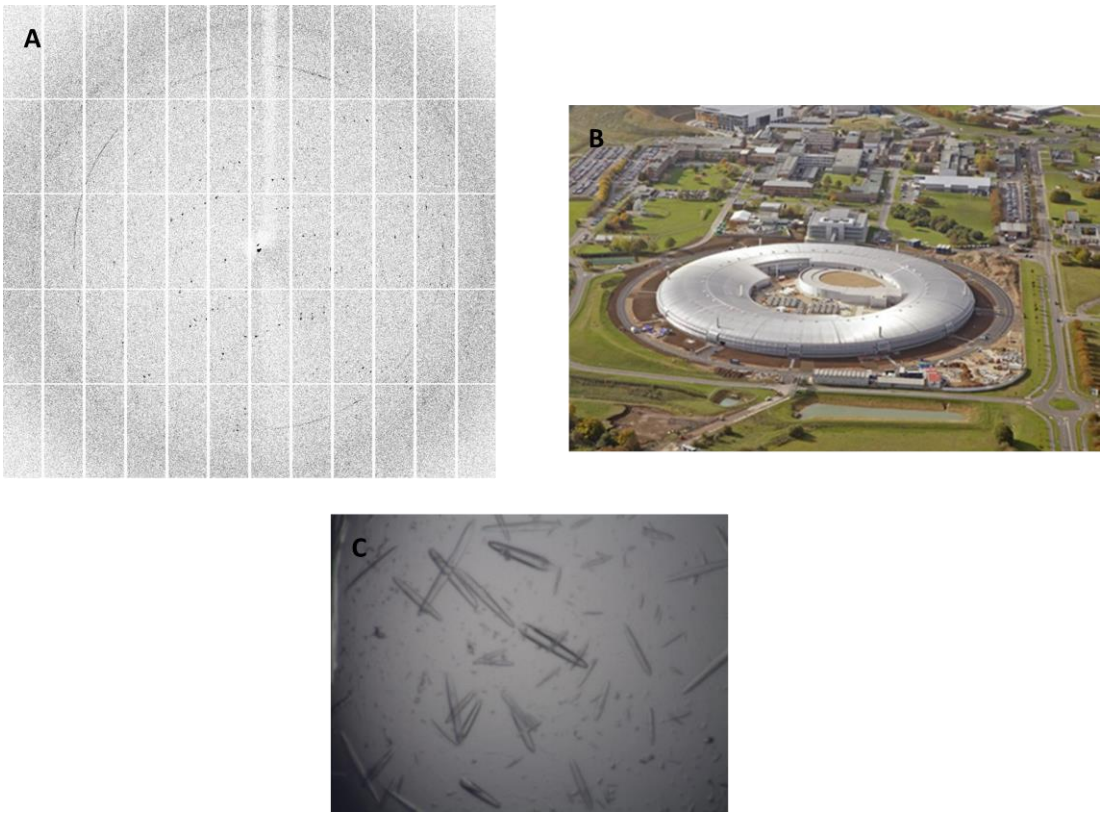

Figure 3-5 The crystallization and X-ray diffraction of LH_D
LH_D crystals have been formed which diffract focused X-rays at the Diamond light source. (A) Crystals of LH_D diffract focused X-rays to a resolution of 3.5Å, collected at Diamond Light Source (station IO3) (B) Diamond Light Source, Oxford, UK. (C) Crystals of LHD grown in 15% PEG 2K MME, 0.3M $(NH_4)_2SO_4$, 0.1M $NaC_2H_4O_2$, pH4.6.

3.2.3.2 *Using affinity chromatography to separate the Light Chain and H_N domain of LH_D*

N-terminal His-tagged LH_D has been expressed and purified for the purpose of separating the H_N and LC domains of the protein. Early attempts to separate the domains of C-terminal His-tagged LH_D using affinity chromatography, failed to produce separation (results not shown). By transferring the His-tag to the LC domain (N-terminal), the H_N and LC domains were separated using a Ni^{2+} chelating column; both a reducing agent and detergent were essential to the separation of the two domains.

Using a pre-optimized cell bank produced by Syntaxin Ltd, N-terminal His-tagged LH_D was expressed in *E*.coli BL21 cells. The protein was then solubilized by lysing cells in the presence of high salt buffer (Figure 3-6, D, Lane 2). Affinity of LH_D's N-terminal His-tag for a

Ni^{2+} chelating column allowed immobilization of the protein and removal of a large proportion of cellular contaminants before eventual elution from the column using Imidazole (Figure 3-6 A, C, Lane 3). Following activation, LH_D was purified using hydrophobic interaction chromatography. Analysis of the eluent through SDS page electrophoresis identified two bands. The LH_D protein (~100kDa) and an unidentified protein (~50kDa) (Figure 3-6, B, D Lane 5). The unidentified 50KDa protein was subsequently removed via size exclusion chromatography under non-reducing conditions (Figure 3-6, C, D Lane 7) leaving a ~100KDa product (Figure 3-6, D Lane 9). Successful activation was determined through SDS-page analysis of LH_D under reducing conditions (two ~50KDa domains) and non-reducing conditions (one ~100KDa domain) respectively (Figure 3-6, D, Lanes 9 and 10).

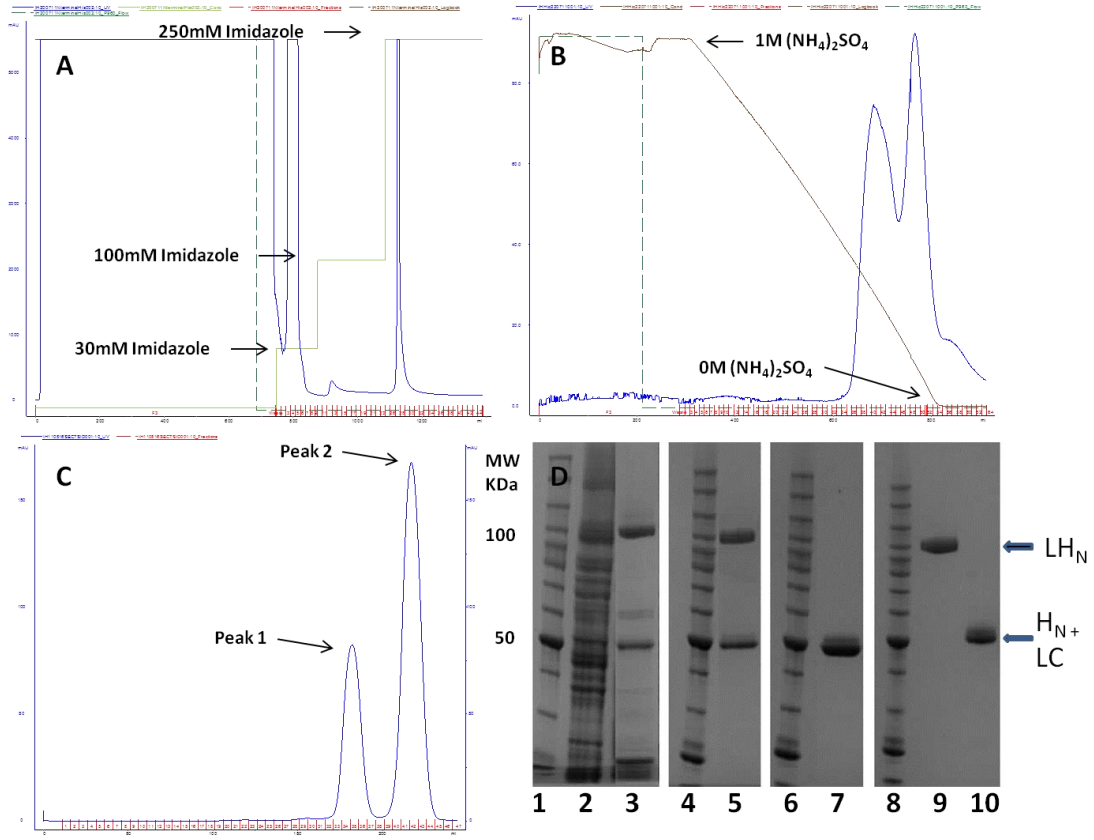

Figure 3-6 Purification of N-terminal His-tagged LH_D for H_N domain purification
(A) Purification step 1 (PS1); Chromatograph of elution from a Ni-charged chelating column at imidazole concentrations of 30, 100 and 250mM respectively. (B) Purification step 2 (PS2); Elution from a hydrophobic interaction column (HIC, Phenyl Sepharose) over a gradient of 1 to 0M $(NH_4)_2SO_4$. (C) Purification step 3 (PS3); Size exclusion chromatography. (D) SDS-page summary of purification; Lane 1, 4, 6 and 8 Benchmark, 2 Cell lysate, 3 PS1

250mM elution, 5 PS2 elution, 7 Post activation +10mM DTT, 9 PS3 elution peak 1 (product) and 10 PS3 elution Peak 2.

By loading N-terminal His-tagged LH_D onto a 3ml Ni-NTA resin column and washing the column with a buffer including a reducing agent (10mM DTT) and detergent (0.5% n-Octyl-β-D-Glucopyranoside) the H_N domain was purified. The separation of the light chain and H_N domains was assessed via western blot (Figure 3-7, A, B). This result was not reproducible and following four further attempts to separate the H_N domain from the light chain the experiment was determined unreliable and the method was discontinued.

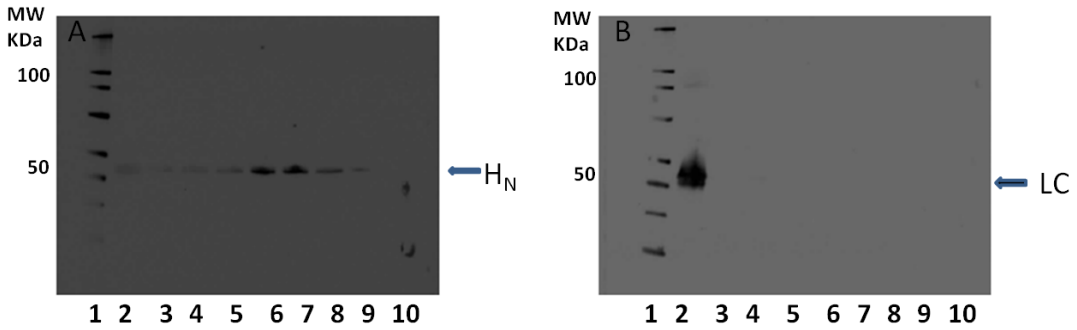

Figure 3-7 Separation of N-terminal His-tagged LH_D using Ni-NTA chromatography
Western blot analysis to identify the H_N domain and Light Chain domain of BoNT serotype D (A) and (B) respectively; Lane 1 Magic Mark protein weight marker, 2 column flow through, 3 1ml wash 1, 4 1ml wash 2, 5 1ml wash 3, 6 1ml wash 4, 7 1ml wash 5, 8 1ml wash 6, 9 1ml wash 7, 10 1ml wash 8 (anti-light chain and anti-H_N domain antibodies used to detect the LC domain and H_N domain respectively (supplied by Syntaxin Ltd)).

3.2.3.3 *Purification of H_N domain (serotypes A and C)*

Due to the low yield and poor reproducibility seen during the separation of LH_N domains, methods to clone, express and purify the H_N domain of BoNT serotypes A and C were developed (methods 3.2.2.6, 3.2.2.7 and 3.2.2.8 respectively).

Genetic constructs for the expression of 10 His-tagged H_N domains (serotypes A and C) were created through the selective endonuclease digestion of LH_N expression plasmids, separation of digested DNA by agarose gel electrophoresis and ligation into pMAL-c2x

vector (NEB, UK). The final sequence was verified via DNA sequencing (Source Bioscience) before transformation into BL21 cells (New England Biolabs) and expression.

Following expression of H_N serotypes A and C respectively, the cells were lysed in the presence of 1% Triton X-100 and 1% Tween 20 according to literature (Lai et al., 2010). Failure to include these detergents in lysis resulted in little to no solubilisation of the H_N protein (data not shown).

H_N serotype A was purified in three stages; firstly affinity chromatography was used to isolate H_N from the lysate solution via Ni-Histidine binding, secondly an ammonium sulphate cut (increasing concentration of $(NH_4)_2SO_4$ to approximately 0.5M whilst stirring in solution) precipitated many contaminants and finally size exclusion chromatography was used to exchange the majority of Triton X-100 and Tween 20 for 0.5% n-Octyl-β-D-Glucopyranoside. The identity of the H_N domain was confirmed thorough western blot analysis (Figure 3-8).

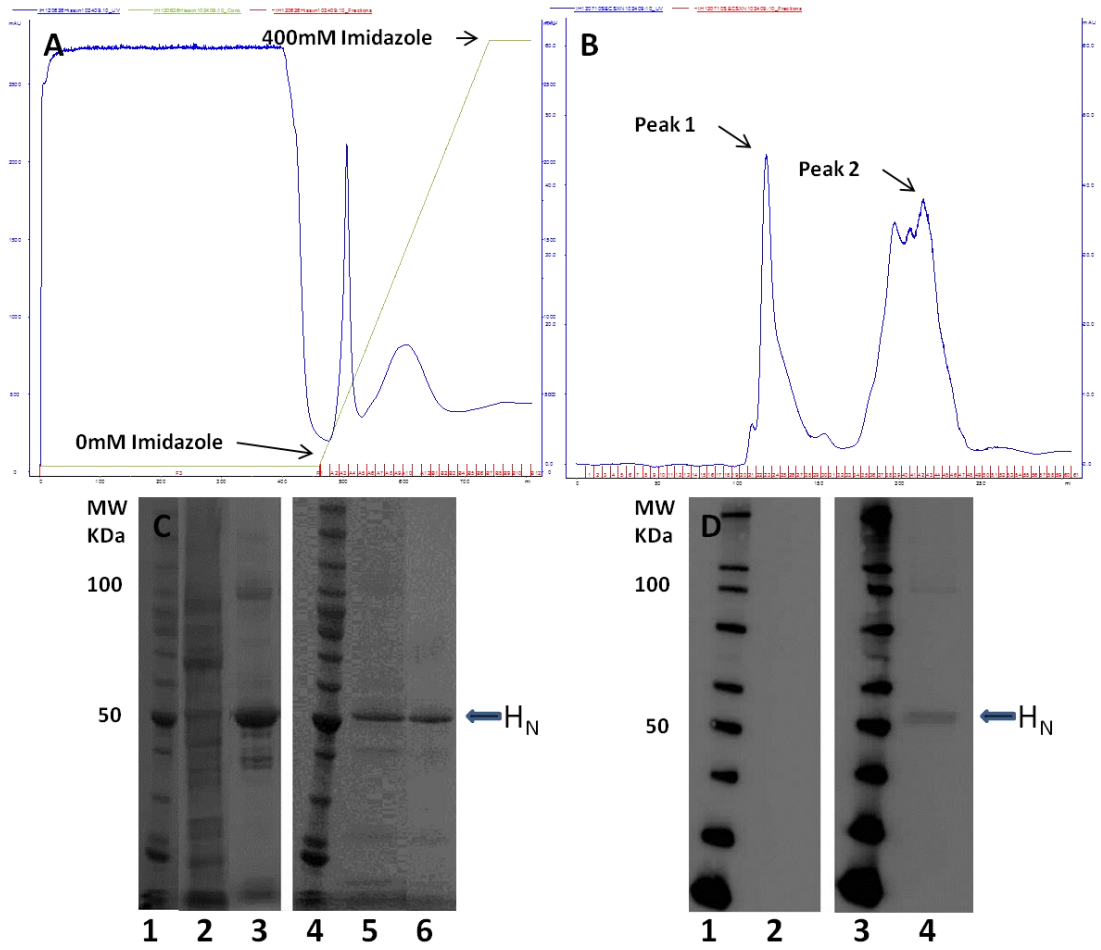

Figure 3-8 Purification of H_N serotype A
(A) Purification step 1 (PS1); Chromatograph of elution from a Ni^{2+} chelating column over a gradient of 0 to 400mM Imidazole. (B) Purification step 2 (PS2); Size exclusion chromatography, peak 1 corresponds to product. (C) SDS-page summary of purification; Lane 1 and 4 Benchmark, 2 Cell lysate, 3 PS1 pooled sample, 5 Sample post (NH4)2SO4 cut 6 PS2 elution peak 1 (product). (D) Western blot analysis of purified protein; Lanes 1 and 3 Magic Mark protein weight marker, 2 BoNT serotype A Light Chain (control), 4 BoNT serotype A HN domain.

The purification of H_N serotype C was completed in three steps; firstly, affinity chromatography was used to isolate H_N from the lysate solution via NTA affinity chromatography; secondly, hydrophobic interaction chromatography removed contaminants eluting between a gradient of 0.5 to 0M $(NH_4)_2SO_4$ (Figure 3-9); finally, size exclusion chromatography was used to exchange the majority of Triton X-100 and Tween 20 for 0.5% n-Octyl-β-D-Glucopyranoside. The purity of the resultant protein was ~60% (determined via SDS page analysis, Figure 3-9). The identity of H_N serotype C could not be confirmed through western blot analysis due to the low sensitivity of the antibody used.

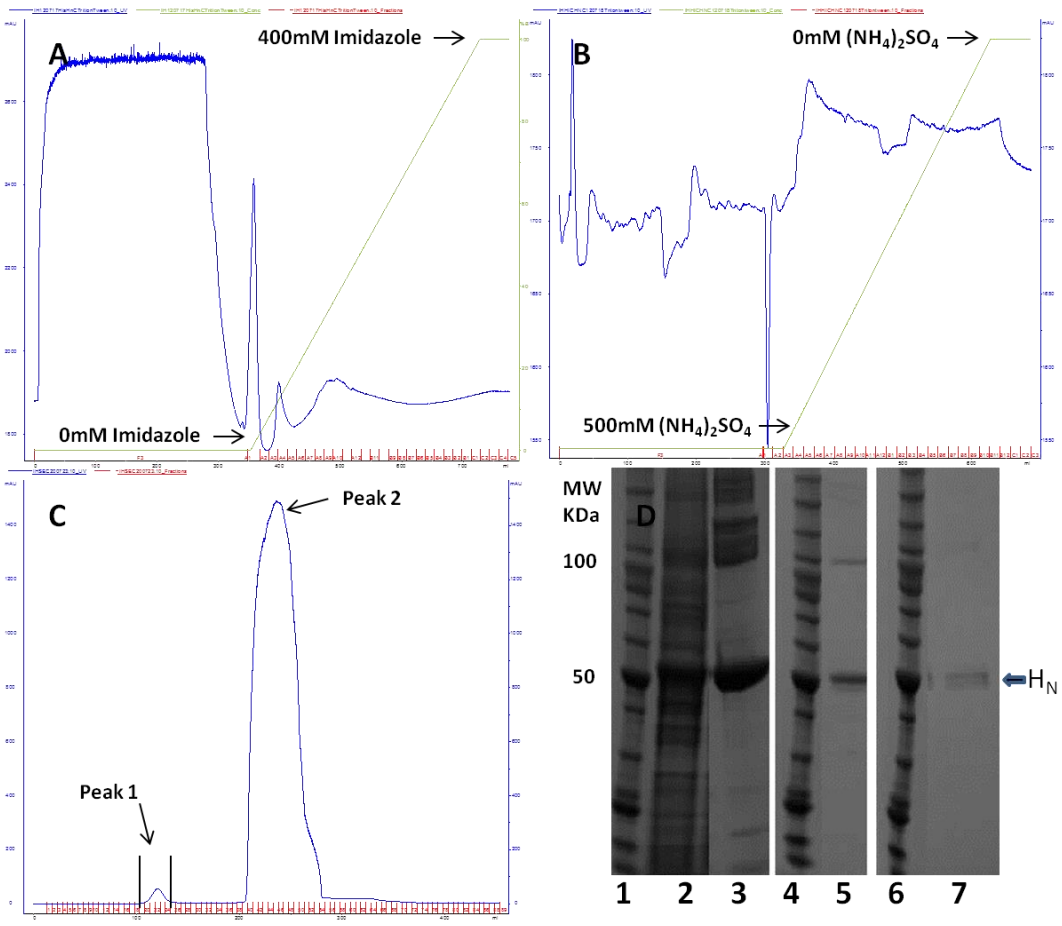

Figure 3-9 Purification of H_N serotype C

(A) Purification step 1 (PS1); Chromatograph of elution from a Ni-charged chelating column over a gradient of 0 to 400mM Imidazole. (B) Purification step 2 (PS2); Elution from a hydrophobic interaction column (HIC, Phenyl Sepharose) over a gradient of 500mM to 0M (NH4)2SO4. (C) Purification step 3 (PS3); Size exclusion chromatography. (D) SDS-page summary of purification; Lane 1, 4 and 6 Benchmark, 2 Cell lysate, 3 PS1 pooled sample, 5 PS2 pooled sample and 7 PS3 elution peak 1 (product).

3.2.4 Discussion

Prior to this investigation only the H_N domain of serotype A had been expressed and purified. Through isolation of the H_N domain, the conditions under which BoNT pore formation occurs were investigated (Galloux et al., 2008; Lai et al., 2010). In a bid to further understand the serotype specific differences inherent in BoNT pore formation and H_N domain structure, other H_N domains must be expressed and purified for analysis through X-ray diffraction or functional assay.

In this chapter I have demonstrated the following; (1) recombinant LH_D can be expressed, purified and, in one trial, crystallised (crystallisation was not reproducible); (2) It is possible to separate the H_N and LC domains of LH_D by affinity chromatography; (3) The H_N domain of BoNT serotype A can be cloned, expressed and purified; (4) The H_N domain of BoNT serotype C has been cloned, expressed and purified for the first time.

3.2.4.1 *The purification, crystallisation and diffraction of LH_D*

In order to further develop our knowledge of the structure and function of BoNTs and their derivatives, LH_D was successfully expressed and purified using an optimised expression plasmid from Syntaxin Ltd. The protein was purified using a combination of affinity and charged based chromatography techniques (Figure 3-4). Furthermore, in one trial, crystals were obtained but subsequent attempts to generate crystals were not successful.

During its purification the protein was “activated” by cleaving a sequence of amino acids between the H_N domain and light chain (LC) in a process designed to emulate post synthetic proteolytic cleavage (Masuyer et al., 2009). This activation process facilitates the removal of all covalent interaction between the two domains. Activation of BoNT proteins is known to be essential for the release and translocation of BoNTs LC domain and consequently was important for the separation of the two domains (Montal, 2010).

LH_D was highly soluble and stable at room temperature at concentrations exceeding 4mg/ml and so was a good candidate for crystallization trials. Through screening over 500 different crystallization conditions the crystallization of LH_D was achieved using the vapor diffusion method. The crystals were taken to the DLS in Oxfordshire where they diffracted to a resolution of approximately 3.5Å. Unfortunately radiation damage, a common problem encountered during X-ray diffraction, irreversibly damaged the crystals preventing a full and solvable data set from being obtained (Ravelli and Garman, 2006). These crystallization conditions could not be repeated over a period of several months culminating in the eventual termination of this project.

3.2.4.2 *Separation of H_N and LC domains*

LH_N proteins contain two domains, namely the light chain domain (LC) and the translocation domain (H_N). The separation and purification of LH_N domains would allow the inclusion of H_N domains in structural studies for the first time whilst concurrently providing new information as to the strength of molecular interactions between H_N and LC domains.

Separating the two domains of LH_N requires the reduction of a disulphide bond and the breaking of non-covalent intermolecular interactions between the belt region of the H_N domain and the LC domain (Figure 3-4) (Masuyer et al., 2011; Masuyer et al., 2009). The two domains of LH_D have been separated by expressing and purifying LH_D with a N-terminal Histidine tag, reducing the disulphide bond between the two domains and washing with a buffer containing a non-ionic detergent (Figure 3-6 and Figure 3-7). This separation was confirmed by western blot analysis (Figure 3-7).

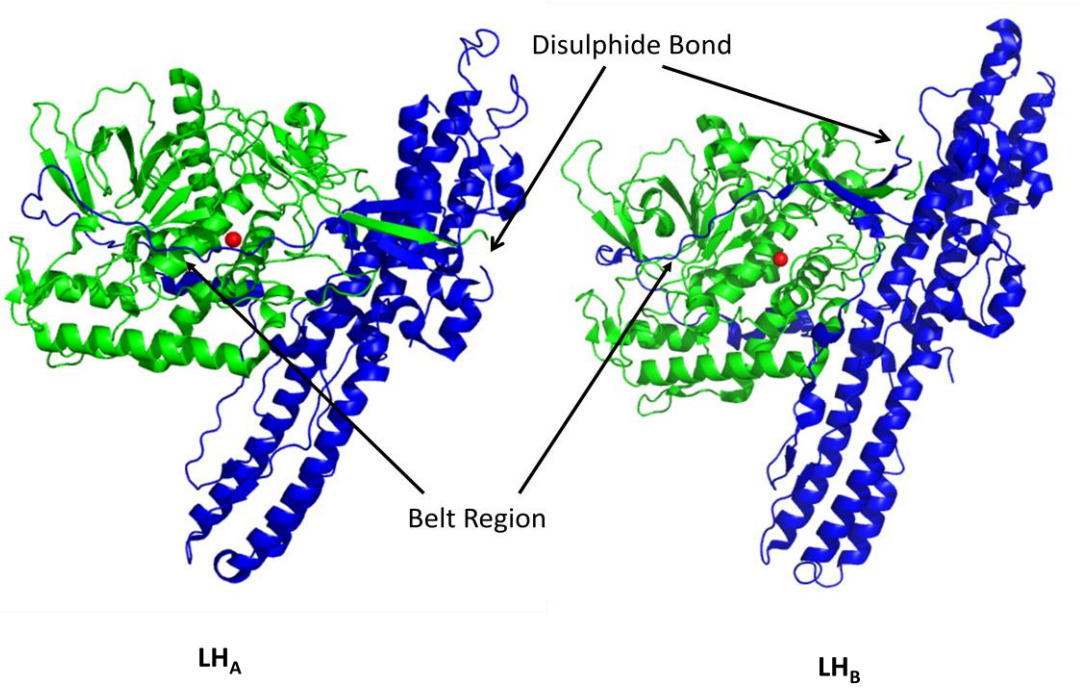

Figure 3-10 The three dimensional structure of LH_N serotypes A and B as determined by X-ray crystallography
The structures of LH_A (2W2D, left) and LH_B (2XHL, right) have been determined by X-ray crystallography. The Light chain (LC) domain of each serotype is highlighted in green and the H_N domain in blue. Disulphide bonds and belt regions have been labeled using arrows. Zn^{2+} atoms associated with the Zn^{2+} metalloprotease function of the light chain domain are highlighted in red (Masuyer et al., 2011; Masuyer et al., 2009).

The need for a detergent, known to be capable of solubalising some membrane proteins (0.5% n-Octyl-β-D-Glucopyranoside), to solubalise H_N is evidence of the domains hydrophobicity. This further supports the hypothesis that BoNTs H_N domain interacts with membrane structures (Fischer et al., 2012).

Unfortunately, this method of separating LH_D's H_N domain and LC was not reproducible as complete separation of the two domains could not be achieved in four further experiments (results not shown). Since, SDS-page analysis of LH_D under the same reducing conditions shows two separate ~50KDa domains (Figure 3-6), we can conclude that the reducing conditions used are sufficient to reduce the inter domain disulphide bond. Many other non-covalent intermolecular interactions seen between the LC and H_N domains of LH_N (Figure 3-10) are therefore presumed responsible for the lack of domain

separation. This observation was supported by literature examples of the separation of the LC domain from the heavy chain domains of BoNT. In these experiments a mixture of dithiothreitol and 2M urea was required to separate the domains; under these conditions the LC domain was found to be unstable (DasGupta and Foley, 1989).

3.2.4.3 *Purification of the BoNT H_N domain*

The inherent difficulty found when trying to separate the two domains of LH_D lead to the decision to separately express and purify the H_N domain of BoNT serotypes A and C respectively. As discussed, purification of the H_N domain is necessary in order to advance our knowledge of H_N domain specific membrane interactions; through purifying multiple serotypes of the H_N domain it may be possible to investigate serotype specific differences in H_N domain physical properties and function for the first time.

The H_N domain of $BoNT_A$ has been expressed and purified using a mixture of affinity chromatography, ammonium sulphate precipitation and size exclusion. This purification was monitored by SDS page and western blot analysis (Figure 3-8). The H_N domain of $BoNT_C$ has similarly been cloned, expressed and purified using a mixture of affinity chromatography, hydrophobic interaction chromatography and size exclusion. This is the first documented case of H_N serotype C expression and purification; the purification was deemed successful through analysis by SDS page. Western blot analysis was not successfully completed as an antibody capable of accurately recognising the H_N domain of $BoNT_C$ was not available. Certain elements of the purification will be discussed as they provide information regarding the physical characteristics of H_N domains.

Literature examples show that in order to solubilise H_N proteins, cells that have expressed H_N must be lysed in the presence of detergent or re-solubilised from urea (Fischer et al., 2012; Galloux et al., 2008; Lai et al., 2010). Both serotypes of H_N purified here have been successfully solubilised by lysing in the presence of a high concentration of detergent (1% Triton X-100 and 1% Tween-20); lysing expressed H_N serotypes A and C in the absence of detergents prevents the proteins from solubalising (results not shown), demonstrating that the H_N domain is insoluble following expression. Aggregation and

insoluble expression is common among hydrophobic proteins expressed in E.coli (Kopito, 2000). The H_N domains solubilisation in detergents is evidence that the domains have potential to interact with the hydrophobic phospholipid environment present in cellular membranes. The decision was made to avoid re-solubalising the proteins using urea to avoid denaturing and refolding of the proteins.

Detergents that form large micells, such as Triton X-100 and Tween-20, are difficult to separate from purified proteins as their size does not allow them to pass though commonly used dialysis tubing. Size exclusion was found to be the most efficient method of removing Tween-20 and Triton X-100 from the protein sample; the UV absorbance (A_{260}) of the detergent allows us to monitor the separation of the protein and detergents through UV absorbance during size exclusion chromatography (Figure 3-8, B and Figure 3-9, C) the identity of each peak was later confirmed through SDS page.

3.2.5 Conclusion

LH_N serotype D has been successfully expressed, purified and crystallised. The crystals produced diffracted to a resolution of ~3.5Å, however, due to radiation damage a full data set could not be collected and consequently the structure of LH_D could not be determined.

In an attempt to purify the H_N domain of LH_D, the LC and H_N domains were separated using affinity chromatography. Separation of the two domains requires reducing conditions and a non-ionic detergent suggesting that the H_N protein possess lipophilic characteristics. Due to the lack of reproducibility, this method of H_N domain purification was discontinued.

The H_N domains of BoNT serotypes A and C were cloned, expressed and purified successfully. This is the first reported cloning, expression and purification method of H_N serotype C. Once again the proteins reliance on detergent to become soluble in an aqueous environment suggests a high level of lipophilicity.

3.3 Developing an assay to assess BoNT and LH_N pore formation

3.3.1 Introduction

Botulinum neurotoxin (BoNT) binds specifically to the pre-synaptic terminal of motor neurones. Once bound, there is evidence to suggest the toxin is endocytosed inside synaptic vesicles (Figure 3-11) (Colasante et al., 2013; Harper et al., 2011; Montecucco et al., 1994) (see section 1.5.2.1).

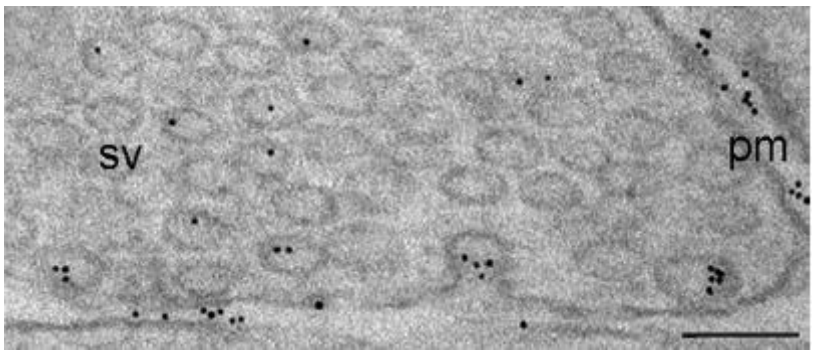

Figure 3-11 The endocytosis of gold labeled $BoNT_A$ H_C domain into synaptic vesicles.
The location of gold labeled $BoNT_A$ H_{CC} domain has been established in hippocampal neurons via immuno-electron microscopy. sv, synaptic vesicles; pm, plasma membrane; scale bar 100nm (Harper et al., 2011).

Once inside the synaptic vesicle, BoNT must translocate its catalytically active protease domain (light chain) through the endosomal membrane into the cell cytosol. The translocation of the light chain is thought to take place though a pore formed by BoNTs H_N domain, following vesicle acidification (Montecucco et al., 1994). Light chain translocation is then thought to be effected by both pH and reducing gradients (Fischer et al., 2009; Montal, 2009).

The way in which BoNTs form pores in vesicular membranes is debated. There are two schools of thought, the first argues that only one molecule of BoNT is taken up into a vesicle and therefore the translocation of the light chain must occur through a singular translocation domain (Colasante et al., 2013); the second states that BoNT forms a multimeric pore, thus requiring more than one molecule to be contained within a vesicle

(Sun et al., 2011). Both possibilities are plausible and are supported by experimental evidence (see sections 1.5.2.4 for evidence and arguments).

There are currently two assays thought to be capable of quantifying BoNT pore formation. These assays are the patch clamp assay and vesicle leakage assay.

Patch clamp assay

A patch clamp assay involves excising a small segment of Neuro 2A or PC12 cell membrane onto the end of a highly polished glass syringe. Through measuring the sodium ion conductance through the excised membrane segment, the pore forming nature of proteins has been qualified (Brunger et al., 2007; Fischer et al., 2008a; Fischer and Montal, 2006; Fischer and Montal, 2007a; Fischer and Montal, 2007b; Fischer et al., 2008b; Fischer et al., 2009; Fischer et al., 2012).

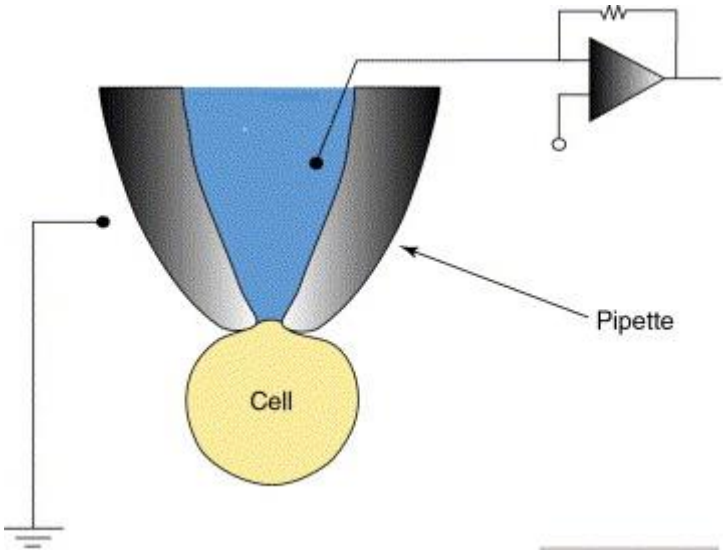

Figure 3-12 The patch clamp technique.
A glass micropipette with a tip diameter of ~1µm is moved onto the cell to form a high-resistance seal with the cell. Suction is applied and a high-resistance seal is obtained between the pipette and cell. The membrane underlying the pipette aperture is then broken to enable the amplifier to control the voltage across the whole of the cell membrane. (Wood et al., 2004)

Vesicle leakage assay:

Vesicle leakage assays quantify the release of a fluorescent marker from inside spherical, unilamellar, liposomes (also known as vesicles) into the "extravesicular" environment upon interaction with pore forming proteins or peptides. The fluorescent marker is quantifiable upon release due to a change in the marker's physical environment, resulting in a change in its potential to fluoresce under experimental conditions. The vesicle leakage technique has been used to detect the pore forming potential of Botulinum neurotoxins and their derivatives, previously confirming that BoNT membrane interaction is pH dependent (Fu and Singh, 1999; Galloux et al., 2008; Lai et al., 2010).

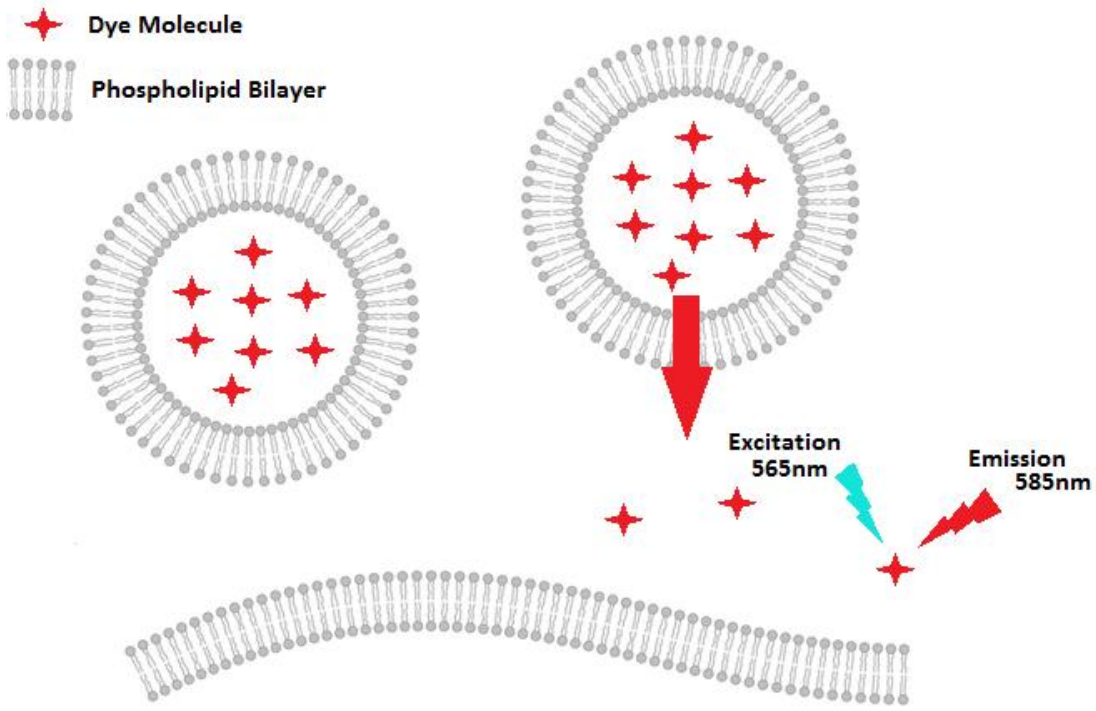

Figure 3-13 The Vesicle Leakage Assay
Highly concentrated self quenching dye is encapsulated inside lipid vesicles. Permeabilization of the vesicle membrane will cause the release of vesicular dye, this release will be recorded as an increase in fluorescence.

Here we show the development of the vesicle leakage assay into a 96 well assay. The assay has been designed to quantify the pore formation of BoNT and its derivatives in vesicle membranes.

3.3.2 Methods

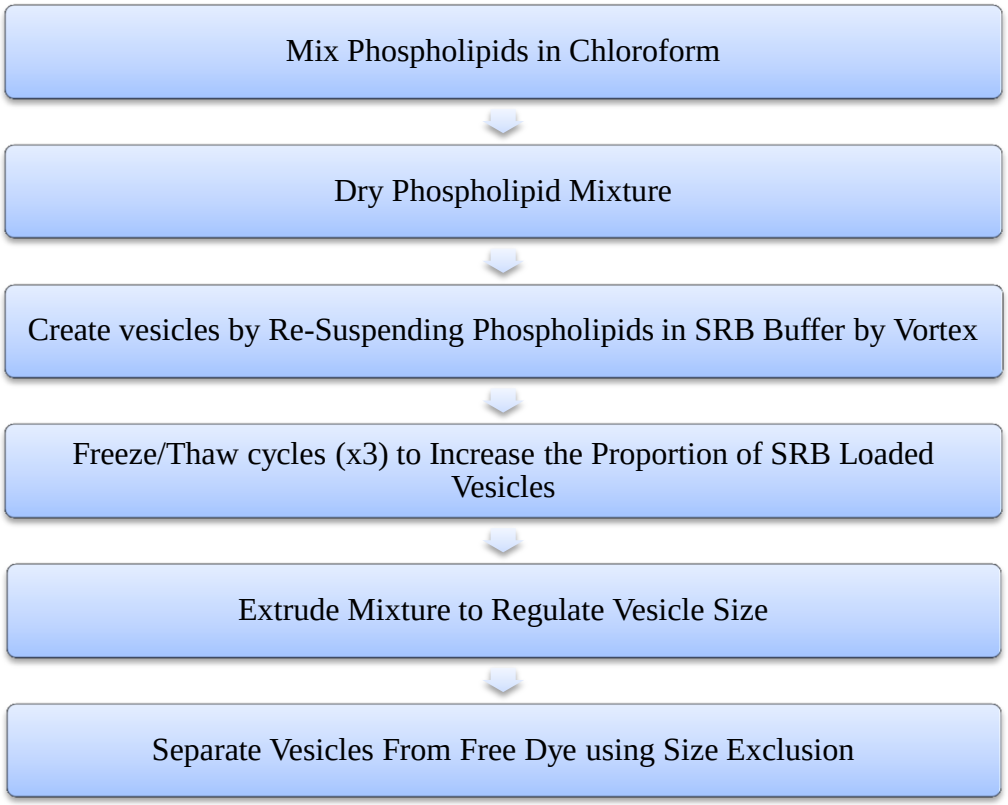

Figure 3-14 Production of Sulforhodamine B loaded lipid vesicles
A simplified protocol for creating vesicles (100nm diameter) which encapsulate 50mM Sulforhodamine B dye.

3.3.2.1 *Vesicle creation*

Large unilamellar vesicles were prepared as follows:

1,2-dioleoyl-sn-glycero-3-phosphocholine (DOPC) and 1,2-dioleoyl-sn-glycero-3-phospho-(-1-race-glycerol) (DOPG) (Avanti Polar Lipids, INC) were solubilised in chloroform (20mg/ml) before they were mixed at a ratio of 3:1 (300µl DOPC: 100µl DOPG) in a glass vial. The solution was dried under a nitrogen jet before the glass vial was placed in a desiccator at room temperature for 1.5 hours to remove excess chloroform. Then, 1ml of 25mM Tris, 50mM NaCl, 50mM Sulforhodamine B (SRB, pH7) buffer was used to re-suspend the phospholipids by vortex for 2mins. The mixture was transferred into a cyro-vial and frozen at -80°C before thawing at 42°C (three times). A mini-extruder (Avanti Polar Lipids, INC) was heated to 50°C (to reduce membrane stability) before it was assembled with a 0.1µm membrane and used to extrude the lipid/buffer mixture ten times. The resultant

mixture was then loaded onto a HiPrep 26/10 desalting column equilibrated with assay buffer. The extravesicular dye was then separated from the formed large unilamellar vesicles (LUV's) at a flow rate of 0.8ml/min. Samples containing LUV's were pooled and dialysed in assay buffer.

3.3.2.2 *Vesicle concentration/calibration assay*

Following LUV purification a calibration assay was used to determine vesicle concentration.

To evaluate the concentration at which the manufactured LUV solution had a low level of background fluorescence, LUV stock solution was diluted in assay buffer to concentrations of 30%, 20%, 10%, 5% and 0% respectively. 250µl of each concentration was mixed to ensure LUV suspension in three individual wells on a black 96-well plate (Costar) before excitation and emission wavelengths of 565nm and 585nm respectively were used to measure SRB fluorescence with a Flexstation 3 plate reader (Molecular Devices). To measure the maximum possible florescence, 25µl of 1% Triton X-100 in assay buffer was added to each well of the 96 well plate and mixed; the plate was then re-read using the same reading protocol. The LUV concentration which demonstrates the lowest level of background florescence and the highest level of maximum fluorescence was chosen for vesicle leakage experiments.

3.3.2.3 *Vesicle leakage assay*

Vesicle leakage assays are performed to measure the disruption of vesicle membranes through tracking the release of SRB contained within those membranes. The leakage of SRB from LUV's was determined by measuring an increase in SRB fluorescence.

200µl of LUV solution (working concentration) was pipetted into black 96-well plates (Costar) where it was mixed with 40µl of test solution. Finally 10µl of pH regulating buffer (phosphate-citrate buffer) was added to determine the pH of the experiment.

Phosphate-citrate buffer was formulated for each experiment by titrating 1M dibasic sodium phosphate and 0.5M citric acid in a water bath at assay temperature; the pH change of assay buffer was then determined following the addition of 1ml phosphate-citrate buffer to 24ml assay buffer at assay temperature. The 96 well plate was placed in the Flexstation 3 reader where it was subjected to the following protocol at a temperature which was set manually; fluorescence was measure every 25 seconds at excitation and emission wavelengths of 565nm and 585nm respectively; the plate was shaken for 5 seconds between every read. The final point of each assay was read after addition of 25µl of assay buffer containing Triton X-100 to each well and mixing with pipette (x3), this stage causes 100% vesicle leakage (F_{max}).

3.3.2.4 *Data analysis*

% Vesicle leakage:

The raw fluorescent data was converted to PDA data files and processed using Microsoft Excel. To determine dye eluted following protein addition as a percentage of total vesicle release, $F_{(t)norm}$ is calculated as a percentage of the maximum fluorescence observed following 0.1% Triton X-100 addition using the following equation,

$$\mathbf{F_{(t)norm} = (F_{(t)} - F_{(0)})/(F_{max} - F_{(0)})x100,}$$

$F_{(0)}$ is the fluorescence level before protein addition, $F_{(t)}$ is the fluorescence at time point (t) and F_{max} is the fluorescence after addition of 1% Triton-X100 before the final reading of each assay (Guo et al., 2003).

3.3.3 Results

3.3.3.1 *Sulforhodamine B dye self quenches at a high concentration*

To set up a vesicle leakage assay, lipid vesicles must be loaded with a chemical marker which is differentially detectable in two different environments (1) when inside lipid vesicles and (2) when in extravesicular media. Sulforhodamine B (SRB) dye is often used in vesicle leakage assays as its fluorescence self quenches at a high concentration (when inside lipid vesicles). Here we assess the concentration dependent fluorescence of 5mM-50nM SRB at 37°C, using excitation and emission wavelengths of 565nm and 585nm respectively.

SRB fluorescence at 585nm increases proportionally with SRB concentration over a concentration range of 20µM-50nM. At concentrations greater than 20µM, SRB fluorescence was inhibited by SRB self quenching. A concentration of 0.1% Triton X-100 appears to have little or no effect on the florescence of SRB dye.

An SRB concentration of 50mM was used in all further experiments because (1) concentrations of SRB greater than 5mM have been shown to quench its fluorescence at an excitation wavelength of 565nm (Figure 3-15) and (2) published vesicle leakage assays use a concentration of 50mM (Lai et al., 2010).

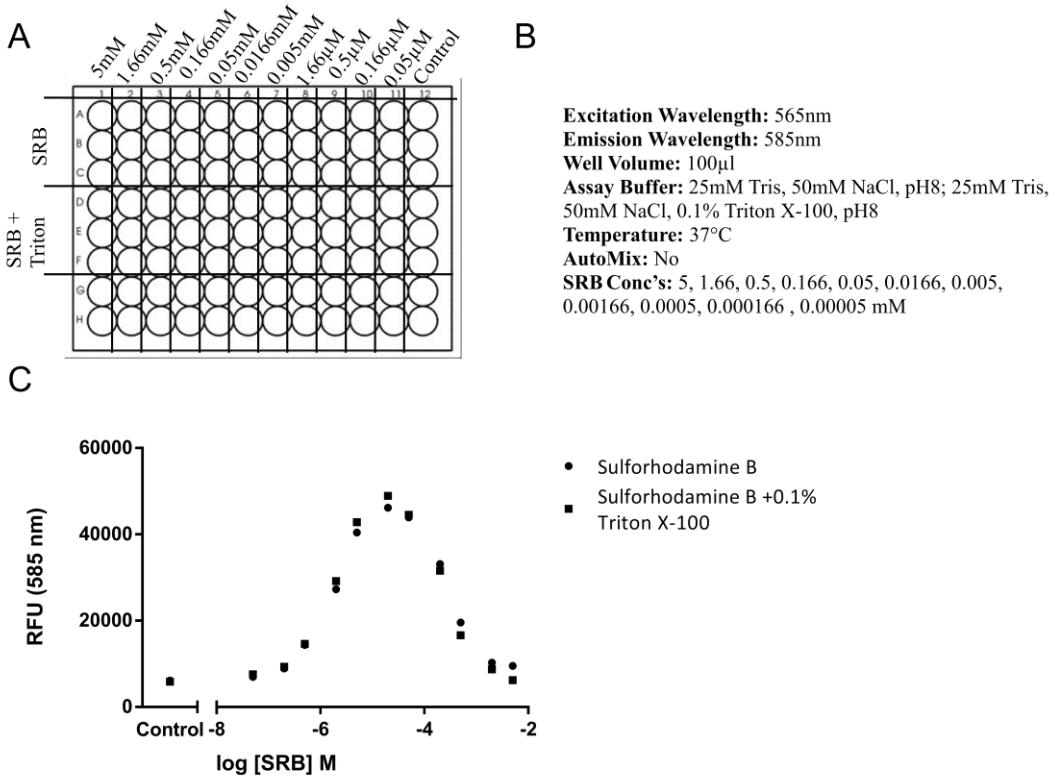

Figure 3-15 Sulforhodamine B dye self-quenches at a high concentration
(A) 96 well plate layout of SRB assay. (B) Assay formulation and Flexstation 3 settings (C) Dose dependent fluorescence of Sulforhodamine B dye (5mM- 50nM) with (■) and without (●) 0.1% Triton X-100. (n=1).

3.3.3.2 *SRB loaded lipid vesicles are stable at pH4 and pH8*

The stability of phospholipid vesicles, loaded with SRB containing buffer, at both neutral and acidic pH is essential for the development of an assay to measure pH dependant vesicle leakage. Vesicle stability has been determined at both neutral and acidic pH by loading vesicles composed of 1,2-dioleoyl-sn-glycero-3-phosphocholine (DOPC) and 1,2-dioleoyl-sn-glycero-3-phospho-(-1-race-glycerol) (DOPG) (3:1 v/v) with 50mM SRB buffer and measuring vesicle leakage at pH 8 and pH 4 respectively (Figure 3-16) over a time course of 15 minutes. The final time point displays complete vesicle lysis after addition of 12.5µl 1% Triton X-100 buffer.

There is no obvious destabilization of vesicles at pH8 or pH4. The addition of Triton X-100 lyses vesicles; vesicle lysis is seen as an increase in SRB fluorescence (~ 30,000 RFU).

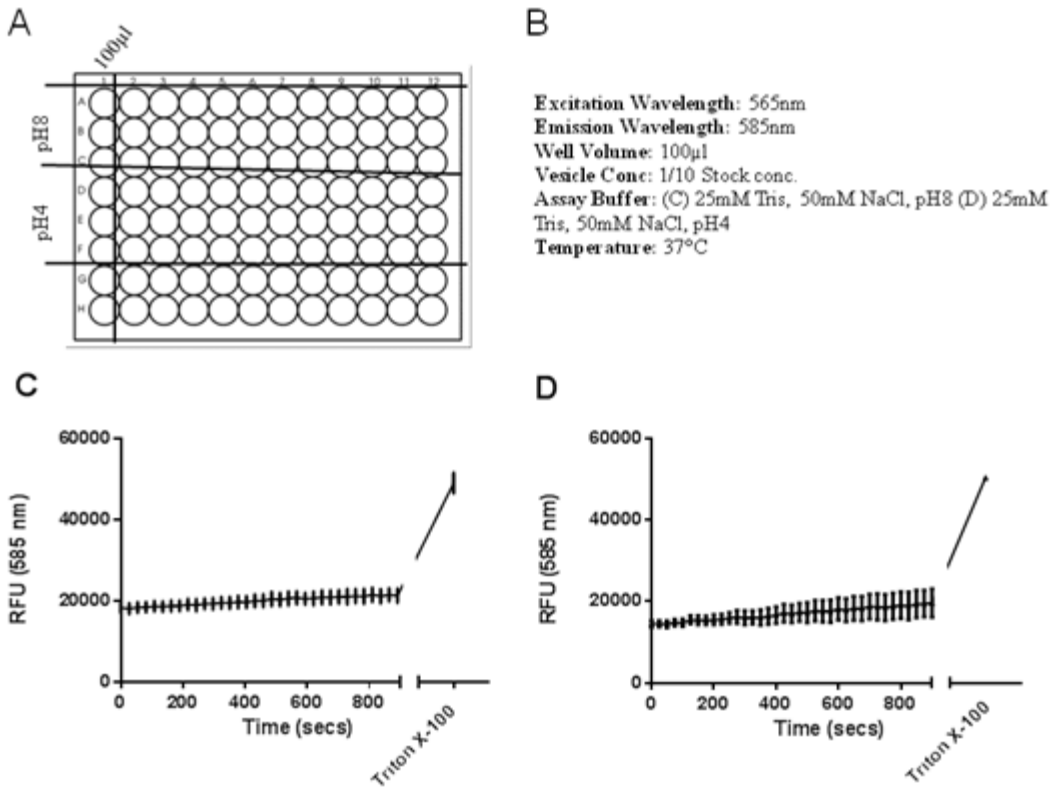

Figure 3-16 Sulforhodamine B loaded lipid vesicles are stable in solution at pH8 and pH4 (n=1)

(A) 96 well plate layout. (B) Assay formulation and Flexstation 3 settings. DOPC/DOPG (3:1 v/v) lipid vesicles loaded with SRB buffer (25mM Tris, 50mM NaCl, 50mM SRB, pH8) were assessed for their stability at (C) pH8 and (D) pH4 for 15 minutes. 12.5µl 1% Triton X-100 was added to each well to show 100% vesicle lysis.

3.3.3.3 *Dehydration effects can be minimized by increasing assay volume*

The effect of dehydration at 37°C has been analyzed using well volumes of 100µl and 200µl respectively over a time course of 3.5 hours. Vesicle stability over this time course was monitored at pH8 and pH4 respectively (Figure 3-17).

A 100µl well volume displays a decrease in fluorescence in both pH8 and pH4 assay buffers (100µl to ~70µl) over a 3.5 hour period. Concurrently, a 200µl well volume shows a steady increase in fluorescence over the time course and a similar ~30µl reduction in volume.

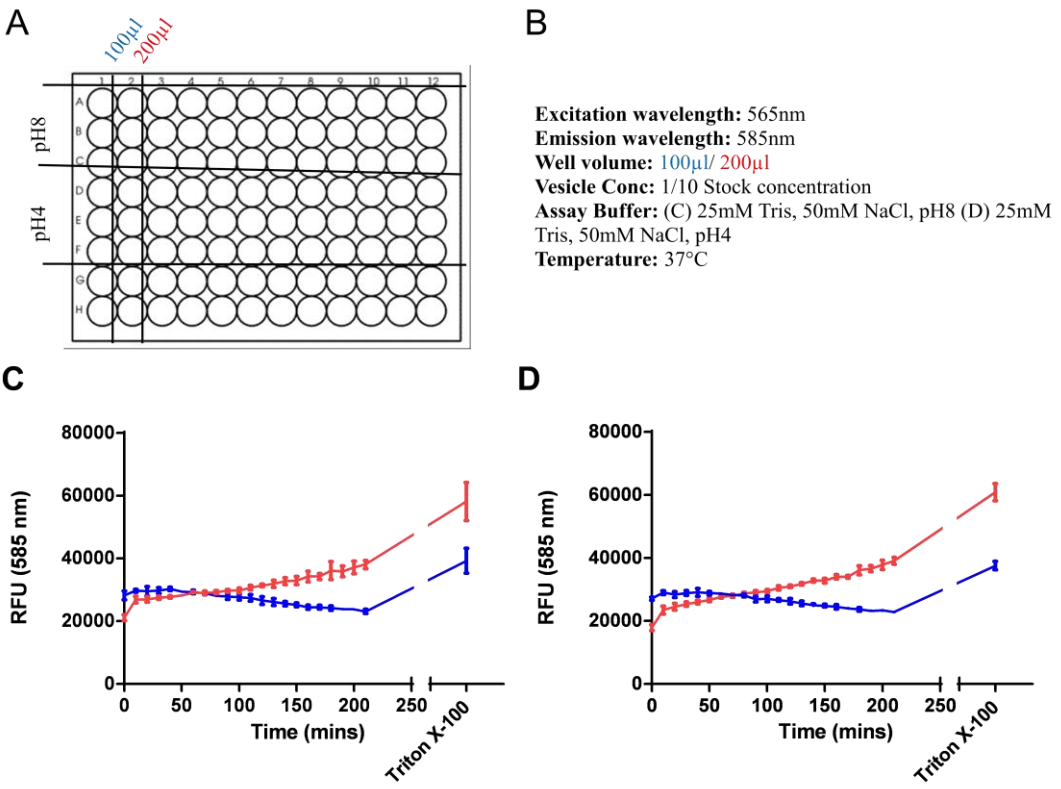

Figure 3-17 Increasing vesicle well volume from 100µl to 200µl reduces the impact of well dehydration (n=1)
(A) 96 well plate layout. (B) Assay formulation and Flexstation 3 settings. Vesicles loaded with 50mM SRB buffer were tested for stability at well volumes of 100µl and 200µl respectively. Vesicle stability is displayed at (C) pH8 and (D) pH4 (37ºC). 12.5µl (C) or 25µl (D) 1% Triton X-100 was added to each well to show 100% vesicle lysis.

3.3.3.4 *Mixing 96 well plates is essential when measuring vesicle-protein interactions*

The purpose of a vesicle leakage assay is to quantify the leakage of vesicle contents following vesicle-protein or vesicle-peptide interactions; vesicle leakage is measured through an increase in SRB florescence (a consequence of SRB leaving lipid vesicles). Here we attempt to further optimize the conditions under which protein-vesicle interactions can be assessed by measuring LH_B induced vesicle leakage at pH4 with and without agitation (mixing).

Vesicles loaded with 50mM SRB dye were formed and diluted in pH4 assay buffer (see materials and methods). 50µl LH_B was then added to each well in order to create LH_B concentrations of 1, 0.1 and 0.01µM respectively at time 0. SRB florescence was measured over a time course of 900 seconds with and without assay agitation (Figure 3-18 C and D respectively).

In the absence of agitation, there was no detectable vesicle leakage caused by LH_B addition. Following plate mixing an increase in fluorescence was detected at a LH_B concentration of 1µM (Figure 3-18, D). This increase in fluorescence is consistent with vesicle disruption and SRB dye leakage (Figure 3-18). No increase in fluorescence was detected when the same experiment was completed at pH7 (results not shown) suggesting that a low pH is necessary for LH_N proteins to interact with vesicular membranes.

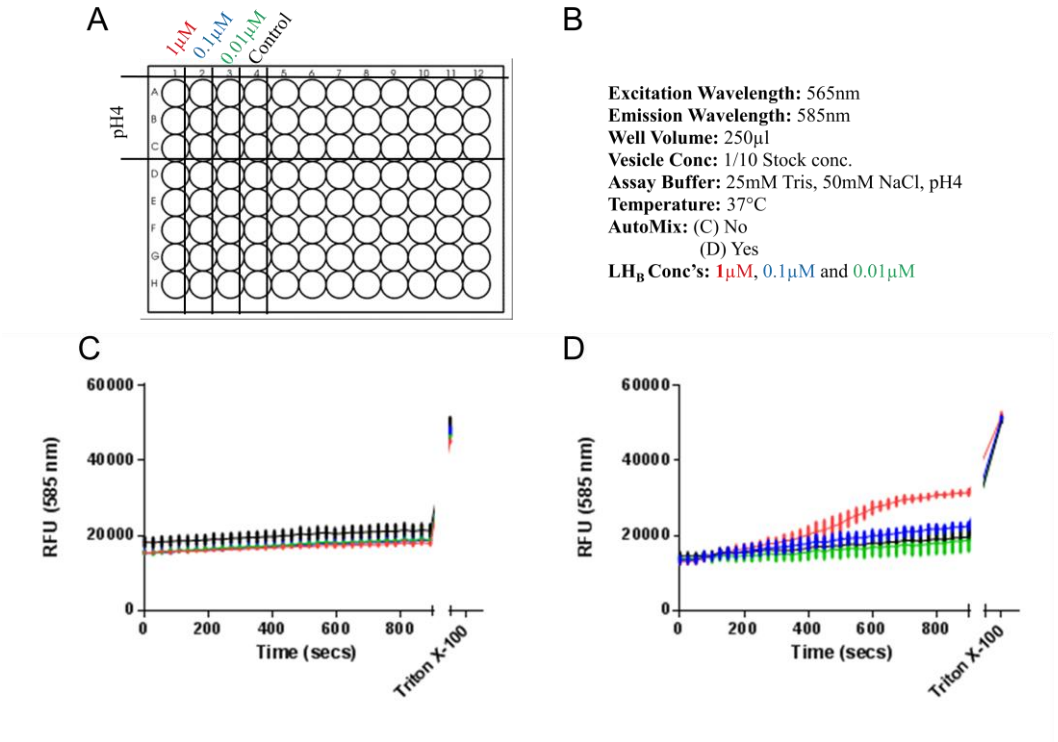

Figure 3-18 Plate mixing is required to measure vesicle leakage (n=1)
(A) 96 well plate layout (B) Assay conditions and Flexstation 3 protocol settings. The addition of various LH_B concentrations (1µM, 0.1µM and 0.01µM respectively) to vesicles was completed with (D) and without (C) a 96 well plate mixing protocol. 25µl 1% Triton X-100 was added to each well to show 100% vesicle lysis.

3.3.3.5 *Determining working vesicle concentration*

The concentration of dye loaded vesicles, used in vesicle leakage assays, must be consistent for vesicle leakage experiments to be comparable. To regulate the concentration of dye loaded vesicles, the fluorescence of vesicle preparations was measured in the presence and absence of 1% Triton X-100. Finally a vesicle concentration was chosen with fluorescence values of <20,000 RFU and >40,000 RFU (with and without 1% Triton X-100 respectively).

Vesicles loaded with 50mM SRB dye are diluted in assay buffer at concentrations of 30, 20, 10 and 5% respectively before loading onto a 96 well plate (250µl well volume). The fluorescence of the vesicles was determined at 0% vesicle leakage (minimum vesicle fluorescence) and at 100% vesicle leakage (after the addition of Triton X-100). An example of this comparison is displayed in Figure 3-19.

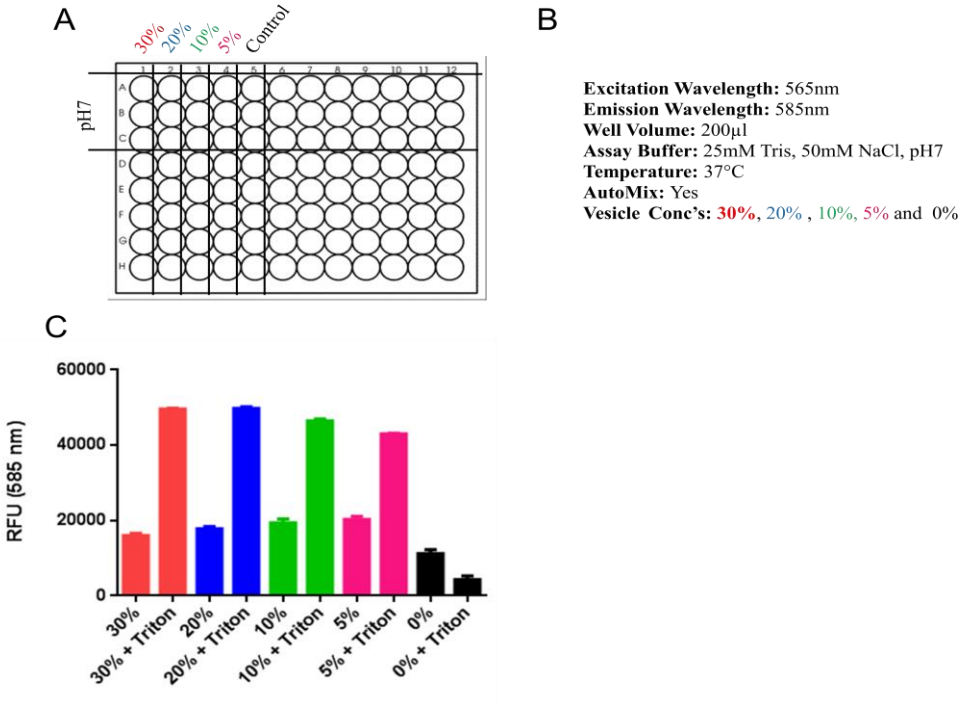

Figure 3-19 Calibration assay to regulate vesicle concentration (n=1)
(A) 96 well plate layout (B) Assay conditions and Flexstation 3 protocol (C) Vesicle concentrations of 30, 20, 10, 5 and 0% were assed for fluorescence with and without the addition of 0.1% Triton X-100.

3.3.3.6 *Pre-incubation of 96 well plates before testing*

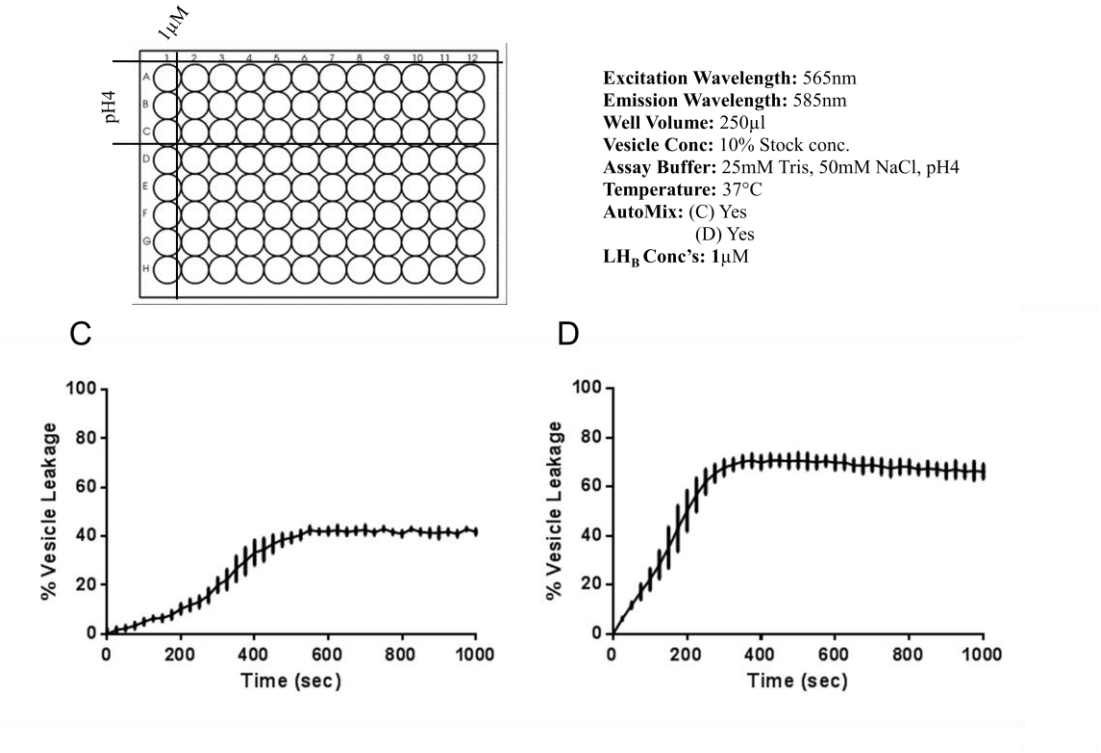

Figure 3-20 Pre-incubation at 37°C increases the initial rate of vesicle leakage (n=3)
(A) 96 well plate layout (B) Assay conditions and Flexstation 3 protocol (C) The addition of 1µM LH_B concentration to vesicles was completed with (D) and without (C) pre-incubation of the 96 well plate at 37°C for 10 minutes before testing. 25µl 1% Triton X-100 was added to each well to show 100% vesicle lysis (not shown).

In order to better regulate the temperature at which vesicle leakage assays are initiated, a pre-incubation step was introduced. All elements used in the assay were pre-incubated at 37°C for 10 minutes prior to commencing the assay.

Here vesicles loaded with 50mM SRB dye were formed and diluted in pH4 assay buffer. Once prepared, solutions were either incubated for 10 minutes at room temperature (Figure 3-20, C) or at 37°C in the Flexstation 3's loading tray (Figure 3-20, D). 50µl LH_B was then added to each well in order to create a final concentration of 1µM at time 0.

The pre-incubation of assay solutions before assay initiation evidently increased the initial rate of vesicle leakage. An assay initiated at room temperature demonstrated vesicle leakage of 9% after 200 seconds in comparison to 53% following pre-incubation.

3.3.4 Discussion

Vesicle leakage is a well-known technique that has previously been used to determine the pore forming properties of Botulinum neurotoxins (BoNTs) and their derivatives (Galloux et al., 2008; Lai et al., 2010). Here a 96-well vesicle leakage assay has been developed to provide a quick and efficient way of measuring the interaction of BoNT proteins and their derivatives with synthetic phospholipid membranes. The qualities essential for setting up a vesicle leakage assay are discussed below.

3.3.4.1 *Generating large unilamellar vesicles*

The first step of creating a vesicle leakage assay is deciding on the composition of the liposome. Ideally the vesicles created in-vitro should mimic those which endocytose BoNT into the presynaptic terminal. This would involve understanding the composition of naturally occurring synaptic vesicles (see section 1.5.4 for synaptic vesicle composition) then optimising a synthetic phospholipid mixture to closely mimic the natural vesicles. However, due to time constraints, for this study we relied on published, peer-reviewed papers detailing vesicle leakage assays used to detect BoNT induced vesicle leakage and used phospholipid mixtures reported as suitable in those papers.

A phospholipid mixture of 75% DOPC and 25% DOPG (Figure 3-21) was decided upon based on information available in literature (Lai et al., 2010). This mixture of phospholipids has been used to determine pore formation by vesicle leakage for both proteins and peptides at various pH conditions and temperatures. Furthermore a DOPC/DOPG vesicle leakage assay has previously been used to determine the pore formation potential of the BoNT/A H_N domain (Lai et al., 2010).

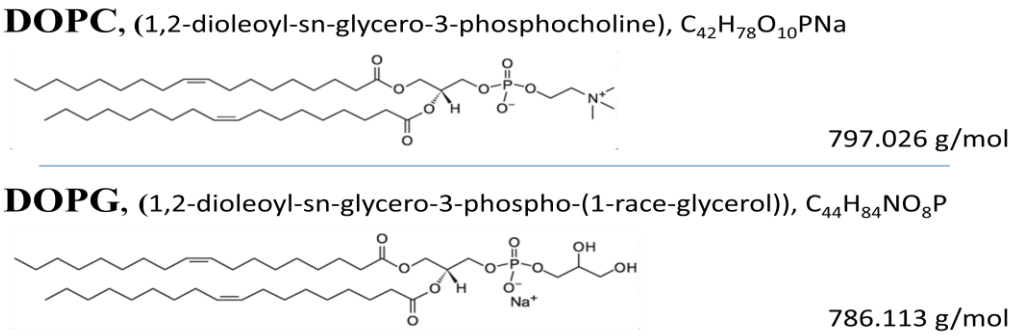

Figure 3-21 DOPC and DOPG phospholipids are used to create large unilamellar vesicles (LUV's)
DOPC and DOPG phospholipid molecules are displayed above along with their molecular formula and molecular weight.

DOPC/DOPG vesicles contain phospholipids with neutral head groups (DOPC) and phospholipids with anionic head groups (DOPG). Increasing the percentage of phospholipids with anionic head groups in vesicles has been shown to increase the interaction of vesicles with BoNT/A (Galloux et al., 2008) suggesting that increasing the surface charge of membranes attracts BoNT molecules. The ratio of DOPC:DOPG in vesicle membranes was ultimately chosen to replicate a successful vesicle leakage assay assessed to show BoNT pore formation in literature (Lai et al., 2010).

3.3.4.2 *Loading large unilamellar vesicles with dye*

Vesicle leakage experiments work on the premise that it is possible to measure the release of intra-vesicular compounds in a quantitative manner following vesicle membrane disruption. In order to achieve this, the intravascular compound must have the following properties.

1. It must be water soluble.

2. It must be possible to form vesicles which trap the compound.

3. When encapsulated in the vesicles it must be possible to separate the loaded vesicles from excess compound.

4. Whether or not the compound is contained within vesicles must be easily detectable.

5. The compound's fluorescence must not be affected by 0.1% Triton X-100 in solution.

Sulforhodamine B (SRB) satisfies the above criteria. It is highly water soluble and concurrently lipophilic. When vesicles are formed in the presence of SRB, the dye is seen to be encapsulated and stable inside vesicles (Figure 3-16). Vesicles loaded with SRB dye adopt a red colour making them easily identifiable.

SRB loaded vesicles were easily separated from excess SRB buffer using size exclusion chromatography. Following a four hour dialysis period, no dye leaked out of the vesicles into the dialysis buffer. This suggests that the liposome's produced are stable and that size exclusion chromatography is sufficient to fully remove extra vesicular dye.

So that we can determine an increase in SRB fluorescence upon vesicle disruption, the vesicles must be loaded with a concentration of SRB that is known to quench florescence. In order to determine the concentration dependence of SRB fluorescence the self quenching nature of SRB was examined (SRB has absorbance and emission wavelengths of 565nm and 585nm respectively). Figure 3-15 shows that a 5mM concentration of SRB is sufficient to quench the dyes fluorescence to basal levels. For this reason vesicles were loaded with a concentration of SRB greater than 5mM during assay development, the concentration chosen for subsequent experiments was 50mM (based on published studies).

3.3.4.3 *Vesicle stability*

After determining that lipid vesicles could be made to encapsulate SRB dye at a self-quenching concentration, the stability of those vesicles was assessed.

BoNTs and their derivatives are known to need acidic conditions to translocate (Montecucco et al., 1994; Mushrush et al., 2011). The vesicles produced must therefore be stable at low pH for pore formation to be assessed. Figure 3-16 shows vesicles were stable at pH8 and pH4 at various concentrations. This figure also shows that, after the addition of 0.1% Triton X-100, fluorescence increased. This observation is further evidence that SRB self-quenches at high concentration (in vesicles) and, when diluted through vesicle leakage, its observed fluorescence increases.

In Figure 3-17 the effect of assay dehydration on background florescence has been assessed. Here we see that by increasing the well volume from 100µl to 200µl it is possible to reduce the effect of dehydration on baseline fluorescence. At 37^{o}C the 100µl well volume decreases over time due to dehydration, consequently, the concentration of SRB in solution increases, resulting in a reduction in SRB fluorescence. Dehydration also occurs at the higher 200µl well volume, however, the volume reduction is proportionally lower resulting in a lower SRB concentration increase and no reduction in fluorescence.

3.3.4.4 *Regulating vesicle concentration*

Vesicle concentration must be regulated so that assays completed with different batches of vesicles are comparable. Figure 3-19 shows how vesicle concentration can be regulated by assessing the difference between baseline vesicle fluorescence and lysed vesicle fluorescence. As the concentration of vesicles is reduced, the baseline florescence increases due to a reduction in SRB self-quenching; concurrently, the fluorescence of SRB from lysed vesicles (using Triton X-100) is reduced as the final SRB concentration in solution is lowered.

Vesicle calibration was completed for every batch of vesicles produced. The vesicle concentration chosen had a baseline fluoresce value below 20,000 RFU and a lysed vesicle fluorescence of above 45,000 RFU.

3.3.4.5 *Pre-incubation*

In order to better regulate the temperature at which the assay is initiated, a 10 minute pre-incubation step was added to the assay protocol. Figure 3-20 displays the effect of pre-incubating the assay reagents for 10 minutes at 37°C prior to initiation. Pre-incubation has evidently had the effect of increasing the initial rate of vesicle leakage and the maximum vesicle leakage achieved by 1µM LH_B.

3.3.5 Conclusion

Here we have successfully demonstrated the creation of a 96 well vesicle leakage assay capable of assessing protein induced vesicle leakage in a quick and efficient manner.

Lipid vesicles have been successfully prepared encapsulating a self-quenching concentration of SRB dye. The resultant vesicles were stable under conditions of low pH and high temperature. Vesicle leakage can only be determined following interaction with proteins at acidic pH and when mixed.

The concentration of SRB loaded lipid vesicles can be assessed prior to vesicle leakage assays by comparing measurements of the normal and lysed fluorescence of vesicle preparations.

3.4 Removal of botulinum neurotoxin's receptor binding domain affects the protein's ability to interact with phospholipid membranes.

3.4.1 Introduction

It is well recognised that Botulinum toxins have the ability to form pores in phospholipid membranes (Montal, 2010). To better understand the structure and function of Botulinum toxins and their domains, I have developed a 96-well vesicle leakage assay to analyse BoNT and LH_N pore forming potential in accordance with published results. Here we set out to analyse vesicle leakage potential to measure protein pore formation and discuss how BoNT and LH_N induced vesicle leakage may allow us to learn more about the activity and functional characteristics of these proteins.

3.4.1.1 *A comparison of BoNT serotypes A and E*

As discussed, both BoNT serotypes A and E block exocytosis of neurotransmitters by cleaving SNAP-25, a protein known to be essential to the fusion of synaptic vesicles to the pre-synaptic membrane (Agarwal et al., 2004). However, major differences have been identified, both structurally and functionally, between the two serotypes.

Functionally, $BoNT_E$ enters cultured neurones more quickly than $BoNT_A$, has a lower potency, cleaves SNAP-25 at a different recognition site and ultimately acts faster to inhibit transmission at the neuromuscular junction (NMJ) (Wang et al., 2008a). $BoNT_E$ also totally inhibits vesicular fusion, in this respect it is similar to BoNTs (such as B, C, D and F) which cleave VAMP or Syntaxin and unlike $BoNT_A$ inhibition which can be rescued (for example by increasing intracellular Ca^{2+}) (Sakaba et al., 2005). Studies have also shown that inhibition of NMJ transmission caused by $BoNT_E$ has a shorter recovery time than that caused by $BoNT_A$ (30-45 days in comparison to more than 90 days in the human Extensor Digitorum Brevis Muscle (EDB) respectively) (Kumaran et al., 2009).

Structurally, although the individual domains of $BoNT_E$ are similar to those of $BoNT_A$ the domain organisation is different (see Figure 1-3). $BoNT_A$'s catalytic (LC) and binding

domains (H_C) flank the long translocation domain with no apparent interactions between them. In contrast, the LC and H_C domains of $BoNT_E$ appear on the same side of the translocation domain and interact with one another, resulting in a tight globular molecule, with each domain having an interaction with the other two domains. It has been hypothesised that the high translocation rate attributed to $BoNT_E$ is a result of the H_N and LC domains high sensitivity to pH changes due to the H_N domains proportionately higher exposure to solvent than in BoNTA (Kumaran et al., 2009).

The different functional characteristics of $BoNT_A$ and $BoNT_E$ have been shown to be transferable though creation of BoNT chimeras comprised of functional domains from both serotypes. When a chimera was created composed of the LC and H_N domains of $BoNT_E$ and H_C domain of $BoNT_A$, the protein was shown to possess the fast translocation characteristics of $BoNT_E$. Concurrently, a chimera composed of the LC and H_N domains of $BoNT_A$ and the H_C domain of $BoNT_E$ showed translocation rates comparable to that of $BoNT_A$. This not only highlights BoNT domain functionality and differences between the functional characteristics of BoNT serotypes but also suggests that a protein composed only of the H_N and LC domain may be capable of displaying pore formation properties representative of those of the full length BoNT toxin (Wang et al., 2008b).

3.4.1.2 *BoNT serotypes A and E form pores in lipid membranes*

Through electrophysiological methods, such as patch clamp assays it has been concluded that BoNT serotypes A and E form pores in lipid membranes under acidic conditions. Membranes from synthesised lipid bilayers ($BoNT_A$), PC12 cells ($BoNT_A$) and Neuro 2A cells ($BoNT_A$ and $BoNT_E$) have all been assessed for their potential to permit BoNT membrane permeation which is thought to be as a consequence of BoNT H_N domain pore formation (Fischer et al., 2008a; Monta et al., 1992; Oblatt-Montal et al., 1995).

Although the manner in which a translocation pore is created is disputed, the field generally agrees that the H_N domain of BoNT and an acidic pH are essential for the formation of a translocation pore. However, the role of the receptor binding domain (H_C) in pore formation is less well understood. In some models the H_C domain recognition of pre-

synaptic membrane receptors is thought to be essential to pore formation ($BoNT_B$) (Sun et al., 2011; Sun et al., 2012), in others the H_C domain is considered as completely non essential to the formation of a pore ($BoNT_A$ and LH_A) (Chaddock and Marks, 2006; Chaddock et al., 2004; Chaddock et al., 2000a; Chaddock et al., 2000b; Fischer et al., 2008b).

The vesicle leakage assay described in section 3.3 provides us with a tool with which we can potentially further evaluate BoNT and LH_N pore formation. In this chapter we evaluate positive and negative pore forming controls in order to evaluate whether this assay is a useful tool to evaluate pore formation at acidic pH. Following this we analyse the concentration, pH and temperature dependant nature of BoNT and LH_N induced vesicle leakage in order to answer the following questions. (1) Can LH_N proteins form pores in vesicle membranes? (2) Does removing the H_C domains from BoNT affect the rate at which it may interact with vesicle membranes? And (3) Do $BoNT_A$ and $BoNT_E$ form pores at different rates respectively and does this compliment evidence that $BoNT_E$ translocates at a faster rate than $BoNT_A$.

3.4.2 Materials and Methods

3.4.2.1 *Vesicle creation*

See section 3.3.2.1.

3.4.2.2 *Vesicle concentration/calibration assay*

Following LUV purification a calibration assay was used to determine vesicle concentration.

To evaluate the concentration at which the manufactured LUV solution had a low level of back ground fluoresce, LUV stock solution was diluted in assay buffer to concentrations of 30%, 20%, 10%, 5% and 0% respectively. 250µl of each concentration was mixed in three individual wells on a black 96-well plate (Costar) before excitation and emission wavelengths of 565nm and 585nm respectively were used to measure SRB fluorescence with a Flexstation 3 plate reader (Molecular Devices). To measure the maximum possible florescence, 25µl of 1% Triton X-100 in assay buffer was added to each well of the 96 well plate and mixed; the plate was then re-read using the same reading protocol. The LUV concentration which shows the lowest level of background florescence and the highest level of maximum fluoresce was chosen for vesicle leakage experiments.

3.4.2.3 *Vesicle leakage assay*

Vesicle leakage assays were performed to measure the disruption of vesicle membranes through tracking the release of SRB buffer contained within those membranes. The leakage of SRB buffer from LUVs was determined by measuring an increase in SRB fluorescence by excitation and emission wavelengths of 565nm and 585nm respectively using a Flexstation 3 plate reader.

200µl of LUV solution (working concentration) was pipetted into black 96-well plates (costar) where it was mixed with 40µl of test solution. Finally 10µl of pH regulating

buffer (phosphate-citrate buffer) was added to set the pH of the reaction. The plate was placed in the Flexstation 3 reader where it was subjected to the following protocol at a temperature which was set manually; fluorescence was measure every 25 seconds at excitation and emission wavelengths of 565nm and 585nm respectively; the plate was shaken for 5 seconds between every read. The final point of each assay was read after addition of 25µl of assay buffer containing Triton X-100 to each well and mixing with pipette (x3), this stage causes 100% vesicle leakage (F_{max}).

3.4.2.4 *Data analysis*

For data analysis method see section 3.3.2.4.

3.4.3 Results

3.4.3.1 *Non-pore forming proteins show vesicle leakage at acidic pH*

To qualify that vesicle leakage was a result of protein or peptide induced pore formation, both pore forming and non-pore forming protein controls were assessed for vesicle leakage at pH7 and pH4. GALA is a pore forming peptide which has been reported to cause vesicle leakage at acidic pH (Nicol et al., 1999); BSA, Transferrin and the LC domain of $BoNT_A$ (LC_A) are considered non-pore forming proteins at pH7 and pH4.

1μM GALA, BSA, Transferrin and LC_A show no appreciable vesicle leakage at pH7 (Figure 3-22, A, B); however, 1μM concentrations of all proteins and peptides tested showed vesicle leakage at pH4 (Figure 3-22, C, D). The assay therefore reported pH dependent effect of proteins on lipid membranes but did not distinguish between known pore forming proteins and proteins with no known pore forming ability. This suggested the assay did not specifically report formation of stable, protein lined channels.

Although we are not confident that this assay measured only stable, protein lined pores, it did measure some physical property, possessed by a protein, that is related to insertion into (and disruption of) lipid bilayers. This property is likely to be related to, and to affect the translocation ability of BoNT proteins.

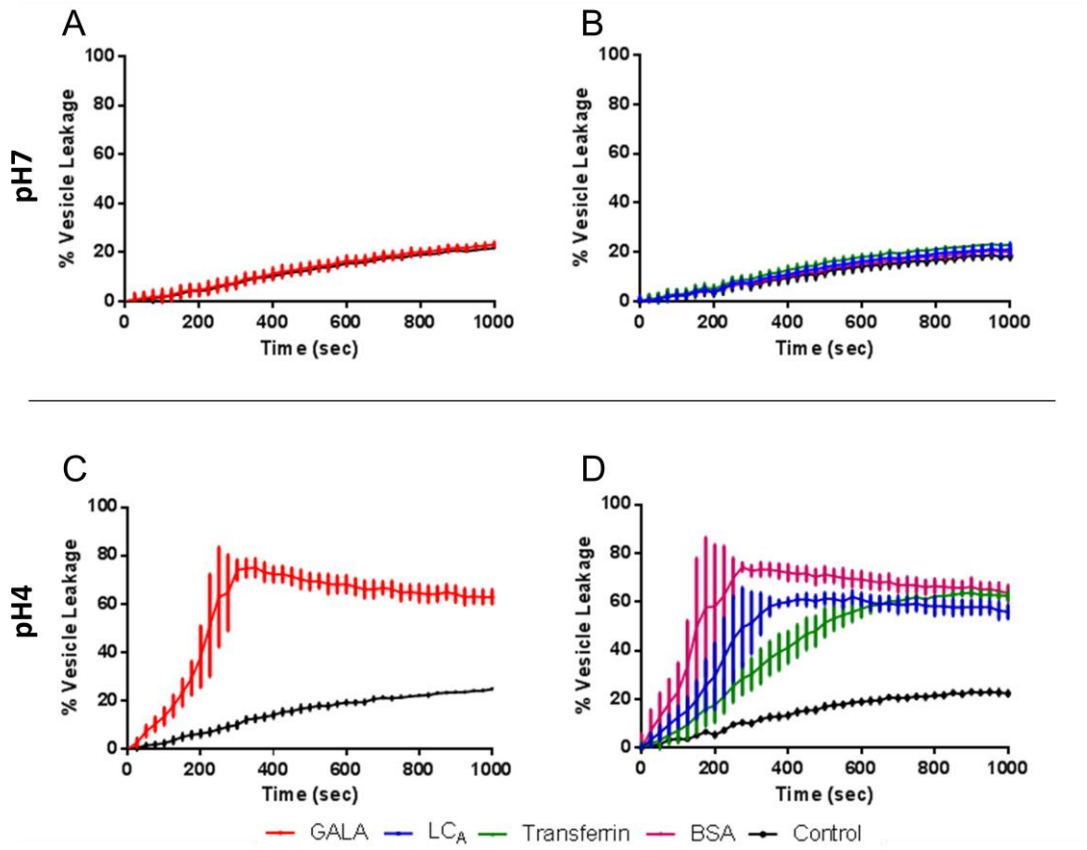

Figure 3-22 Positive and negative control proteins show vesicle leakage at pH4.
Vesicle leakage is measured over a time course of 1000 seconds at 37°C at either pH4 or pH7 (A) Vesicle leakage induced by the addition of 1µM GALA at pH7 (n=3). (B) Vesicle leakage induced by the addition of 1µM LC_A, Transferrin and BSA respectably at pH7 (n=3). (C) Vesicle leakage induced by the addition of 1µM GALA at pH4 (n=3). (D) Vesicle leakage induced by the addition of 1µM LC_A, Transferrin and BSA respectively at pH4 (n=3).

	T50% (Seconds)	% Vesicle leakage at 1000 seconds
GALA	222.75	62.93
LC_A	281.00	55.99
Transferrin	489.55	62.62
Bovine Serum Albumin (BSA)	151.03	63.65

Table 3-2 Summary of the rate at which GALA, LC_A, Transferrin and BSA cause vesicle leakage.

3.4.3.2 *Botulinum neurotoxins and LH_N derivatives cause vesicle leakage in a concentration dependent manner*

The concentration dependent manner in which Botulinum neurotoxins and LH_N molecules cause vesicle leakage was assessed using a 96-well vesicle leakage assay. Vesicle leakage induced by 1, 0.1, 0.01 and 0.001µM concentrations of $BoNT_A$, $BoNT_E$, LH_A and LH_E was assessed at pH7 and pH4 respectively.

$BoNT_A$ and LH_A demonstrate vesicle leakage in a concentration dependent manner at pH4. At 1 and 0.1µM, $BoNT_A$ induces a faster rate of vesicle leakage in comparison to LH_A, demonstrated by T50% values of 182.16 and 394.24 to 330.86 and 467.33 seconds respectively.

$BoNT_E$ and LH_E both induce vesicle leakage in a concentration dependent manner at pH4; the rate at which these proteins do this is generally very similar. For example, the vesicle leakage caused by 1µM $BoNT_E$ and LH_E is similar with T50% values of 243.15 and 193.58 seconds respectively. Some specific differences were recognized, including at a concentration of 0.01µM where $BoNT_E$ demonstrates a faster rate of vesicle leakage than LH_E with T50% values of 590.55 and 709.01 seconds respectively.

The rate of vesicle leakage induced by a 0.01µM concentration of $BoNT_A$ and $BoNT_E$ at pH4 shows a definable difference between the two serotypes potential to cause vesicle leakage. $BoNT_E$ demonstrates a T50% value of 590.55 seconds whereas $BoNT_A$ does not reach 50% vesicle leakage over the 1000 second time course.

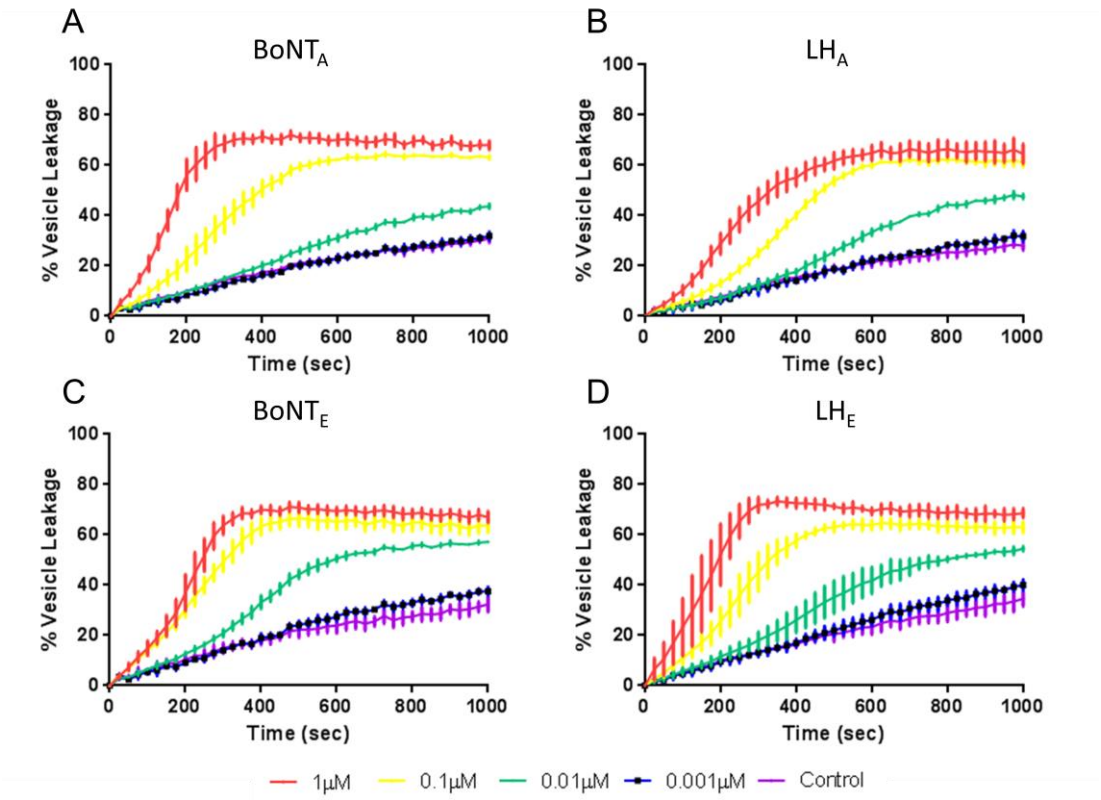

Figure 3-23 Removing the H_C domain of BoNT serotypes A and E effects vesicle leakage in a concentration dependent manner

Vesicle leakage is measured over a time course of 1000 seconds at 37°C (pH4) (A) Vesicle leakage induced by 1, 0.1, 0.001 and 0.0001µM $BoNT_A$ respectively (n=3). (B) Vesicle leakage induced 1, 0.1, 0.001 and 0.0001µM LH_A respectively (n=3). (C) Vesicle leakage induced by 1, 0.1, 0.001 and 0.0001µM $BoNT_E$ respectively (n=3). (D) Vesicle leakage induced by 1, 0.1, 0.001 and 0.0001µM LH_E respectively (n=3).

	Concentration (µM)	T50% (Seconds)	% Vesicle leakage at 1000 seconds
$BoNT_A$	1	182.16	67.99
	0.1	394.24	63.25
	0.01	n/a	43.72
	0.001	n/a	31.94
$BoNT_E$	1	243.15	67.08
	0.1	303.67	63.664
	0.01	590.55	57.233
	0.001	n/a	37.50
LH_A	1	330.86	64.361
	0.1	467.33	61.32
	0.01	n/a	47.66
	0.001	n/a	31.78
LH_E	1	193.58	68.60
	0.1	329.38	62.98
	0.01	709.01	54.47
	0.001	n/a	40.01

Table 3-3 Summary of the rate at which $BoNT_A$, $BoNT_E$, LH_A and LH_E cause vesicle leakage over a concentration range of 1 to 0.001µM at pH4

3.4.3.3 *The rate at which BoNT and LH_N proteins interact with lipid vesicles is pH dependent*

Botulinum neurotoxins are known to require a low pH to form pores in membranes (Montecucco et al., 1994). Here we investigate the role of the receptor binding domain in modulating pH dependency of vesicle leakage induced by $BoNT_A$, $BoNT_E$, LH_A and LH_E whilst varying the pH level at which the interaction occurs.

The rate of vesicle leakage induced by the addition of 0.05µM $BoNT_A$, $BoNT_E$, LH_A and LH_E is reduced by increasing the extra-vesicular pH (Figure 3-24). Removing the H_C domain of $BoNT_A$ has the effect of reducing the rate of vesicle leakage achieved at pH3, 4 and 4.5 (Figure 3-24 A and B). In contrast to serotype A, removing the H_C domain of $BoNT_E$ did not have a pronounced effect on the rate of vesicle leakage initiated at pH3, 4 and 4.5. The most notable difference between $BoNT_E$ and LH_E induced vesicle leakage was seen at pH4 with T50% values of 432.16 and 455.88 seconds respectively. A striking difference

between BoNT serotype A and serotype E proteins was that serotype E caused vesicle leakage at pH5 whereas serotype A did not. Leakage caused by serotype E is less pH dependent than that caused by serotype A.

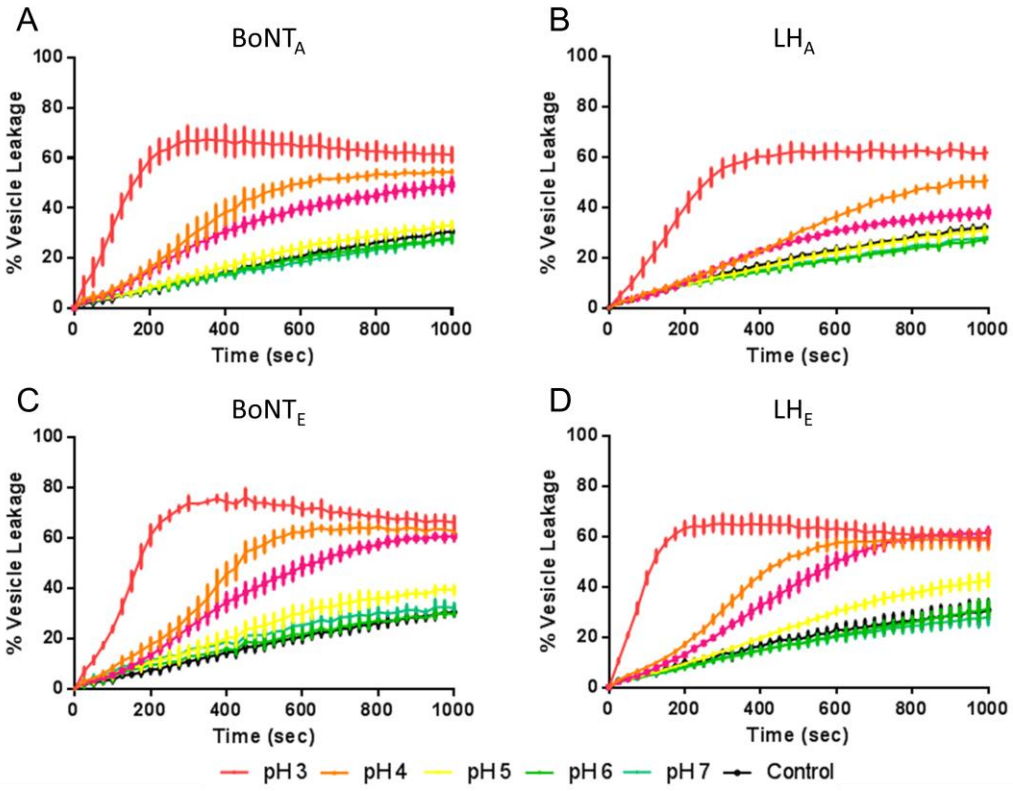

Figure 3-24 Removing the H_C domain of BoNT serotypes A and E affects the rate of vesicle leakage at pH 3-7.

Vesicle leakage is measured over a time course of 1000 seconds at 37°C following the addition of 0.05µM BoNT and LH_N serotypes A and E. (A) Vesicle leakage induced by 0.05µM $BoNT_A$ at pH 3, 4, 5, 6 and 7 respectively (n=3). (B) Vesicle leakage induced by 0.05µM LH_A at pH 3, 4, 5, 6 and 7 respectively (n=3). (C) Vesicle leakage induced by 0.05µM $BoNT_E$ at pH 3, 4, 5, 6 and 7 respectively (n=3). (D) Vesicle leakage induced by 0.05µM LH_E at pH 3, 4, 5, 6 and 7 respectively (n=3).

	pH	T50% (Seconds)	% Vesicle leakage at 1000 seconds
$BoNT_A$	3	157.77	61.22
	4	606.45	54.47
	4.5	n/a	49.37
	5	n/a	33.10
	6		27.88
	7		27.46
$BoNT_E$	3	168.19	66.17
	4	432.16	62.83
	4.5	630.12	60.86
	5	n/a	39.24
	6	n/a	29.78
	7	n/a	32.30
LH_A	3	256.77	62.01
	4	920.10	50.96
	4.5	n/a	38.22
	5	n/a	31.19
	6	n/a	26.45
	7	n/a	28.38
LH_E	3	118.52	59.52
	4	455.88	58.62
	4.5	596.56	61.73
	5	n/a	42.74
	6	n/a	31.23
	7	n/a	27.89

Table 3-4 Summary of the rate at which $BoNT_A$, $BoNT_E$, LH_A and LH_E cause vesicle leakage over a pH range of pH 7- pH 3

3.4.3.4 *Removing the H_C domain of BoNT effects the proteins ability to cause vesicle leakage at 20°C, 30°C and 40°C*

By controlling the temperature at which we assessed both BoNT and LH_N induced vesicle leakage we have attempted to gain insight into how removing the H_C domain of BoNT effects protein-vesicle interactions. Vesicle leakage induced by the addition of 0.1µM $BoNT_A$, $BoNT_E$, LH_A and LH_E to lipid vesicles at 20°C, 30°C and 40°C respectively elucidated differences in the temperature dependent way these molecules cause vesicle leakage.

$BoNT_A$ induced a faster rate of vesicle leakage than LH_A at 20°C, 30°C and 40°C respectively. The most remarkable difference can been seen at 20°C where the percentage vesicle leakage seen after 1000 seconds has been reduced from 47.18% to 18.22%, demonstrating the importance of the H_C domain to vesicle leakage at 20°C. At 30°C the removal of $BoNT_A$'s H_C domain reduces the proteins ability to induce vesicle leakage demonstrated by an increase in T50% time from 304.17 ($BoNT_A$) to 877.49 seconds (LH_A).

Variation in the rate at which serotype E molecules ($BoNT_E$ and LH_E) induced vesicle leakage at 20°C, 30°C and 40°C was not as pronounced as seen for serotype A ($BoNT_A$ and LH_A). In stark contrast to serotype A proteins, the vesicle leakage exhibited by both serotype E proteins at 20°C was similar, demonstrated by T50% values of 632.89 and 613.11 seconds for $BoNT_E$ and LH_E respectively. The most notable difference between $BoNT_E$ and LH_E induced vesicle leakage was at 30°C where LH_E has a slower rate of vesicle leakage (T50% values of 248.51 and 373.98 seconds respectively).

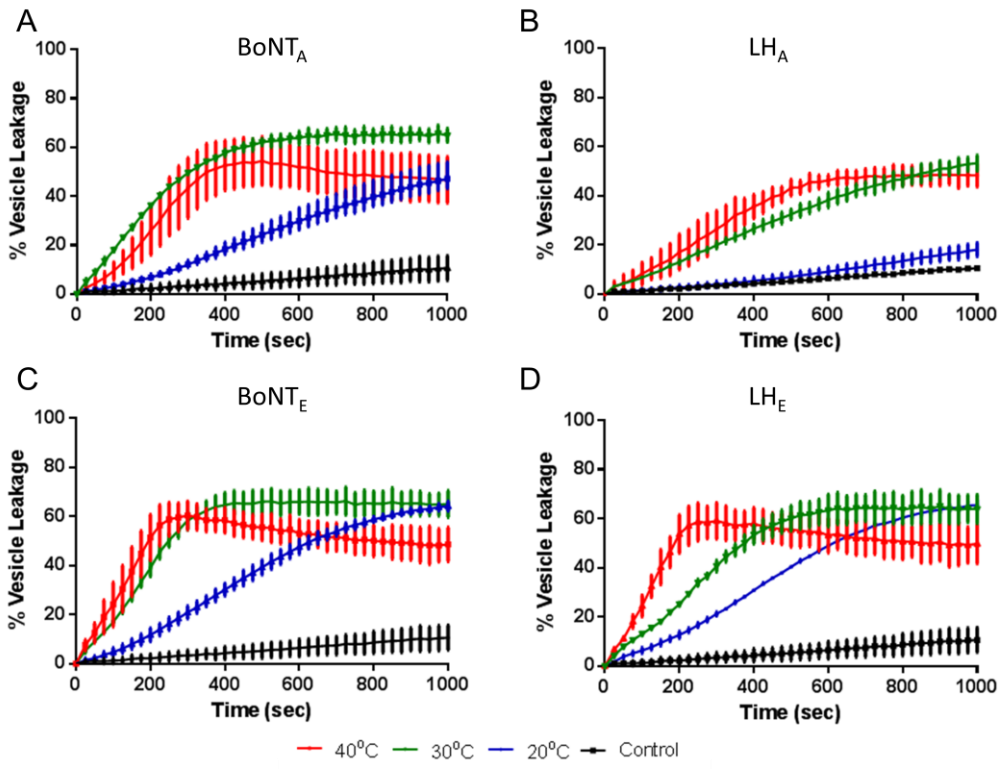

Figure 3-25 Removing the H_C domain of BoNT serotypes A and E affects the rate at which the proteins cause vesicle leakage.

Vesicle leakage measured over a time course of 1000 seconds following the addition of 0.1µM BoNT and LH_N serotypes A and E respectively (pH4). (A) Vesicle leakage induced by 0.1µM $BoNT_A$ at 40, 30 and 20°C respectively (n=3) (B) Vesicle leakage induced by 0.1µM LH_A at 40, 30 and 20°C respectively (n=3) (C) Vesicle leakage induced by 0.1µM $BoNT_E$ at 40, 30 and 20°C respectively (n=3) (D) Vesicle leakage induced by 0.1µM LH_E at 40, 30 and 20°C respectively (n=3).

	Temperature (Celsius)	T50% (Seconds)	% Vesicle leakage at 1000 seconds
$BoNT_A$	20°C	n/a	47.18
	30°C	304.17	64.94
	40°C	248.81	49.42
$BoNT_E$	20°C	632.89	64.22
	30°C	248.51	65.04
	40°C	194.58	48.57
LH_A	20°C	n/a	18.22
	30°C	877.49	53.40
	40°C	466.40	49.74
LH_E	20°C	613.11	65.59
	30°C	373.98	63.93
	40°C	187.22	49.74

Table 3-5 Summary of the rate at which $BoNT_A$, $BoNT_E$, LH_A and LH_E cause vesicle leakage at 20°C, 30°C and 40°C (pH4)

3.4.4 Discussion

In the previous chapter (3.3) an assay was set up which was expected, based on correlation with literature (Galloux et al., 2008; Lai et al., 2010), to possess the ability to determine BoNT induced pore formation in phospholipid membranes. Here we evaluated the assay by testing whether proteins with no known pore forming ability (negative control proteins) disrupted dye loaded vesicles at acidic pH. Following this, the potential of endonegative versions of $BoNT_A$ and $BoNT_E$ to cause vesicle leakage was compared to that of LH_A and LH_E molecules in an attempt to assess the effect of removing the receptor binding domain (H_C domain) on pore formation.

3.4.4.1 *All proteins interacted with DOPC:DOPG phospholipid vesicles at acidic pH*

In order to determine whether this vesicle leakage assay was an effective method of measuring pore formation in liposomes, a known pore forming peptide and three proteins with no known pore forming ability, were assessed for vesicle leakage at pH7 and pH4. GALA, a peptide reported to form pores in lipid vesicles at low pH (Nicol et al., 1999) was used to demonstrate that pH sensitive vesicle leakage could be achieved in accordance with literature. A 1µM concentration of GALA showed vesicle leakage at pH4 but not at pH7, this confirms that the assay used is capable of detecting pH sensitive peptide-membrane interactions that have been reported to be evidence of pore formation.

BSA, Transferrin and the light chain domain of $BoNT_A$ (LC_A) have no recognized ability to form pores; yet all three proteins induced vesicle leakage under acidic conditions (Figure 3-22). If proteins with no known pore forming ability are capable of causing vesicle leakage, then it is likely that the assay (at least under these conditions) cannot distinguish between *bona fide* pH regulated protein pore formation and a more general disruption of phospholipid membranes.

Acidic pH does not appear to destabilize phospholipid vesicles (Figure 3-22) (Lin et al., 2012), this suggests that any vesicle leakage that occurs at low pH does so via vesicle-protein interactions. If vesicle leakage does not occur as a direct result of a proteins known

pore forming ability, it must be due to non-specific vesicle-protein interactions. At acidic pH the charge presented by free electron pairs present on amino acid side chains will become neutralized via protonation. This will reduce the solubility of the protein and concurrently increase its lipophilicity which in turn may be responsible for an increase in protein-vesicle interaction and consequently vesicle leakage.

The lack of protein controls for low pH induced vesicle leakage in literature has been confirmed through correspondence with a respective author (Lai et al., 2010). This suggests that many vesicle leakage assays reported in literature may also report a more general lipophilicity of proteins at acidic pH rather than a specific pore forming activity of specialized proteins. This does not necessarily mean that pore formation does not occur, but suggests that some vesicle leakage assays may not report pore formation in isolation. One published example of a well controlled vesicle leakage assay, set up to report BoNT pore formation, showed the heavy chain of $BoNT_A$ to induce the release of K^+ ions from vesicles composed of phosphatidyl choline and phosphatidyl glycerol where the LC domain (negative protein control) did not (Shone et al., 1987).

3.4.4.2 *A comparison between $BoNT_A$ and $BoNT_E$ vesicle interaction*

Given that, in our assay, vesicle leakage was stimulated by proteins with no known pore forming ability, protein induced vesicle leakage in this assay could not be assumed to measure pore formation. Rather it represented protein interaction with a phospholipid membrane which may or may not have included a protein lined pore component. Here I discuss the effect of endonegative BoNT molecules (serotypes A and E) on phospholipid vesicles in order to further investigate their general interactions with membranes.

A comparison of the ability of BoNT serotypes A and E to cause vesicle leakage was conducted to identify whether $BoNT_E$'s faster rate of translocation (Kumaran et al., 2009) translated into a faster rate of vesicle leakage. $BoNT_E$ causes vesicle leakage at a faster rate in comparison to $BoNT_A$ over almost all of the conditions tested. The most striking comparison between the two molecules was seen at 0.01µM, pH 5 and 20°C where $BoNT_E$'s faster rate of vesicle leakage suggested that it possesses structural qualities which allow it

to associate with vesicles in a way which is more energetically favorable than $BoNT_A$. $BoNT_E$'s propensity to induce a faster rate of vesicle leakage at 20°C may be suggestive of structural properties needed to sustain toxin activity in cold blooded animals such as fish (Piazza et al., 2011).

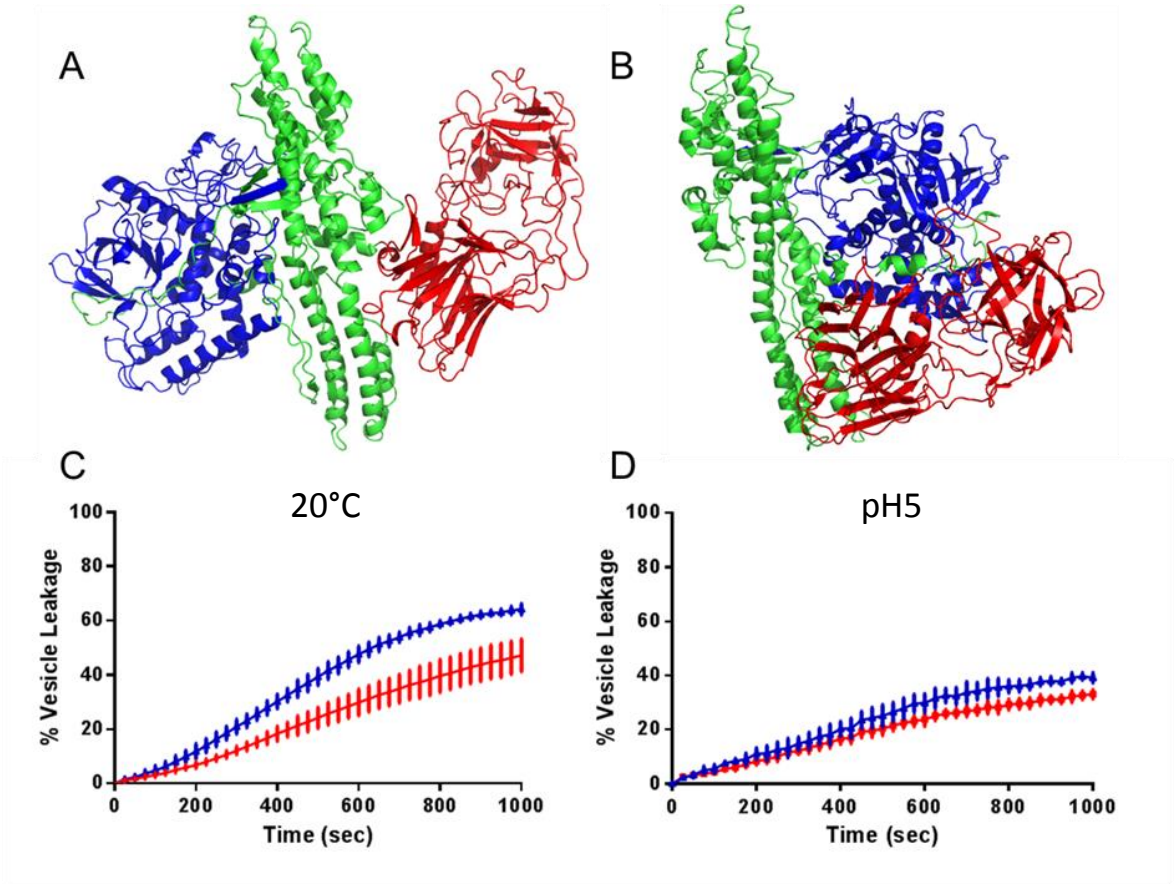

Figure 3-26 $BoNT_E$ induces a faster rate of vesicle leakage than $BoNT_A$ at 20°C and pH5
(A) and (B) The crystal structure of Botulinum neurotoxin serotype A (3BTA) and E (3FFZ) respectively (Kumaran et al., 2009; Lacy et al., 1998); the receptor binding domain (H_C domain) is displayed in red, the translocation domain (H_N domain) in green and the catalytic domain (Light chain, LC domain) in blue. (C) Vesicle leakage induced by $BoNT_A$ (red) and $BoNT_E$ (blue) at 20°C over 1000s (pH4). (D) Vesicle leakage induced by $BoNT_A$ (red) and $BoNT_E$ (blue) at pH5 over 1000s.

3.4.4.3 *Vesicle leakage is induced by BoNT and LH_N molecules*

As discussed earlier, by removing the H_C domain of BoNT's we create LH_N proteins. LH_N proteins are known to form pores in Neuro2A cell membranes (Fischer and Montal, 2007b), cleave endogenous SNARE proteins (Chaddock et al., 2002) and are suggested to be

responsible for the translocation function of BoNT. As a result of this it is hypothesised that they could be considered a good and safe model to investigate BoNT pore formation.

Here we compare and contrast vesicle leakage caused by BoNT and LH_N proteins of the same serotype, thus elucidating the effect of removing the H_C domain on BoNT-vesicle interaction.

Removing the H_C domain of $BoNT_A$ affects the proteins ability to cause vesicle leakage in three ways; (1) the rate of vesicle leakage is reduced at high concentrations; (2) the rate of vesicle leakage is reduced at pH4; (3) little to no vesicle leakage occurs at 20°C. The third factor is by far the most pronounced; if vesicle leakage is drastically reduced by removing the H_C domain of $BoNT_A$ this may be evidence that the protein adopts a stable conformation that has less propensity to be lipophilic. Whether or not this change in the proteins lipophilicity identifies properties of LH_A that would be relevant in a physiological environment is unclear as the conditions under which this change has been observed are not physiological. Further analysis of the protein by Circular dichroism at various pH levels and temperatures would allow further analysis of this point.

Removing the receptor binding domain of $BoNT_E$ has a very minimal effect on the proteins propensity to cause vesicle leakage. The concentration and pH range at which LH_E is able to induce vesicle leakage is very similar to that of $BoNT_E$ suggesting that the proteins behave very similarly in interaction with lipid membranes under the conditions tested. The only notable difference between $BoNT_E$ and LH_E induced vesicle leakage occurs at 30°C for a reason not apparent in these experiments. Unlike removing the H_C domain of $BoNT_A$, removing the H_C domain of $BoNT_E$ does not seem to inhibit the protein's ability to cause vesicle leakage at 20°C, why this may be the case is not clear but could be related to a difference in the three-dimensional structures of these two serotypes.

3.4.5 Conclusion

Proteins with known and no-known pore forming ability have been assessed for their potential to cause vesicle leakage at pH4 and pH7. This has revealed that this vesicle

leakage assay is not capable of distinguishing between pore forming and non-pore forming proteins at acidic pH. Consequently, based on these results, we cannot conclude that BoNT induced vesicle leakage is as a direct result of BoNT pore formation and H_N domain membrane insertion.

Removing the receptor binding domain (H_C domain) of BoNT serotype A has a more pronounced effect on the rate at which it is capable of causing vesicle leakage than removing the H_C domain of $BoNT_E$. Removing the H_C domain of $BoNT_A$ reduces the proteins potential to cause vesicle leakage over a range of concentrations, pH values and temperatures; the most remarkable of these is LH_A's lack of ability to cause vesicle leakage at 20°C suggesting that LH_A possesses different structural characteristics in comparison to $BoNT_A$. Concurrently, the removal of $BoNT_E$'s H_C domain has little effect on the proteins ability to cause vesicle leakage.

3.5 The serotype specific interaction of LH_N proteins with phospholipid membranes.

3.5.1 Introduction

Botulinum neurotoxins have evolved simultaneously in a range of genetically diverse clostridia species. This evolution has resulted in seven genetically and functionally distinct serotypes (serotypes A-H) and an unknown number of sub serotypes. How these seven serotypes are functionally distinct is still an area of great potential discovery (Figure 3-27).

Current evidence for sterotypically distinct BoNT function can be broken down into four areas; receptor binding, pore formation, LC domain translocation and SNARE cleavage (Chapter 1, Introduction). Here we attempt to investigate the relationship between serotype and pore formation, perhaps the least understood mechanism of BoNT intoxication.

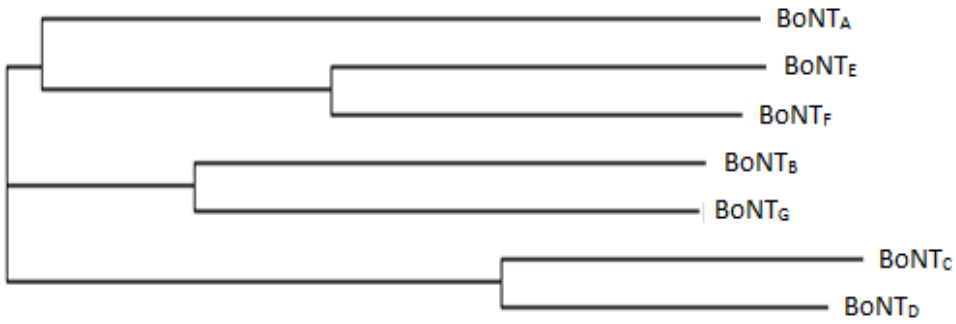

Figure 3-27 Comparison of the translated genetic sequences of BoNT serotypes A-G.
Shown above is a neighbor-joining alignment of the nucleotide coding regions of the seven serotypes of BoNT (A through G).

3.5.1.1 *Aim*

In the previous chapter non-specific protein-vesicle interactions were determined to disrupt phospholipid vesicles at acidic pH. In order to investigate whether at least some

component of the observed vesicle leakage can be attributed to protein pore formation in vesicle membranes, an attempt has been made to visualise vesicle-protein interaction through electron-microscopy.

Whether or not LH_N proteins form pores in lipid vesicles, the rate at which they disrupt lipid vesicles over various concentration, pH and temperature conditions is evidence of the proteins lipophilicity and potentially their propensity to insert into vesicle membranes. For this reason, five different serotypes of LH_N (serotypes A-E) were compared for their potential to cause vesicle leakage under various concentrations, pH levels and temperatures. Furthermore, the effect of reducing the disulphide bond between the H_N and LC domains of LH_N molecules (serotypes A-D) was examined to see whether removing this interaction would influence the lipophicitiy of H_N domains.

3.5.2 Methods

3.5.2.1 *Electron microscopy*

50µl of 1mg/ml protein solution was mixed with 100µl of phospholipid vesicles for one hour in low pH buffer to mirror conditions seen during vesicle leakage assays (25mM Tris, 50mM NaCl, pH4) at room temperature. The samples were then loaded onto glow discharged carbon-coated copper grids and negative staining with 0.75% (w/v) Uranyl Formate. Micrographs were recorded at a nominal magnification of 50,000x on a Philips CM100 electron microscope operating at 100kV.

3.5.2.2 *Vesicle creation*

See section 3.4.2.1

3.5.2.3 *Vesicle concentration/calibration assay*

See section 3.4.2.2

3.5.2.4 *Vesicle leakage assay*

See section 3.4.2.3.

3.5.2.5 *Data analysis*

See section 3.3.2.4.

3.5.3 Results

3.5.3.1 *Using electron microscopy to visualize pore formation*

To qualify whether $BoNT_A$, LH_A, GALA or the light chain domain of BoNT serotype A (LC_A) form pores in phospholipid vesicles, election microscopy was used to directly visualise protein-vesicle interactions. The stain used for electron microscopy (Uranyl Formate) binds to proteins but not to phospholipids allowing the distinction to be made between protein and lipid structures; consequently proteinous patches appear dark and vesicle membranes appear transparent (Lai et al., 1984).

In the absence of protein, no intact vesicles were visualised (Figure 3-28, A). This is the expected result because the stain does not bind to phospholipids. Pre-incubation of vesicles with LH_A, LC_A or $BoNT_A$ revealed intact vesicle structures; this visualisation was not apparent following pre-incubation with the GALA pore forming peptide or with reduced LH_A protein.

Following pre-incubation with $BoNT_A$ and LH_A (proteins with known pore forming activity), vesicles had a dark coating and small round dark patches (Figure 3-28 B, C and D). In contrast, vesicles pre-incubated with LC_A had a dark proteinous coating, but no small dark circular patches Figure 3-29, C). This is suggestive of a difference between the protein-vesicle interactions of known pore forming proteins and non-pore forming proteins.

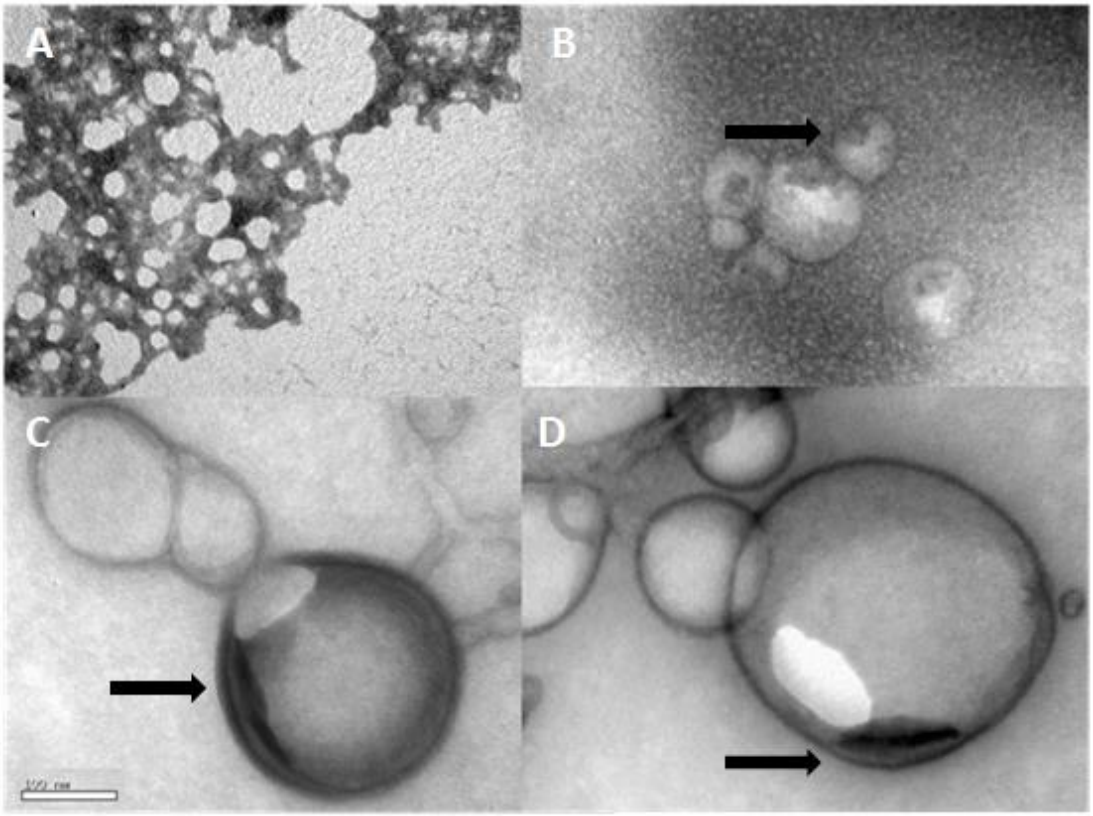

Figure 3-28 Electron micrographs of vesicle-protein interactions.
DOPC/DOPG vesicle membranes were incubated with assay buffer, LH_A and $BoNT_A$ respectively at pH4. (A) Electron micrograph depicting the effect of assay buffer on vesicles. (B) Electron micrograph of the effect of 1µM LH_A on lipid vesicles after a ten minute incubation. (C and D) Electron micrograph of the effect of 1µM $BoNT_A$ on lipid vesicles after a ten minute incubation. Dark patches attributed to protein aggregation have been identified using black arrows.

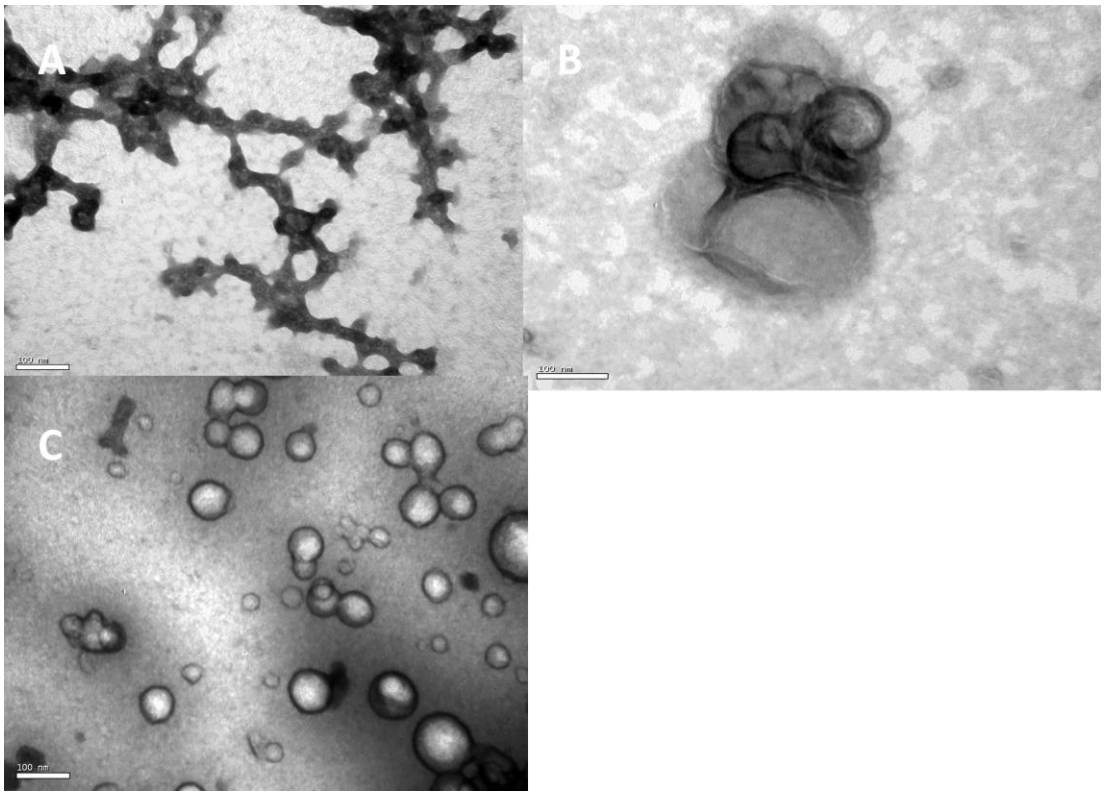

Figure 3-29 Electron micrographs of vesicle-protein interactions.
DOPC/DOPG vesicle membranes were incubated with reduced LH_A, GALA and LC_A respectively at pH4. (A) Electron micrograph of the effect of 1 µM reduced LH_A on phospholipid vesicles. (B) Electron micrograph of the effect of 1 µM GALA on phospholipid vesicles. (C) Electron micrograph of the effect of 1µM LC_A on lipid vesicles.

3.5.3.2 *Concentration dependent/ serotype specific vesicle leakage*

The vesicle leakage assay was used as a tool to define serotype specific differences in the rate at which LH_N proteins disrupt vesicular membranes. Here the concentration dependency of vesicle-LH_N interaction is assessed for LH_N serotypes A-E (all experiments were completed at pH4).

After 1000 seconds LH_A concentrations of 1, 0.1, and 0.001µM caused vesicle leakage of 64.36, 63.25 and 43.72% respectively at pH4. No other concentrations of LH_A tested showed vesicle leakage. 1µM LH_A demonstrated a time to 50% vesicle leakage (T50%) value of 330.86 seconds, consequently LH_A showed the slowest rate of vesicle leakage at a 1µM concentration (Figure 3-30, A) (pH4).

LH_B is distinctive in vesicle leakage assays as it was the only serotype to induce no vesicle leakage at 0.01µM (Figure 3-30, B), pH4. After 1000 seconds LH_B concentrations of 1 and 0.1µM caused vesicle leakage of 66.13 and 56.86% respectively. LH_B demonstrated a T50% time of 199.26 and 462.92 seconds at concentrations of 1 and 0.1µM respectively demonstrating the second fastest rate of vesicle leakage at 1µM.

When tested at a concentration of 0.001µM, LH_C showed the highest level of vesicle leakage after 1000 seconds (42.51%) (Figure 3-30, C). LH_C demonstrates a T50% time of 228.31, 303.93 and 567.44 seconds at concentrations of 1, 0.1 and 0.01µM respectively.

LH_D displayed the highest rate of vesicle leakage at concentrations of 0.1 and 0.01 µM respectively (Figure 3-30, D). After 1000 seconds LH_D concentrations of 1, 0.1, 0.01, 0.001µM caused vesicle leakage of 71.40, 65.96, 57.97 and 39.18% respectively. LH_D demonstrated a T50% time of 209.40, 228.04 and 398.84 seconds at concentrations of 1, 0.1 and 0.01µM respectively.

LH_E displayed the highest rate of vesicle leakage at 1µM (Figure 3-30, E). After 1000 seconds LH_E concentrations of 1, 0.1, 0.01, 0.001µM caused vesicle leakage of 68.60, 62.98,

54.47 and 40.01% respectively. LH_E demonstrated a T50% time of 193.58, 329.38 and 790.01 seconds at concentrations of 1, 0.1 and 0.01µM respectively.

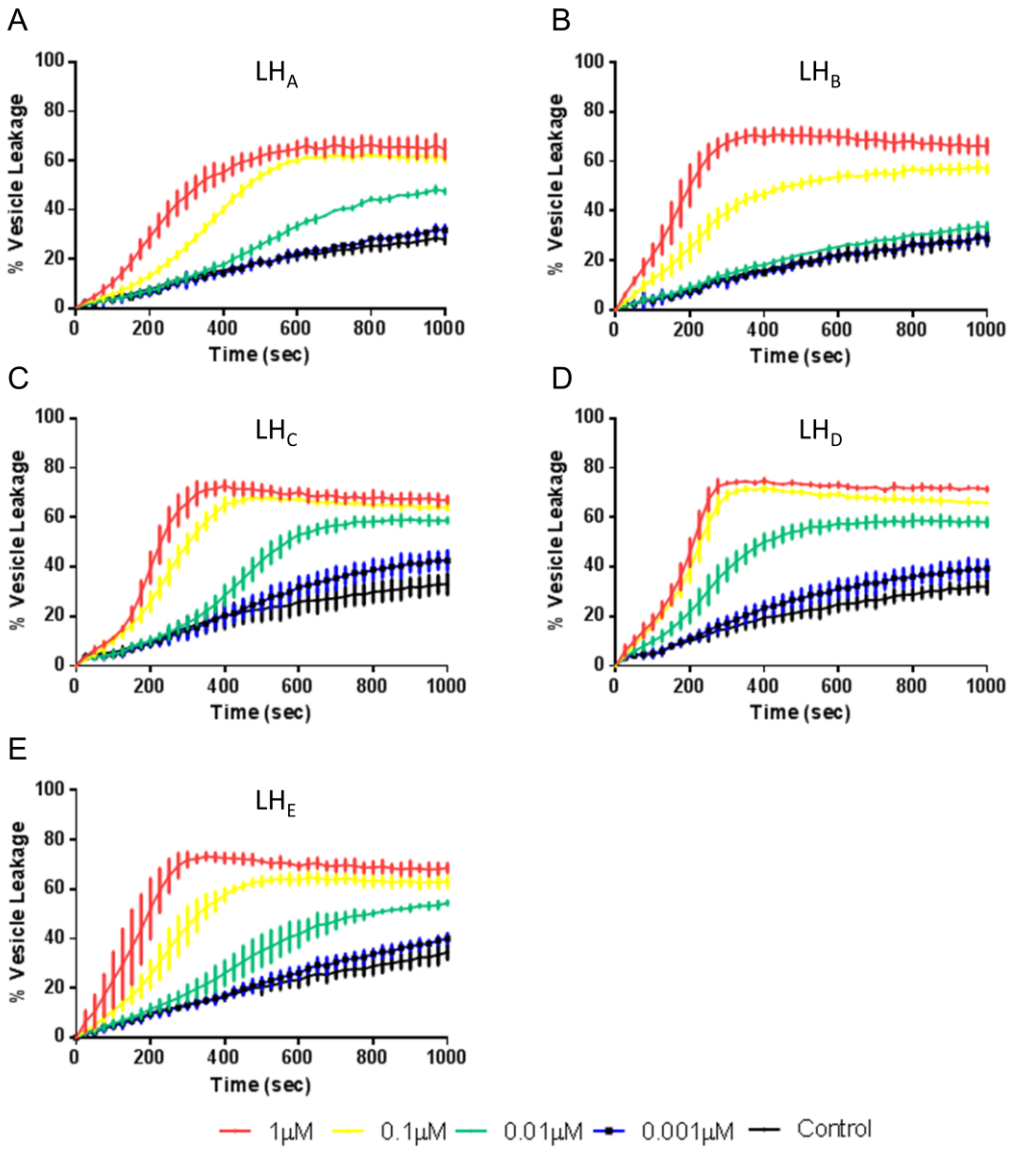

Figure 3-30 LH_N serotypes A-E cause vesicle leakage in a concentration dependent manner.

Vesicle leakage is measured over a time course of 1000 seconds at 37°C (pH4) (A) Vesicle leakage induced by 1, 0.1, 0.001 and 0.0001µM LH_A respectively (n=3). (B) Vesicle leakage induced by 1, 0.1, 0.001 and 0.0001µM LH_B respectively (n=3). (C) Vesicle leakage induced by 1, 0.1, 0.001 and 0.0001µM LH_C respectively (n=3). (D) Vesicle leakage induced by 1, 0.1, 0.001 and 0.0001µM LH_D respectively (n=3). (E) Vesicle leakage induced by 1, 0.1, 0.001 and 0.0001µM LH_E respectively (n=3).

	Concentration (µM)	T50% (Seconds)	% Vesicle leakage at 1000 seconds
LH_A	1	330.86	64.36
	0.1	394.24	63.25
	0.01	n/a	43.72
	0.001	n/a	31.94
LH_B	1	199.26	66.13
	0.1	462.928	56.86
	0.01	n/a	33.57
	0.001	n/a	28.73
LH_C	1	228.31	66.98
	0.1	303.93	64.03
	0.01	567.44	58.74
	0.001	n/a	42.51
LH_D	1	209.40	71.40
	0.1	228.04	65.96
	0.01	398.84	57.97
	0.001	n/a	39.18
LH_E	1	193.58	68.60
	0.1	329.38	62.98
	0.01	790.01	54.47
	0.001	n/a	40.01

Table 3-6 Summary of the rate at which LH_N seortypes A-E cause vesicle leakage over a concentration range of 1 to 0.001µM.

3.5.3.3 *pH dependent / serotype specific vesicle leakage*

It has long been established that acidification of the endosomal compartment is essential to the action of Botulinum neurotoxins (Montecucco et al., 1994). Here we demonstrate how LH_N serotypes A-E interact with vesicular membranes under different pH conditions in an attempt to provide insight into the lipophilicity of various LH_N serotypes over a range of pH conditions. As LH_N molecules (serotypes A-E) were shown to cause vesicle leakage in a concentration dependent manner, it has been necessary to complete the analysis of pH dependent vesicle leakage using concentrations of LH_N molecules which allow both positive and negative trends in pH dependant vesicle leakage to be assessed.

A 0.05μM concentration of LH_A caused vesicle leakage at pH3 and pH4 respectively. The rate at which LH_A caused vesicle leakage at pH3 was approximately 3.5x greater than at pH4 (T50% values of 256.77 and 920.10 seconds respectively).

A 0.1μM concentration of LH_B caused vesicle leakage at pH3, pH4 and pH5 respectively. The rate at which LH_B caused vesicle leakage at pH3 was approximately 2x greater than at pH4 (T50% values of 457.88 and 901.35 seconds respectively). In comparison to other serotypes, LH_B demonstrated the lowest rate of vesicle leakage at pH3 even though it is tested at the highest concentration.

A 0.01μM concentration of LH_C caused vesicle leakage at pH3 and pH4 respectively. The rate at which LH_C caused vesicle leakage at pH3 was approximately 0.75x greater than at pH4 (T50% values of 513.30 and 682.36 seconds respectively). LH_C showed the lowest increase in rate between pH4 and pH3 of all serotypes.

A 0.01μM concentration of LH_D caused vesicle leakage at pH3, pH4 and pH5 respectively. The rate at which LH_D caused vesicle leakage at pH3 was approximately 1.3x greater than at pH4 (T50% values of 294.00 and 379.01 seconds respectively) and approximately 3.2x greater than at pH5 (T50% value of 953.25 seconds respectively). LH_D demonstrated the highest rate of vesicle leakage seen at pH5 even though it was tested at the lowest concentration.

A 0.05μM concentration of LH_E caused vesicle leakage at pH3, pH4 and pH5 respectively. The rate at which LH_E caused vesicle leakage at pH3 was approximately 3.8x greater than at pH4 (T50% values of 455.88 and 118.52 seconds respectively). LH_E had the fastest rate of vesicle leakage at pH3 although it was tested at a higher concentration than LH_C and LH_D respectively.

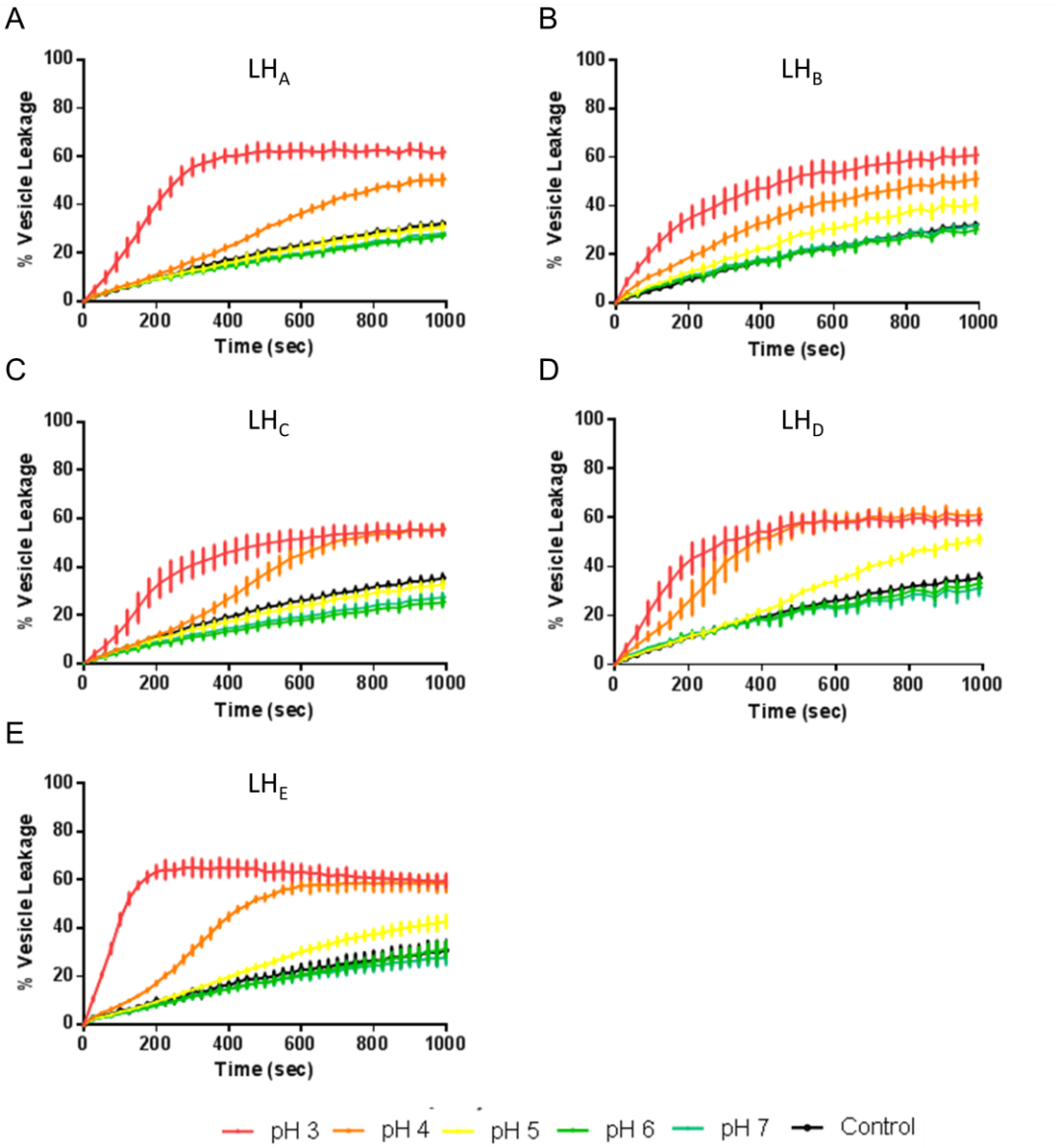

Figure 3-31 LH_N serotypes A-E cause vesicle leakage in a pH dependent manner at pH 3-7. Vesicle leakage is measured over a time course of 1000 seconds at 37°C following the addition of 0.05µM LH_A, 0.1µM LH_B, 0.01µM LH_C, 0.01µM LH_D and 0.05µM LH_E respectively. (A) Vesicle leakage induced 0.05µM LH_A at pH 3, 4, 5, 6 and 7 respectively (n=3). (B) Vesicle leakage induced by 0.1µM LH_B at pH 3, 4, 5, 6 and 7 respectively (n=3). (C) Vesicle leakage induced by 0.01µM LH_C at pH 3, 4, 5, 6 and 7 respectively (n=3). (D) Vesicle leakage induced by 0.01µM LH_D at pH 3, 4, 5, 6 and 7 respectively (n=3). (E) Vesicle leakage induced by 0.05µM LH_E at pH 3, 4, 5, 6 and 7 respectively (n=3).

	pH	T50% (Seconds)	% Vesicle leakage at 1000 seconds
LH_A	3	256.77	62.01
	4	920.10	50.96
	5	n/a	31.19
	6	n/a	26.45
	7	n/a	28.38
LH_B	3	457.88	61.04
	4	901.35	51.27
	5	n/a	41.50
	6	n/a	30.45
	7	n/a	32.35
LH_C	3	513.30	55.64
	4	682.36	56.06
	5	n/a	33.29
	6	n/a	25.74
	7	n/a	27.7
LH_D	3	294.00	59.30
	4	379.01	61.47
	5	953.25	51.61
	6	n/a	33.25
	7	n/a	31.47
LH_E	3	118.52	59.52
	4	455.88	58.62
	5	n/a	42.74
	6	n/a	31.23
	7	n/a	27.89

Table 3-7 Summary of the rate at which LH_N seortypes A-E cause vesicle leakage over a pH range of pH7-pH3.

3.5.3.4 *The serotype specific temperature dependence of LH_N induced vesicle leakage*

Botulinum neurotoxins are known to intoxicate cold and warm blooded organisms. The temperature dependent nature of a serotype's interaction with lipid membranes may provide evidence of why different serotypes induce a toxic effect at different temperatures. All experiments were completed using an LH_N concentration of 0.1µM at pH4, this allows direct comparisons to be drawn between the rate at which all five serotypes of LH_N cause vesicle leakage at 20°C, 30°C and 40°C.

LH_A caused little or no vesicle leakage at 20°C in stark contrast with all other serotypes (18.22% vesicle leakage after 1000 seconds). However, LH_A did induce vesicle leakage at 40°C and 30°C with T50% values of 466.40 and 877.49 seconds respectively. Increasing the temperature from 30°C to 40°C caused an approximate 1.8x increase in the rate of LH_A induced vesicle leakage.

LH_B induced vesicle leakage at 20°C, 30°C and 40°C, this caused vesicle leakage of 38.72, 53.73 and 46.38% respectively after 1000 seconds. Due to this comparatively low level of vesicle leakage, LH_B only presented a T50% value at 30°C (761.48 seconds).

Vesicle leakage occurred at 20°C, 30°C and 40°C following the introduction of 0.1µM LH_C to lipid vesicles, showing T50% values of 961.74, 448.12 and 246.85 respectively. The rate of vesicle leakage induced by LH_A increased by approximately 2.2x after increasing the temperature from 20°C to 30°C and approximately 1.8x after increasing the temperature from 30°C to 40°C.

LH_D caused a higher rate of vesicle leakage than LH_N serotypes A, B, C and E at 20°C, 30°C and 40°C. Increasing the temperature of the assay from 20°C to 30°C increased the rate of vesicle leakage by approximately 1.2x, further increasing the temperature from 30°C to 40°C caused a further 1.7x increase in the rate of vesicle leakage.

LH_E caused a higher rate of vesicle leakage than LH_N serotype A, B and C at 20°C, 30°C and 40°C. Increasing the temperature of the assay from 20°C to 30°C increased the rate of vesicle leakage by approximately 1.6x, further increasing the temperature from 30°C to 40°C caused a further 2x increase in the rate of vesicle leakage.

The stability of lipid vesicles at 20°C, 30°C and 40°C was assessed through measuring spontaneous vesicle leakage under assay conditions (Figure 3-32, C). The lowest level of spontaneous vesicle leakage was seen at 20°C suggesting that vesicles show a higher level of stability below a temperature of 30°C.

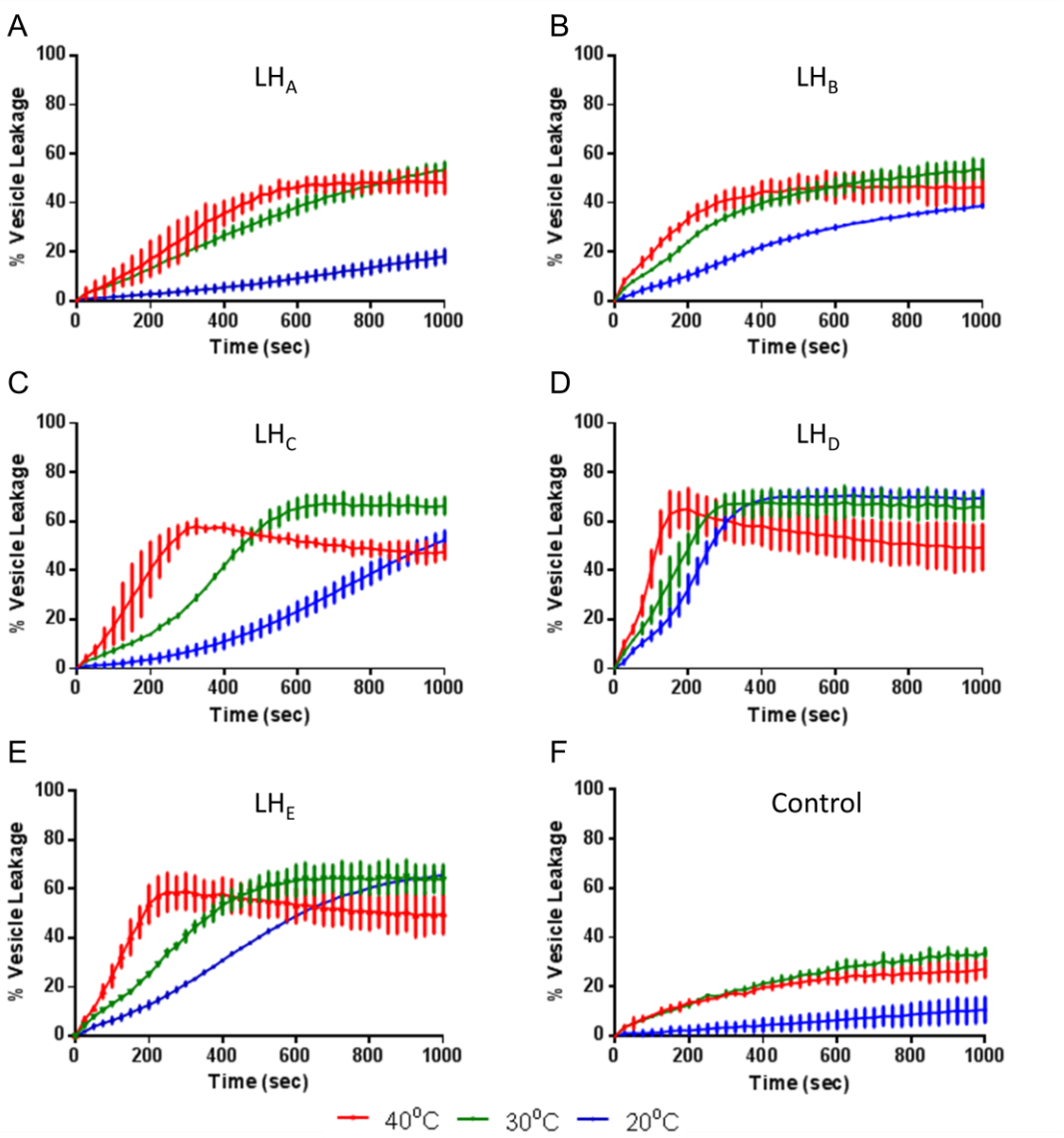

Figure 3-32 LH$_N$ proteins (serotypes A-E) cause vesicle leakage in a temperature dependent manner.

Vesicle leakage is measured over a time course of 1000 seconds following the addition of 0.1µM LH$_N$ serotypes A to E respectively (pH4). (A) Vesicle leakage induced by 0.1µM LH$_A$ at 40, 30 and 20°C respectively (n=3) (B) Vesicle leakage induced by 0.1µM LH$_B$ at 40, 30 and 20°C respectively (n=3) (C) Vesicle leakage induced by 0.1µM LH$_C$ at 40, 30 and 20°C respectively (n=3) (D) Vesicle leakage induced by 0.1µM LH$_D$ at 40, 30 and 20°C respectively (n=3). (E) Vesicle leakage induced by 0.1µM LH$_E$ at 40, 30 and 20°C respectively (n=3). (F) Vesicle leakage induced by assay buffer at 40, 30 and 20°C respectively (n=3).

	Temperature (Celsius)	T50% (Seconds)	% Vesicle leakage at 1000 seconds
LH_A	20°C	n/a	18.22
	30°C	877.49	53.40
	40°C	466.40	49.74
LH_B	20°C	n/a	38.72
	30°C	761.48	53.73
	40°C	n/a	46.38
LH_C	20°C	961.74	52.43
	30°C	448.12	66.26
	40°C	246.85	47.52
LH_D	20°C	260.70	69.35
	30°C	204.04	65.59
	40°C	115.58	49.41
LH_E	20°C	613.11	65.59
	30°C	373.98	63.93
	40°C	187.22	49.74

Table 3-8 Summary of the rate at which LH_N serotypes A-E cause vesicle leakage at 20°C, 30°C and 40°C.

3.5.3.5 *LH_N induced vesicle leakage in reducing and non-reducing conditions*

Vesicle leakage induced by a 1µM concentration of LH_N serotypes A-D has been assessed under non-reducing and reducing conditions (±10mM DTT) respectively. This has been completed to assess whether reducing the di-sulphide bond present between the H_N domain and LC domain of LH_N proteins affects the way in which the proteinous domains of LH_N interact with phospholipid vesicles.

Two serotypes of LH_N interact differently with phospholipid vesicles under reducing and non-reducing conditions respectively, namely LH_A and LH_C. Under reducing conditions, LH_A and LH_C caused vesicle leakage at a slightly faster rate than under non-reducing conditions (T50% values of 361.21 and 281.57 in comparison to 476.55 and 363.59 seconds, respectively).

Vesicle leakage induced through the interaction of LH_B and LH_D with phospholipid vesicles did not markedly change between reducing and non-reducing conditions (T50%

values for reducing 240.15 and 185.02 and non-reducing conditions 222.22 and 147.04 seconds respectively). Furthermore, lipid vesicles were found not to be destabilised in the presence and absence of 10mM DTT (reducing and non-reducing conditions respectively).

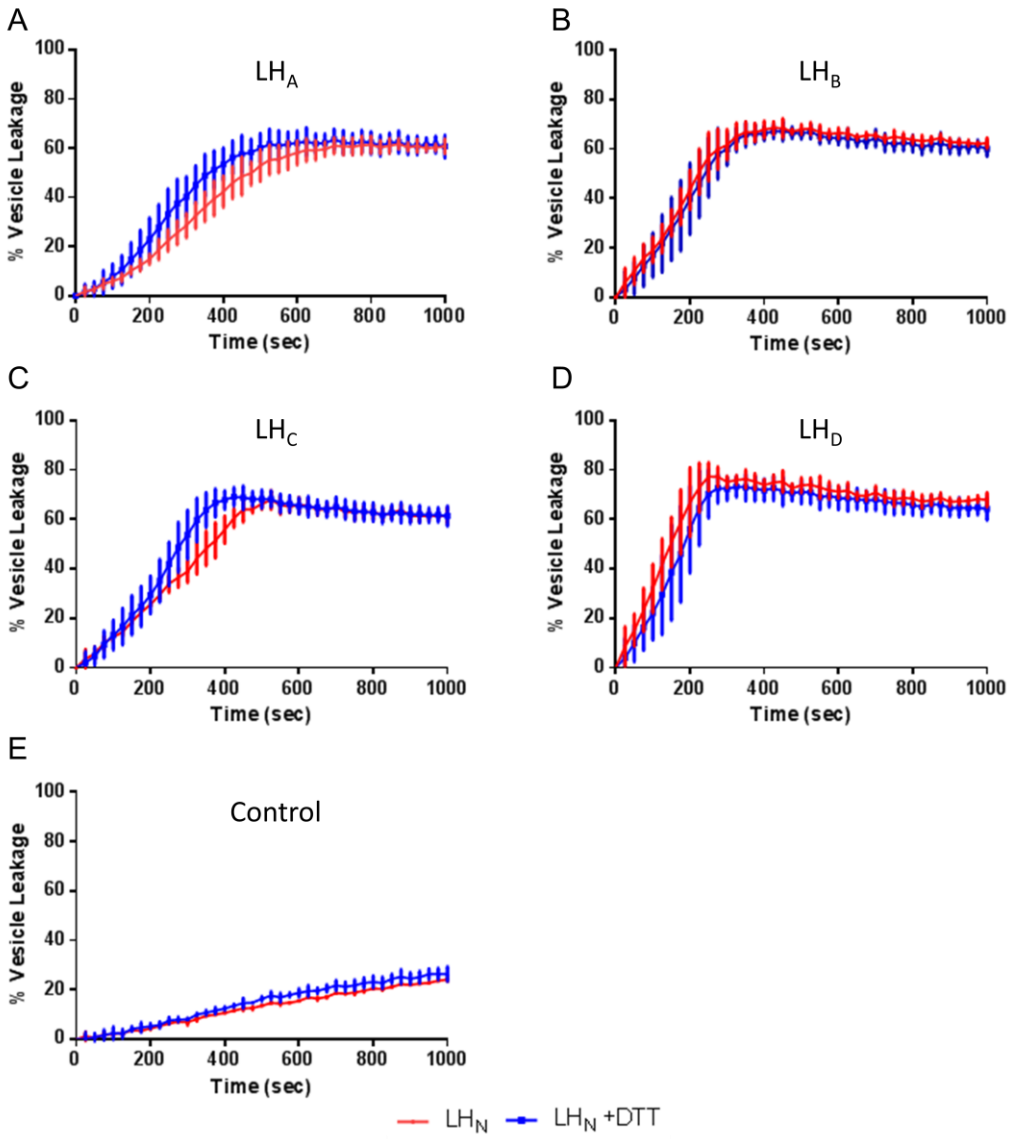

Figure 3-33 LH_N proteins cause vesicle leakage under reducing conditions.
Vesicle leakage is measured over a time course of 1000 seconds following the addition of 1µM LH_N serotypes A to D respectively (pH4). (A) Vesicle leakage induced by 1µM LH_A with and without 10mM DTT respectively (n=3) (B) Vesicle leakage induced by 1µM LH_B with and without 10mM DTT respectively (n=3) (C) Vesicle leakage induced by 1µM LH_C with and without 10mM DTT respectively (n=3) (D) Vesicle leakage induced by 1µM LH_D with and without 10mM DTT respectively (n=3) (E) Vesicle leakage induced by assay buffer with and without 10mM DTT respectively (n=3)

		T50% (Seconds)	% Vesicle leakage at 1000 seconds
LH_A	+DTT	361.21	60.79
	n/a	476.55	60.83
LH_B	+DTT	240.15	60.13
	n/a	222.22	62.38
LH_C	+DTT	281.57	61.27
	n/a	363.59	61.50
LH_D	+DTT	185.02	64.22
	n/a	147.94	67.88
Control	+DTT	n/a	26.45
	n/a	n/a	24.23

Table 3-9 Summary of the rate at which LH_N serotype A-D cause vesicle leakage in reducing and non-reducing conditions.

3.5.4 Discussion

Here we attempt to measure serotype specific differences in the way in which LH_N molecules interact with lipid vesicles, through this we attempt to determine serotype specific differences in LH_N pore formation. Firstly, electron microscopy was used to directly visualise whether BoNT or LH_N pores were formed in vesicle membranes. Secondly, vesicle leakage was used to analyse serotype specific differences in the way LH_N molecules interact with vesicular membranes through varying the concentration, pH and temperature at which interactions occur. Thirdly, we analysed the effect of reducing the disulphide bond between the H_N and LC domains of LH_N molecules on vesicle leakage (serotypes A-D).

3.5.4.1 *Electron microscopic analysis of protein-vesicle interactions*

In the previous chapter, it was discovered that vesicle leakage could not conclusively report protein or peptide pore formation but instead reports the more general destabilization of phospholipid membranes by proteins. Here we assess whether or not we are able to visualize a BoNT or LH_N pore forming in lipid vesicles using electron microscopy. The effect of known pore forming proteins and peptides, such as endonegative $BoNT_A$, LH_A, and GALA, were compared to the effect of a protein with no known non-pore forming ability (light chain domain of $BoNT_A$ (LC_A) at pH4.

Literature examples of protein pores formed by toxins in lipid vesicles (Diphtheria toxin and Hemolysin E toxin, (Figure 3-34, A and B respectively)), demonstrate that the negative stain (Uranly Formate), stains protein molecules and leaves phospholipids translucent (Lai et al., 1984). Whilst both have been determined to show evidence of protein pore formation in lipid vesicles only the Hemolysin shows clear and definable pores which are thought to consist of eight 34KDa subunits (Wallace et al., 2000). Electron microscopic analysis of the interaction between BoNT and LH_N proteins with lipid vesicles was completed at pH4 (Figure 3-28, B, C and D); both BoNT and LH_N proteins line the outside of lipid vesicles in a manner similar to diphtheria toxin, suggesting that BoNT and LH_N molecules have affinity for a lipid environment at acidic pH. Dark circles which appear on the membrane surface may represent pores in vesicle membranes but are most likely

protein aggregation. There is no clear and definable pore like structure evident following vesicle incubation with either BoNT or LH_N.

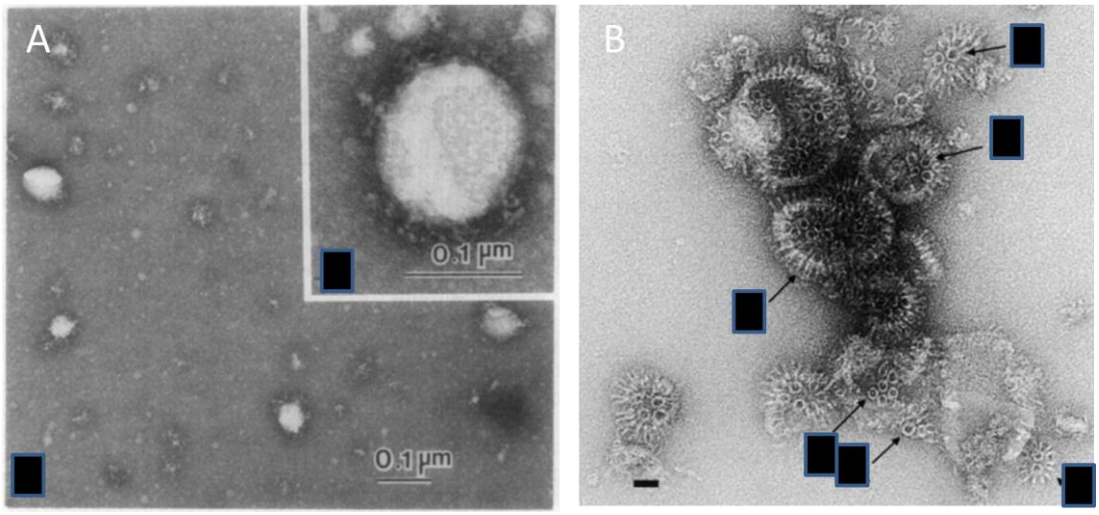

Figure 3-34 Diphtheria toxin and Hemolysin E toxin form pores in vesicle membranes
(A) Electron microscopic analysis of the interaction between Diphtheria toxin with phospholipid membranes at acidic pH (B) Electron microscopic analysis of the interaction between Hemolysin E toxin and phospholipid membranes at neutral pH (Lai et al., 1984; Wallace et al., 2000)

Liposomes were found not to be visible under the conditions of electron microscopy without the presence of protein in solution (Figure 3-29, A). This casts doubt over the structural integrity of the liposomes and could explain why proteins with no known pore forming ability have been seen to cause vesicle leakage (section 3.4.3.1). Concurrently, a protein control with no known pore forming activity (LC_A) appears to line the outside of and stabilize phospholipid vesicles in a manner consistent with BoNT and LH_N proteins (Figure 3-28, C). Unlike BoNT and LH_N proteins, LC_A does not show dark circles on the surface of vesicles. This demonstrates that a perceived non-pore forming protein shows affinity for phospholipid vesicles at acidic pH; this affinity may be sufficient to induce vesicle leakage without the formation of a pore if the liposome is considered structurally unsound.

3.5.4.2 *LH_N serotypes A-E disrupt vesicle membranes in a serotype specific fashion*

As electron microscopic analysis has not validated the presence of specific pore formation in lipid vesicles, it is not possible to derive evidence of LH_N pore formation from

this vesicle leakage assay. However, we can study the conditions under which LH_N serotypes A-E become lipophilic and thus the conditions under which they would be most likely to form pores.

LH_A is evidently the least lipophilic of the LH_N serotypes tested. This is demonstrated comparatively by its low rate of vesicle leakage at high concentration, its inability to cause vesicle leakage at pH5 and its near inability to cause vesicle leakage at 20°C. This apparent lack of lipophilicity may suggest that the protein is more stable at low pH, further analysis through circular dichroism may elucidate why LH_A is more stable and less lipophilic in these conditions.

LH_B concentrations lower than 0.01µM fail to induce vesicle leakage; consequently LH_B demonstrates the highest level of concentration dependency of all serotypes. This may suggest that LH_B has a tendency to aggregate in a multimeric form effectively decreasing the number of free molecules in solution and thus the probability of disrupting lipid vesicles. LH_B may form a multimeric conformation similar to $BoNT_B$'s trimeric pore forming structure (Sun et al., 2011).

LH_C demonstrates the fastest rate of vesicle leakage at a concentration of 0.001µM showing that in comparison to other serotypes it only needs a very low concentration to initiate vesicle leakage. Like LH_A, LH_C does not disrupt vesicle membranes at pH5 and shows a exceptionally temperature dependant form of vesicle leakage. This suggests that it takes a very acidic pH and a high temperature for LH_C to adopt a lipophilic conformation. This may mean that the protein is less hydrophobic than other LH_N proteins.

LH_D displays the fastest rate of vesicle leakage at concentrations of 0.1µM and 0.01µM respectively. Serotype D also shows the highest rate of vesicle leakage at pH5 and at 20°C, 30°C and 40°C respectively. As serotype D shows the highest rate of vesicle leakage both at pH5 and 20°C this suggests that it requires less energy to adopt a conformation capable of permeabilising membranes. The stoichiometry with which LH_D permeabilises membranes may be simpler than the multimer proposed for LH_B allowing this serotype to form pores over a wider range of concentrations. The wide range of conditions over which

LH_D is capable of causing liposome permeabilisation may be related to why $BoNT_D$ is such a quick acting toxin in rats and mice in comparison to other serotypes (Eleopra et al., 2013). The rapid rate at which LH_D is able to cause vesicle leakage over an array of concentrations may suggest that the structure of LH_D is the most hydrophobic of the serotypes tested.

As well as demonstrating the highest rate of vesicle leakage at 1µM, LH_E demonstrates the greatest increase in the rate of vesicle leakage seen when decreasing the extravesicular pH from pH4 to pH3 (a ~3.8x increase in rate of vesicle leakage). This suggests that LH_E is affected greatly by a change in pH conditions and readily adopts a lipophilic structural organisation. This may be related to the fast rate of $BoNT_E$ translocation, thought to be brought about by the molecules readiness to adopt a multimeric pore like structure at pH5 in contrast to $BoNT_B$ which requires more acidic conditions (Sun et al., 2012).

As we have concluded that the lipophilicity of LH_N molecules at acidic pH is responsible for the rate at which they cause vesicle leakage, a comparison between the surface charge of LH_N proteins at low pH may be seen to correlate with the rate of vesicle leakage observed. However, there is a lack of sufficient structural information to draw such a comparison.

3.5.4.3 *Reducing the disulfide linkage between the heavy and light chain of LH_N molecules*

Patch clamp experiments have shown BoNT and LH_N to form pores in excised segments of cell membranes (see section 1.5.2.5). The pore formed was considered to be in a closed conformation if the LC domain occupied the pore and an open conformation if it did not (Fischer and Montal, 2007b). Reducing the disulphide bond connecting the LC and H_N domains prior to pore formation has been shown to only allow the formation of open pores (Fischer and Montal, 2007a). To see whether we could detect evidence of the proposed closed (or blocked) and open pores in vesicular membranes, a comparison was made between vesicle leakage induced by LH_N (serotypes A-D) with and without a reducing agent known to reduce the inter-domain disulphide bond (10mM DTT, see section 3.2.2.5) in the extra-vesicular environment.

A small difference in the rate of vesicle leakage achieved by LH_A and LH_C under reducing and non-reducing conditions was detectable. In both cases the rate of vesicle leakage was seen to be slightly higher under reducing conditions suggesting that it may be possible to see blocked and open pore formations though a change in the rate of vesicle leakage.

LH_B and LH_D do not show any significant difference in the rate at which they cause vesicle leakage in reducing and non-reducing conditions. Clarity on this issue might be provided by analyzing the rates of LH_N serotypes A-D over a range of concentrations under reducing and non-reducing conditions.

3.5.5 Conclusion

Firstly, the interaction of BoNT and LH_N proteins with lipid vesicles at low pH was visualized using electron microscopy. Analysis of these interactions did not show clear evidence of stable pores formed in lipid vesicles. However, all proteins incubated with vesicles at low pH (including LC_A) showed a lipophilic affinity for the liposomes. This correlated well with our previous findings that all proteins tested caused dye leakage at acidic pH (Figure 3-22).

Secondly, the ability of LH_N serotypes A, B, C, D and E to cause vesicle leakage was concentration, pH and temperature dependent. We conclude that serotype specific differences in ability to permeate phospholipid vesicles represents each serotypes propensity to adopt a lipophilic conformation, differences in this property must affect each H_N domains pore formation activity.

Finally, it could not be concluded that differences demonstrated between vesicle leakage caused by reduced and non-reduced LH_N proteins (serotypes A and C) was a result of the formation of open and blocked pores respectively.

4 General Discussion

The *Clostridium botulinum* neurotoxin (BoNT) is a fascinating example of the specific and intricate nature in which toxins manipulate cellular function. The seven different serotypes of BoNT specifically target and enter the cholinergic neuromuscular synapse where they cause flaccid muscular paralysis (with great potency) through inhibiting the cells ability to perform exocytosis (Montal, 2010). This mechanism is thought to be dependent on BoNTs tri-modular domain structure which includes the following domains: receptor binding domain (H_C), translocation domain (H_N) and catalytic domain (LC). Much is known about the mechanism through which the H_C domain binds with specificity to the pre-synaptic terminal of the neuromuscular junction and the mechanism by which the LC domain cleaves SNARE proteins preventing exocytotic vesicular secretion but very little is known about the way in which the H_N domain interacts with cellular membranes.

In this investigation we have set out to shed light on the most elusive mechanism of BoNT intoxication, namely, the serotype specific way in which the H_N domain of BoNT interacts with cellular membranes. Through analyzing the expression, purification, cellular interaction and artificial membrane interaction of BoNTs and their LH_N and H_N derivatives we have been able to determine the physical properties of BoNT, LH_N and H_N molecules.

4.1 LH_D effects an increase in CHO-K1 cell intracellular Ca^{2+} levels

The interaction of LH_D with CHO-K1 cell membranes was determined through the protein's ability to cause an influx of extracellular Ca^{2+} into CHO-K1 cells at high concentration (Figure 3-1). Reducing extracellular Ca^{2+} concentration reduces the LH_D induced increase in intracellular Ca^{2+}, suggesting that LH_D was capable of facilitating the movement of Ca^{2+} from the extracellular to intracellular environment (Figure 3-2). Whilst it was hypothesized that this movement of Ca^{2+} may be as a result of a pore formed by LH_D in the CHO-K1 cell membrane, the difficulty associated with reliably reproducing this response resulted in the eventual termination of this study. However, the idea that LH_D may be

capable of forming a pore in cellular membranes at physiological pH and that BoNT and LH_N pore formation is serotype specific was intriguing and required further investigation.

4.2 LH_N and H_N domain physical properties were determined through expression and purification

In order to visualize if LH_D might interact with cellular membranes in a different way to other serotypes and to elucidate the structure of its H_N domain for the first time, LH_D was expressed, purified and crystallized in an attempt to elucidate its three dimensional structure via X-ray crystallography (Figure 3-4). Unfortunately, these crystallization trials were unsuccessful which, in turn, lead to attempts to purify the H_N domain of serotype D for inclusion in crystallization trials.

To isolate the H_N domain of LH_D, the LC and H_N domains of LH_D were successfully separated via affinity chromatography (Figure 3-6 and Figure 3-7). A detergent was required to separate the domains of LH_D, confirming that the H_N domain of LH_D was hydrophobic. Due to a lack of reproducibility seen when attempting to isolate the H_N domain of serotype D from its LH_N construct, attempts were made to express and purify the H_N domains of BoNT serotypes A and C. This lead to the successful expression and purification of H_N serotype A (Figure 3-8) and the never before seen, successful expression and purification of H_N serotype C (Figure 3-9). Notably, both serotypes required high levels of detergent to keep them soluble following expression and throughout the purification procedure, again displaying the hydrophobic nature of the H_N domain. Due to time constraints the H_N domains of BoNT serotypes A, C and D were not transferred into crystallization trials.

4.3 Investigating the pore forming potential of BoNT and LH_N proteins through vesicle leakage

In an attempt to evaluate the conditions under which BoNT and LH_N form pores, a vesicle leakage assay was designed and developed (based on literature examples of vesicle leakage (Galloux et al., 2008; Lai et al., 2010)) in a novel 96 well format.

During the development of this vesicle leakage assay, it was determined that proteins with no known pore forming ability (e.g. BSA, LC_A and Transferrin) were capable of inducing vesicle leakage at acidic but not neutral pH. Due to the surprising nature of these results, two authors who had studied the pore forming nature of BoNT using a vesicle leakage assay, were contacted to confirm whether or not they had also used non-pore forming (negative) protein controls (Lai et al., 2010). Upon confirmation that they had not, we began to question the ability of this vesicle leakage assay to determine protein pore formation at acidic pH. The ability of negative control proteins to cause vesicle leakage suggests that we do not specifically measure protein pore formation under these conditions but rather the lipophilicity of a protein at acidic pH. Specifically, as LC_A molecules induced vesicle leakage at acidic but not neutral pH, it was thought that an increase in the molecules lipophilicity, known to be a result of protein refolding (Cai et al., 2006), was responsible for the molecules increased interaction with lipid vesicles.

To verify whether or not pore forming proteins were capable of forming pores in lipid vesicles, the interaction of BoNT and LH_N toxins with lipid vesicles was investigated via electron microscopy. This analysis neither confirmed nor excluded the presence of a pore formed by either BoNT or LH_N proteins in lipid vesicles (Figure 3-28 and Figure 3-29). We therefore have to conclude that this vesicle leakage assay does not provide sufficient evidence to determine whether or not proteins or peptides form pores at acidic pH regardless of its similarity with published assays (Galloux et al., 2008; Lai et al., 2010). However, as the lipophilicity gained by BoNT domains at acidic pH has been determined to be important for the membrane interaction and pore formation of BoNT proteins (Colasante et al., 2013; Fischer et al., 2012), the rate at which vesicle leakage occurs in this assay may provide insight into the pore forming potential of the molecules tested.

It was demonstrated that removing the H_C domain of BoNT serotypes A and E affects the rate at which they interact with phospholipid vesicles (Figure 3-23, Figure 3-24 and Figure 3-25). In particular removing the H_C domain of $BoNT_A$ inhibited its ability to permeate phospholipid vesicles at lower than physiological temperatures. It is plausible that removing the H_C domain of BoNT will remove hydrophobic yet solvent exposed loops

located on the H_{CN} subdomain (Muraro et al., 2009) causing a reduction in the molecule's lipophilicity. However, why this affects the temperature at which the LH_N molecule can induce vesicle leakage is not clear. Circular dichroism (CD) may be able to identify whether LH_A adopts a significantly different structural arrangement over the temperature range tested (40°C-20°C), which in turn may identify why the lipophilicity of this molecule seemed to vary so markedly without the H_C domain. (Lalli et al., 1999; Zhang et al., 2010).

As this vesicle leakage assay is comparable with others, published in literature, used to determine the conditions under which $BoNT_A$ and its derivatives form pores in vesicle membranes (e.g. (Galloux et al., 2008; Lai et al., 2010)), we may need to reinterpret some published examples of BoNT domain induced vesicle leakage. For example, in 2010 it was demonstrated that reducing the concentration of NaCl increased the rate at which vesicle leakage occurred following H_N domain interaction with dye loaded lipid vesicles at pH4 (Lai et al., 2010). This was previously determined to be as a result of H_N domain pore formation in lipid vesicles, however, given that negative protein controls were not run (e.g. BSA or Transferrin) we can only conclude that the H_N domain possessed a higher lipophilicity at low NaCl concentration, suggesting that NaCl prevents protonation of the charged residues on the surface of the H_N domain thus reducing the molecules lipophilicity.

LH_N proteins were assessed to cause vesicle leakage in a serotype specific way which has the potential to highlight differences between the lipophilicity of LH_N serotypes A-E under various conditions. Most remarkably LH_D was shown to induce the fastest rate of vesicle leakage at pH5 (Figure 3-31) (the least acidic pH where vesicle leakage was detectable). Once again CD analysis of the change in LH_N structure under various conditions may be instrumental in demonstrating why various serotypes of LH_N molecules adopt more or less lipophilic arrangements under different conditions.

Finally, the effect of reducing the disulphide bond between the H_N and LC domains of LH_N molecules did not affect the rate of vesicle leakage determined. Therefore we could not conclude that either an open or closed pore was formed in lipid vesicles (Brunger et al., 2007).

4.4 Further development of the vesicle leakage assay

It may yet be possible to develop a 96 well vesicle leakage assay that it is capable of determining whether or not a protein or peptide has the potential to form a pore in vesicle membranes at acidic pH. To facilitate this, we would need to develop a phospholipid mixture that created a more stable vesicle, not disrupted by non-specific protein-vesicle interactions. The inclusion of molecules such as Cholesterol, known to be essential to the integrity of plasma membrane microdomains and the composition of cellular vesicles, may serve to stabilize vesicle structure and thus prevent disruption of vesicle membranes by non-pore forming proteins (Goluszko and Nowicki, 2005).

The leakage of fluorescent dye from lipid vesicles has been shown to require a very high concentration of BoNT, LH_N and H_N protein respectively (Galloux et al., 2008; Lai et al., 2010). In contrast the leakage of K^+ ions from lipid vesicles has been shown to require a far lower concentration of $BoNT_A$ derivatives in order to determine pore formation (Shone et al., 1987). Furthermore, the assays ability to work at a lower concentration appears to allow it to distinguish between pore forming and non-pore forming proteins at acidic pH. Prospectively, it may be possible to load phospholipid vesicles with a high concentration of Ca^{2+} ions and monitor the BoNT induced leakage of Ca^{+2} into the extra-vesicular media through an increase in Ca^{2+} sensitive dye florescence.

Electrophysiological methods that have been used in the past to detect the conditions under which BoNT forms pores in cellular membranes (e.g. the patch clamp assay) still appear to be the most sensitive and accurate method for detecting BoNT, LH_N and H_N induced pore formation (Fischer and Montal, 2007b). Furthermore, the patch clamp assay is capable of determining both the open and closed H_N pore conformations (Fischer et al., 2008b). If a vesicle leakage assay can be produced which can distinguish between pore forming and non-pore forming proteins, a direct comparison of BoNT and LH_N induced pore formation (between the patch clamp and vesicle leakage assay) may enable a detailed and thorough analysis of vesicle leakage data. A 96 well vesicle leakage assay which has the capability of determining the formation of protein pores in lipid membranes would greatly advance the field of botulinum neurotoxin research and potentially allow the development

of a new range of BoNT based therapeutics with variable ability to form pores in cellular membranes.

5 References

Agarwal, R., Binz, T., and Swaminathan, S. (2005). Structural analysis of botulinum neurotoxin serotype F light chain: implications on substrate binding and inhibitor design. Biochemistry *44*, 11758-11765.

Agarwal, R., Eswaramoorthy, S., Kumaran, D., Binz, T., and Swaminathan, S. (2004). Structural analysis of botulinum neurotoxin type E catalytic domain and its mutant Glu212-->Gln reveals the pivotal role of the Glu212 carboxylate in the catalytic pathway. Biochemistry *43*, 6637-6644.

Agarwal, R., Schmidt, J.J., Stafford, R.G., and Swaminathan, S. (2009). Mode of VAMP substrate recognition and inhibition of Clostridium botulinum neurotoxin F. Nature Structural & Molecular Biology *16*, 789-794.

Aoki, K.R., and Guyer, B. (2001). Botulinum toxin type A and other botulinum toxin serotypes: a comparative review of biochemical and pharmacological actions. European Journal of Neurology : the Official Journal of the European Federation of Neurological Societies *8 Suppl 5*, 21-29.

Arndt, J.W., Chai, Q., Christian, T., and Stevens, R.C. (2006). Structure of botulinum neurotoxin type D light chain at 1.65 A resolution: repercussions for VAMP-2 substrate specificity. Biochemistry *45*, 3255-3262.

Arndt, J.W., Yu, W., Bi, F., and Stevens, R.C. (2005). Crystal structure of botulinum neurotoxin type G light chain: serotype divergence in substrate recognition. Biochemistry *44*, 9574-9580.

Balfanz, J., Rautenberg, P., and Ullmann, U. (1996). Molecular mechanisms of action of bacterial exotoxins. Zentralblatt für bakteriologie *284*, 170-206.

Barash, J.R., and Arnon, S.S. (2014). A novel strain of Clostridium botulinum that produces type B and type H botulinum toxins. The Journal of Infectious Diseases *209*, 183-191.

Benson, M.A., Fu, Z., Kim, J.J., and Baldwin, M.R. (2011). Unique ganglioside recognition strategies for clostridial neurotoxins. The Journal of Biological Chemistry *286*, 34015-34022.

Berntsson, R.P., Peng, L., Dong, M., and Stenmark, P. (2013). Structure of dual receptor binding to botulinum neurotoxin B. Nature Communications *4*, 2058.

Binz, T. (2013). Clostridial neurotoxin light chains: devices for SNARE cleavage mediated blockade of neurotransmission. Current topics in Microbiology and Immunology *364*, 139-157.

Binz, T., Bade, S., Rummel, A., Kollewe, A., and Alves, J. (2002). Arg(362) and Tyr(365) of the botulinum neurotoxin type a light chain are involved in transition state stabilization. Biochemistry *41*, 1717-1723.

Brunger, A.T., Breidenbach, M.A., Jin, R., Fischer, A., Santos, J.S., and Montal, M. (2007). Botulinum neurotoxin heavy chain belt as an intramolecular chaperone for the light chain. PLoS Pathogens *3*, 1191-1194.

Cai, S., Kukreja, R., Shoesmith, S., Chang, T.W., and Singh, B.R. (2006). Botulinum neurotoxin light chain refolds at endosomal pH for its translocation. The Protein Journal *25*, 455-462.

Caya, J.G., Agni, R., and Miller, J.E. (2004). Clostridium botulinum and the clinical laboratorian: a detailed review of botulism, including biological warfare ramifications of botulinum toxin. Archives of Pathology & Laboratory Medicine *128*, 653-662.

Chaddock, J.A., Herbert, M.H., Ling, R.J., Alexander, F.C., Fooks, S.J., Revell, D.F., Quinn, C.P., Shone, C.C., and Foster, K.A. (2002). Expression and purification of catalytically active, non-

toxic endopeptidase derivatives of Clostridium botulinum toxin type A. Protein Expression and Purification *25*, 219-228.
Chaddock, J.A., and Marks, P.M. (2006). Clostridial neurotoxins: structure-function led design of new therapeutics. Cellular and Molecular Life Sciences *63*, 540-551.
Chaddock, J.A., Purkiss, J.R., Alexander, F.C., Doward, S., Fooks, S.J., Friis, L.M., Hall, Y.H., Kirby, E.R., Leeds, N., Moulsdale, H.J*., et al.* (2004). Retargeted clostridial endopeptidases: inhibition of nociceptive neurotransmitter release in vitro, and antinociceptive activity in in vivo models of pain. Movement Disorders : Official Journal of the Movement Disorder Society *19 Suppl 8*, S42-47.
Chaddock, J.A., Purkiss, J.R., Duggan, M.J., Quinn, C.P., Shone, C.C., and Foster, K.A. (2000a). A conjugate composed of nerve growth factor coupled to a non-toxic derivative of Clostridium botulinum neurotoxin type A can inhibit neurotransmitter release in vitro. Growth Factors *18*, 147-155.
Chaddock, J.A., Purkiss, J.R., Friis, L.M., Broadbridge, J.D., Duggan, M.J., Fooks, S.J., Shone, C.C., Quinn, C.P., and Foster, K.A. (2000b). Inhibition of vesicular secretion in both neuronal and nonneuronal cells by a retargeted endopeptidase derivative of Clostridium botulinum neurotoxin type A. Infection and Immunity *68*, 2587-2593.
Chai, Q., Arndt, J.W., Dong, M., Tepp, W.H., Johnson, E.A., Chapman, E.R., and Stevens, R.C. (2006). Structural basis of cell surface receptor recognition by botulinum neurotoxin B. Nature *444*, 1096-1100.
Coffield, J.A., Considine, R.V., and Simpson, L.L. (1994). Clostridial neurotoxins in the age of molecular medicine. Trends Microbiol *2*, 67-69.
Colasante, C., Rossetto, O., Morbiato, L., Pirazzini, M., Molgo, J., and Montecucco, C. (2013). Botulinum neurotoxin type A is internalized and translocated from small synaptic vesicles at the neuromuscular junction. Molecular Neurobiology, 48, 120-127.
Collins, and East (1998). Phylogeny and taxonomy of the food-borne pathogen Clostridium botulinum and its neurotoxins. Journal of Applied Microbiology *84*, 5-17.
Darios, F., and Davletov, B. (2006). Omega-3 and omega-6 fatty acids stimulate cell membrane expansion by acting on syntaxin 3. Nature *440*, 813-817.
DasGupta, B.R., and Foley, J., Jr. (1989). C. botulinum neurotoxin types A and E: isolated light chain breaks down into two fragments. Comparison of their amino acid sequences with tetanus neurotoxin. Biochimie *71*, 1193-1200.
de Haan, L., and Hirst, T.R. (2000). Cholera toxin and related enterotoxins: a cell biological and immunological perspective. Journal of Natural Toxins *9*, 281-297.
Dias, J.P., Ismael, M.A., Pilon, M., de Champlain, J., Ferrari, B., Carayon, P., and Couture, R. (2007). The kinin B1 receptor antagonist SSR240612 reverses tactile and cold allodynia in an experimental rat model of insulin resistance. British Journal of Pharmacology *152*, 280-287.
Dobell, C. (1923). A Protozoological bicentenary: Antony van Leeuwenhoek (1632–1723) and Louis Joblot (1645–1723). Parasitology *15*, 308-319.
Donovan, J.J., Simon, M.I., and Montal, M. (1982). Insertion of diphtheria toxin into and across membranes: role of phosphoinositide asymmetry. Nature *298*, 669-672.
Duggan, M.J., Quinn, C.P., Chaddock, J.A., Purkiss, J.R., Alexander, F.C.G., Doward, S., Fooks, S.J., Friis, L.M., Hall, Y.H.J., Kirby, E.R*., et al.* (2002). Inhibition of release of neurotransmitters from rat dorsal root ganglia by a novel conjugate of a Clostridium botulinum Toxin A endopeptidase fragment and Erythrina cristagalli lectin. Journal of Biological Chemistry *277*, 34846-34852.
Eleopra, R., Montecucco, C., Devigili, G., Lettieri, C., Rinaldo, S., Verriello, L., Pirazzini, M., Caccin, P., and Rossetto, O. (2013). Botulinum neurotoxin serotype D is poorly effective in

humans: an in vivo electrophysiological study. Clinical Neurophysiology : Official Journal of the International Federation of Clinical Neurophysiology *124*, 999-1004.
Eswaramoorthy, S., Kumaran, D., Keller, J., and Swaminathan, S. (2004). Role of metals in the biological activity of clostridium botulinum neurotoxins. Biochemistry *43*, 2209-2216.
Fdez, E., Jowitt, T.A., Wang, M.C., Rajebhosale, M., Foster, K., Bella, J., Baldock, C., Woodman, P.G., and Hilfiker, S. (2008). A role for soluble N-ethylmaleimide-sensitive factor attachment protein receptor complex dimerization during neurosecretion. Molecular Biology of the Cell *19*, 3379-3389.
Fernandez-Salas, E., Steward, L.E., Ho, H., Garay, P.E., Sun, S.W., Gilmore, M.A., Ordas, J.V., Wang, J., Francis, J., and Aoki, K.R. (2004). Plasma membrane localization signals in the light chain of botulinum neurotoxin. Proc Natl Acad Sci U S A *101*, 3208-3213.
Fischer, A., Garcia-Rodriguez, C., Geren, I., Lou, J., Marks, J.D., Nakagawa, T., and Montal, M. (2008a). Molecular architecture of botulinum neurotoxin E revealed by single particle electron microscopy. The Journal of Biological Chemistry *283*, 3997-4003.
Fischer, A., and Montal, M. (2006). Characterization of Clostridial botulinum neurotoxin channels in neuroblastoma cells. Neurotox res *9*, 93-100.
Fischer, A., and Montal, M. (2007a). Crucial role of the disulfide bridge between botulinum neurotoxin light and heavy chains in protease translocation across membranes. The Journal of Biological Chemistry *282*, 29604-29611.
Fischer, A., and Montal, M. (2007b). Single molecule detection of intermediates during botulinum neurotoxin translocation across membranes. Proceedings of the National Academy of Sciences of the United States of America *104*, 10447-10452.
Fischer, A., Mushrush, D.J., Lacy, D.B., and Montal, M. (2008b). Botulinum neurotoxin devoid of receptor binding domain translocates active protease. PLoS Pathogens *4*, e1000245.
Fischer, A., Nakai, Y., Eubanks, L.M., Clancy, C.M., Tepp, W.H., Pellett, S., Dickerson, T.J., Johnson, E.A., Janda, K.D., Montal, M*., et al.* (2009). Bimodal modulation of the botulinum neurotoxin protein-conducting channel. Proceedings of the National Academy of Sciences of the United States of America *106*, 1330-1335.
Fischer, A., Sambashivan, S., Brunger, A.T., and Montal, M. (2012). Beltless translocation domain of botulinum neurotoxin A embodies a minimum ion-conductive channel. The Journal of Biological Chemistry *287*, 1657-1661.
Foster, K., Bigalke, H., and Aoki, K.R. (2006). Botulinum neurotoxin — from laboratory to bedside. Neurotox res *9*, 133-140.
Fred, E.B. (1933). Antony van Leeuwenhoek: On the three-hundredth anniversary of his birth. Journal of Bacteriology *25*, iv 2-18.
Fu, F.-N., Busath, D.D., and Singh, B.R. (2002). Spectroscopic analysis of low pH and lipid-induced structural changes in type A botulinum neurotoxin relevant to membrane channel formation and translocation. Biophysical Chemistry *99*, 17-29.
Fu, F.-N., and Singh, B. (1999). Calcein permeability of liposomes mediated by type A botulinum neurotoxin and Its light and heavy chains. J Protein Chem *18*, 701-707.
Galloux, M., Vitrac, H., Montagner, C., Raffestin, S., Popoff, M.R., Chenal, A., Forge, V., and Gillet, D. (2008). Membrane interaction of botulinum neurotoxin A translocation (T) domain. Journal of Biological Chemistry *283*, 27668-27676.
Goluszko, P., and Nowicki, B. (2005). Membrane cholesterol: a crucial molecule affecting interactions of microbial pathogens with mammalian cells. Infection and Immunity *73*, 7791-7796.

Goodnough, M.C., Oyler, G., Fishman, P.S., Johnson, E.A., Neale, E.A., Keller, J.E., Tepp, W.H., Clark, M., Hartz, S., and Adler, M. (2002). Development of a delivery vehicle for intracellular transport of botulinum neurotoxin antagonists. FEBS Lett *513*, 163-168.
Gouaux, E., Hobaugh, M., and Song, L. (1997). Alpha-hemolysin, gamma-hemolysin, and leukocidin from Staphylococcus aureus: distant in sequence but similar in structure. Protein Science : a publication of the protein society *6*, 2631-2635.
Guo, X., MacKay, J.A., and Szoka, F.C., Jr. (2003). Mechanism of pH-triggered collapse of phosphatidylethanolamine liposomes stabilized by an ortho ester polyethyleneglycol lipid. Biophysical Journal *84*, 1784-1795.
Harper, C.B., Martin, S., Nguyen, T.H., Daniels, S.J., Lavidis, N.A., Popoff, M.R., Hadzic, G., Mariana, A., Chau, N., McCluskey, A.*, et al.* (2011). Dynamin inhibition blocks botulinum neurotoxin type A endocytosis in neurons and delays botulism. The Journal of Biological Chemistry *286*, 35966-35976.
Hatheway, C.L. (1990). Toxigenic clostridia. Clinical Microbiology Reviews *3*, 66-98.
Hedeland, M., Moura, H., Baverud, V., Woolfitt, A.R., Bondesson, U., and Barr, J.R. (2011). Confirmation of botulism in birds and cattle by the mouse bioassay and Endopep-MS. Journal of Medical Microbiology *60*, 1299-1305.
Hill, K.K., Smith, T.J., Helma, C.H., Ticknor, L.O., Foley, B.T., Svensson, R.T., Brown, J.L., Johnson, E.A., Smith, L.A., Okinaka, R.T.*, et al.* (2007). Genetic diversity among botulinum neurotoxin-producing clostridial strains. Journal of Bacteriology *189*, 818-832.
Hill, K.K., Xie, G., Foley, B.T., Smith, T.J., Munk, A.C., Bruce, D., Smith, L.A., Brettin, T.S., and Detter, J.C. (2009). Recombination and insertion events involving the botulinum neurotoxin complex genes in Clostridium botulinum types A, B, E and F and Clostridium butyricum type E strains. BMC Biology *7*, 66.
Hoch, D.H., Romero-Mira, M., Ehrlich, B.E., Finkelstein, A., DasGupta, B.R., and Simpson, L.L. (1985). Channels formed by botulinum, tetanus, and diphtheria toxins in planar lipid bilayers: Relevance to translocation of proteins across membranes. Proceedings of the National Academy of Sciences of the United States of America *82*, 1692-1696.
Holdsworth, G., Slocombe, P., Hutchinson, G., and Milligan, G. (2005). Analysis of endogenous S1P and LPA receptor expression in CHO-K1 cells. Gene *350*, 59-63.
Inglis, T.J. (2007). Principia aetiologica: taking causality beyond Koch's postulates. Journal of Medical Microbiology *56*, 1419-1422.
Jin, R., Rummel, A., Binz, T., and Brunger, A.T. (2006). Botulinum neurotoxin B recognizes its protein receptor with high affinity and specificity. Nature *444*, 1092-1095.
Jin, R., Sikorra, S., Stegmann, C.M., Pich, A., Binz, T., and Brunger, A.T. (2007). Structural and biochemical studies of botulinum neurotoxin serotype C1 light chain protease: implications for dual substrate specificity. Biochemistry *46*, 10685-10693.
Kaneko, J., and Kamio, Y. (2004). Bacterial two-component and hetero-heptameric pore-forming cytolytic toxins: structures, pore-forming mechanism, and organization of the genes. Bioscience, Biotechnology, and Biochemistry *68*, 981-1003.
Karalewitz, A.P., Fu, Z., Baldwin, M.R., Kim, J.J., and Barbieri, J.T. (2012). Botulinum neurotoxin serotype C associates with dual ganglioside receptors to facilitate cell entry. The Journal of Biological Chemistry *287*, 40806-40816.
Karalewitz, A.P., Kroken, A.R., Fu, Z., Baldwin, M.R., Kim, J.J., and Barbieri, J.T. (2010). Identification of a unique ganglioside binding loop within botulinum neurotoxins C and D-SA. Biochemistry *49*, 8117-8126.
Kopito, R.R. (2000). Aggresomes, inclusion bodies and protein aggregation. Trends in Cell Biology *10*, 524-530.

Koriazova, L.K., and Montal, M. (2003). Translocation of botulinum neurotoxin light chain protease through the heavy chain channel. Nature Structural Biology *10*, 13-18.
Kozaki, S., Kamata, Y., Watarai, S., Nishiki, T., and Mochida, S. (1998). Ganglioside GT1b as a complementary receptor component for Clostridium botulinum neurotoxins. Microbial Pathogenesis *25*, 91-99.
Kroken, A.R., Karalewitz, A.P., Fu, Z., Kim, J.J., and Barbieri, J.T. (2011). Novel ganglioside-mediated entry of botulinum neurotoxin serotype D into neurons. The Journal of Biological Chemistry *286*, 26828-26837.
Kubota, T., Yonekura, N., Hariya, Y., Isogai, E., Isogai, H., Amano, K.-i., and Fujii, N. (1998). Gene arrangement in the upstream region of Clostridium botulinum type E and Clostridium butyricum BL6340 progenitor toxin genes is different from that of other types. FEMS Microbiology Letters *158*, 215-221.
Kumaran, D., Eswaramoorthy, S., Furey, W., Navaza, J., Sax, M., and Swaminathan, S. (2009). Domain organization in clostridium botulinum neurotoxin type E Is unique: Its implication in faster translocation. Journal of Molecular Biology *386*, 233-245.
Lacy, D.B., Tepp, W., Cohen, A.C., DasGupta, B.R., and Stevens, R.C. (1998). Crystal structure of botulinum neurotoxin type A and implications for toxicity. Nature Structural Biology *5*, 898-902.
Lai, B., Agarwal, R., Nelson, L.D., Swaminathan, S., and London, E. (2010). Low pH-induced pore formation by the T domain of botulinum toxin type A is dependent upon NaCl concentration. The Journal of Membrane Biology *236*, 191-201.
Lai, C.-S., Kushnaryov, V., Panz, T., and Basosi, R. (1984). Diphtheria toxin induces leakage of acidic liposomes. Archives of Biochemistry and Biophysics *234*, 1-6.
Lalli, G., Herreros, J., Osborne, S.L., Montecucco, C., Rossetto, O., and Schiavo, G. (1999). Functional characterisation of tetanus and botulinum neurotoxins binding domains. Journal of Cell Science *112 (Pt 16)*, 2715-2724.
Leeb-Lundberg, L.M., Marceau, F., Muller-Esterl, W., Pettibone, D.J., and Zuraw, B.L. (2005). International union of pharmacology. XLV. Classification of the kinin receptor family: from molecular mechanisms to pathophysiological consequences. Pharmacological Reviews *57*, 27-77.
Leggett, J., Harper, E., Waite, E., Marks, P., Martinez, A., and Lightman, S. (2013). GHRH receptor-targeted botulinum neurotoxin selectively inhibits pulsatile GH secretion in male rats. Endocrinology 154, 3305-3318.
Li, L., and Singh, B.R. (2000). Spectroscopic analysis of pH-induced changes in the molecular features of type A botulinum neurotoxin light chain. Biochemistry *39*, 6466-6474.
Lin, B.F., Missirlis, D., Krogstad, D.V., and Tirrell, M. (2012). Structural effects and lipid membrane interactions of the pH-responsive GALA peptide with fatty acid acylation. Biochemistry *51*, 4658-4668.
Lopez, P.H.H., and Schnaar, R.L. (2009). Gangliosides in cell recognition and membrane protein regulation. Current opinion in Structural Biology *19*, 549-557.
Maclennan, J.D. (1962). The histotoxic clostridial infections of man. Bacteriological Reviews *26*, 177-276.
Masuyer, G., Beard, M., Cadd, V.A., Chaddock, J.A., and Acharya, K.R. (2011). Structure and activity of a functional derivative of Clostridium botulinum neurotoxin B. Journal of Structural Biology *174*, 52-57.
Masuyer, G., Thiyagarajan, N., James, P.L., Marks, P.M.H., Chaddock, J.A., and Acharya, K.R. (2009). Crystal structure of a catalytically active, non-toxic endopeptidase derivative of

Clostridium botulinum toxin A. Biochemical and Biophysical Research Communications *381*, 50-53.
Mathis, S.A., Criscimagna, N.L., and Leeb-Lundberg, L.M. (1996). B1 and B2 kinin receptors mediate distinct patterns of intracellular Ca^{2+} signaling in single cultured vascular smooth muscle cells. Molecular Pharmacology *50*, 128-139.
Monta, M.S., Blewitt, R., Tomich, J.M., and Montal, M. (1992). Identification of an ion channel-forming motif in the primary structure of tetanus and botulinum neurotoxins. FEBS Letters *313*, 12-18.
Montal, M. (2009). Translocation of botulinum neurotoxin light chain protease by the heavy chain protein-conducting channel. Toxicon *54*, 565-569.
Montal, M. (2010). Botulinum neurotoxin: A marvel of protein design. Annual Review of Biochemistry *79*, 591-617.
Montecucco, C. (1986). How do tetanus and botulinum toxins bind to neuronal membranes? Trends in Biochemical Sciences *11*, 314-317.
Montecucco, C., Papini, E., and Schiavo, G. (1994). Bacterial protein toxins penetrate cells via a four-step mechanism. FEBS Letters *346*, 92-98.
Montecucco, C., and Schiavo, G. (1995). Structure and function of tetanus and botulinum neurotoxins. Quarterly Reviews of Biophysics *28*, 423-472.
Muraro, L., Tosatto, S., Motterlini, L., Rossetto, O., and Montecucco, C. (2009). The N-terminal half of the receptor domain of botulinum neurotoxin A binds to microdomains of the plasma membrane. Biochemical and Biophysical Research Communications *380*, 76-80.
Mushrush, D.J., Koteiche, H.A., Sammons, M.A., Link, A.J., McHaourab, H.S., and Lacy, D.B. (2011). Studies of the mechanistic details of the pH-dependent association of botulinum neurotoxin with membranes. The Journal of Biological Chemistry *286*, 27011-27018.
Nicol, F., Nir, S., and Szoka, F.C., Jr. (1999). Orientation of the pore-forming peptide GALA in POPC vesicles determined by a BODIPY-avidin/biotin binding assay. Biophysical Journal *76*, 2121-2141.
Niemann, H.H., Schubert, W.D., and Heinz, D.W. (2004). Adhesins and invasins of pathogenic bacteria: a structural view. Microbes and infection / Institut Pasteur *6*, 101-112.
Nishiki, T.-i., Tokuyama, Y., Kamata, Y., Nemoto, Y., Yoshida, A., Sato, K., Sekiguchi, M., Takahashi, M., and Kozaki, S. (1996). The high-affinity binding of Clostridium botulinum type B neurotoxin to synaptotagmin II associated with gangliosides GT1b/GD1a. FEBS Letters *378*, 253-257.
Nishiki, T., Kamata, Y., Nemoto, Y., Omori, A., Ito, T., Takahashi, M., and Kozaki, S. (1994). Identification of protein receptor for Clostridium botulinum type B neurotoxin in rat brain synaptosomes. Journal of Biological Chemistry *269*, 10498-10503.
Oblatt-Montal, M., Yamazaki, M., Nelson, R., and Montal, M. (1995). Formation of ion channels in lipid bilayers by a peptide with the predicted transmembrane sequence of botulinum neurotoxin A. Protein science : a publication of the protein society *4*, 1490-1497.
Odumosu, O., Nicholas, D., Yano, H., and Langridge, W. (2010). AB toxins: a paradigm switch from deadly to desirable. Toxins *2*, 1612-1645.
Peck, M.W. (2009). Biology and genomic analysis of Clostridium botulinum. In advances in microbial physiology, K.P. Robert, ed. (Academic Press), pp. 183-320.
Peng, L., Berntsson, R.P., Tepp, W.H., Pitkin, R.M., Johnson, E.A., Stenmark, P., and Dong, M. (2012). Botulinum neurotoxin D-C uses synaptotagmin I and II as receptors, and human synaptotagmin II is not an effective receptor for type B, D-C and G toxins. Journal of Cell Science *125*, 3233-3242.

Piazza, T.M., Blehert, D.S., Dunning, F.M., Berlowski-Zier, B.M., Zeytin, F.N., Samuel, M.D., and Tucker, W.C. (2011). In vitro detection and quantification of botulinum neurotoxin type E activity in avian blood. Applied and Environmental Microbiology *77*, 7815-7822.
Pirazzini, M., Bordin, F., Rossetto, O., Shone, C.C., Binz, T., and Montecucco, C. (2013). The thioredoxin reductase-thioredoxin system is involved in the entry of tetanus and botulinum neurotoxins in the cytosol of nerve terminals. FEBS Letters *587*, 150-155.
Pirazzini, M., Rossetto, O., Bolognese, P., Shone, C.C., and Montecucco, C. (2011). Double anchorage to the membrane and intact inter-chain disulfide bond are required for the low pH induced entry of tetanus and botulinum neurotoxins into neurons. Cellular Microbiology *13*, 1731-1743.
Ravelli, R.B., and Garman, E.F. (2006). Radiation damage in macromolecular cryocrystallography. Curr Opin Struct Biol *16*, 624-629.
Rietschel, E.T., Kirikae, T., Schade, F.U., Mamat, U., Schmidt, G., Loppnow, H., Ulmer, A.J., Zähringer, U., Seydel, U., and Di Padova, F. (1994). Bacterial endotoxin: molecular relationships of structure to activity and function. The FASEB Journal *8*, 217-225.
Sakaba, T., Stein, A., Jahn, R., and Neher, E. (2005). Distinct kinetic changes in neurotransmitter release after SNARE protein cleavage. Science *309*, 491-494.
Schmid, M.F., Robinson, J.P., and DasGupta, B.R. (1993). Direct visualization of botulinum neurotoxin-induced channels in phospholipid vesicles. Nature *364*, 827-830.
Schmitt, J., Karalewitz, A., Benefield, D.A., Mushrush, D.J., Pruitt, R.N., Spiller, B.W., Barbieri, J.T., and Lacy, D.B. (2010). Structural analysis of botulinum neurotoxin type G receptor binding. Biochemistry *49*, 5200-5205.
Scott, A.B., and Suzuki, D. (1988). Systemic toxicity of botulinum toxin by intramuscular injection in the monkey. Movement Disorders *3*, 333-335.
Segelke, B., Knapp, M., Kadkhodayan, S., Balhorn, R., and Rupp, B. (2004). Crystal structure of Clostridium botulinum neurotoxin protease in a product-bound state: Evidence for noncanonical zinc protease activity. Proc Natl Acad Sci U S A *101*, 6888-6893.
Shone, C.C., Hambleton, P., and Melling, J. (1985). Inactivation of Clostridium botulinum type A neurotoxin by trypsin and purification of two tryptic fragments. European Journal of Biochemistry *151*, 75-82.
Shone, C.C., Hambleton, P., and Melling, J. (1987). A 50-kDa fragment from the NH2-terminus of the heavy subunit of Clostridium botulinum type A neurotoxin forms channels in lipid vesicles. European Journal of Biochemistry *167*, 175-180.
Shukla, H.D., and Sharma, S.K. (2005). Clostridium botulinum: a bug with beauty and weapon. Critical Reviews in Microbiology *31*, 11-18.
Simpson, L.L., Coffield, J.A., and Bakry, N. (1994). Inhibition of vacuolar adenosine triphosphatase antagonizes the effects of clostridial neurotoxins but not phospholipase A2 neurotoxins. The Journal of Pharmacology and Experimental Therapeutics *269*, 256-262.
Simpson, P.B., Woollacott, A.J., Hill, R.G., and Seabrook, G.R. (2000). Functional characterization of bradykinin analogues on recombinant human bradykinin B1 and B2 receptors. European Journal of Pharmacology *392*, 1-9.
Stenmark, P., Dupuy, J., Imamura, A., Kiso, M., and Stevens, R.C. (2008). Crystal structure of botulinum neurotoxin type A in complex with the cell surface co-receptor GT1b-insight into the toxin-neuron interaction. PLoS Pathogens *4*, e1000129.
Strotmeier, J., Lee, K., Volker, A.K., Mahrhold, S., Zong, Y., Zeiser, J., Zhou, J., Pich, A., Bigalke, H., Binz, T*., et al.* (2010). Botulinum neurotoxin serotype D attacks neurons via two carbohydrate-binding sites in a ganglioside-dependent manner. The Biochemical Journal *431*, 207-216.

Südhof, T.C., and Rothman, J.E. (2009). Membrane fusion: grappling with SNARE and SM proteins. Science *323*, 474-477.
Sun, J. (2012). Roles of cellular redox factors in pathogen and toxin entry in the endocytic pathways. ISBN 978-953-51-0662-3
Sun, S., Suresh, S., Liu, H., Tepp, W.H., Johnson, E.A., Edwardson, J.M., and Chapman, E.R. (2011). Receptor binding enables botulinum neurotoxin B to sense low pH for translocation channel assembly. Cell Host & Microbe *10*, 237-247.
Sun, S., Tepp, W.H., Johnson, E.A., and Chapman, E.R. (2012). Botulinum neurotoxins B and E translocate at different rates and exhibit divergent responses to GT1b and low pH. Biochemistry *51*, 5655-5662.
Swaminathan, S. (2011). Molecular structures and functional relationships in clostridial neurotoxins. The FEBS Journal *278*, 4467-4485.
Swaminathan, S., and Eswaramoorthy, S. (2000). Structural analysis of the catalytic and binding sites of Clostridium botulinum neurotoxin B. Nature Structural Biology *7*, 693-699.
Takamori, S., Holt, M., Stenius, K., Lemke, E.A., Gronborg, M., Riedel, D., Urlaub, H., Schenck, S., Brugger, B., Ringler, P*., et al.* (2006). Molecular anatomy of a trafficking organelle. Cell *127*, 831-846.
Turton, K., Chaddock, J.A., and Acharya, K.R. (2002). Botulinum and tetanus neurotoxins: structure, function and therapeutic utility. Trends in Biochemical Sciences *27*, 552-558.
Verderio, C., Rossetto, O., Grumelli, C., Frassoni, C., Montecucco, C., and Matteoli, M. (2006). Entering neurons: botulinum toxins and synaptic vesicle recycling. EMBO reports *7*, 995-999.
Wallace, A.J., Stillman, T.J., Atkins, A., Jamieson, S.J., Bullough, P.A., Green, J., and Artymiuk, P.J. (2000). E. coli hemolysin E (HlyE, ClyA, SheA): X-ray crystal structure of the toxin and observation of membrane pores by electron microscopy. Cell *100*, 265-276.
Wang, J., Meng, J., Lawrence, G.W., Zurawski, T.H., Sasse, A., Bodeker, M.O., Gilmore, M.A., Fernandez-Salas, E., Francis, J., Steward, L.E*., et al.* (2008a). Novel chimeras of botulinum neurotoxins A and E unveil contributions from the binding, translocation, and protease domains to their functional characteristics. Journal of Biological Chemistry *283*, 16993-17002.
Wang, Q., Venkataramanan, K.P., Huang, H., Papoutsakis, E.T., and Wu, C.H. (2013). Transcription factors and genetic circuits orchestrating the complex, multilayered response of Clostridium acetobutylicum to butanol and butyrate stress. BMC Systems Biology *7*, 120.
Wileman, T., Harding, C., and Stahl, P. (1985). Receptor-mediated endocytosis. The Biochemical Journal *232*, 1-14.
Wood, C., Williams, C., and Waldron, G.J. (2004). Patch clamping by numbers. Drug Discovery Today *9*, 434-441.
Wu, D., Lin, X., Bernloehr, C., Hildebrandt, T., and Doods, H. (2012). Effects of a novel bradykinin B1 receptor antagonist and angiotensin II receptor blockade on experimental myocardial infarction in rats. PLoS ONE *7*, e51151.
Yowler, B.C., Kensinger, R.D., and Schengrund, C.L. (2002). Botulinum neurotoxin A activity is dependent upon the presence of specific gangliosides in neuroblastoma cells expressing synaptotagmin I. The Journal of Biological Chemistry *277*, 32815-32819.
Zhang, Y., Buchko, G.W., Qin, L., Robinson, H., and Varnum, S.M. (2010). Structural analysis of the receptor binding domain of botulinum neurotoxin serotype D. Biochemical and Biophysical Research Communications *401*, 498-503.
Zimmermann, H., Volknandt, W., Wittich, B., and Hausinger, A. (1993). Synaptic vesicle life cycle and synaptic turnover. Journal of Physiology, Paris *87*, 159-170.